Title: THE HAND OF *AUSTRALOPITHECUS SEDIBA*

TRACY L. KIVELL
Animal Postcranial Evolution (APE) Lab, Skeletal Biology Research Centre, School of Anthropology and Conservation, University of Kent, Marlowe Building, Canterbury, Kent, CT2 7NR UK; Department of Human Evolution, Max Planck Institute for Evolutionary Anthropology, Deutscher Platz 6, Leipzig, 04103, Germany; Evolutionary Studies Institute and Centre for Excellence in PalaeoSciences, University of the Witwatersrand, Private Bag 3, Wits 2050, South Africa; t.l.kivell@kent.ac.uk

STEVEN E. CHURCHILL
Department of Evolutionary Anthropology, Duke University, Box 90383, Durham, North Carolina 27708-9976, USA; Evolutionary Studies Institute and Centre for Excellence in PalaeoSciences, University of the Witwatersrand, Private Bag 3, Wits 2050, South Africa; churchy@duke.edu

JOB M. KIBII
Division of Palaeontology and Palaeoanthropology, National Museums of Kenya, PO Box 40658-00100, Nairobi, Kenya; Evolutionary Studies Institute and Centre for Excellence in PalaeoSciences, University of the Witwatersrand, Private Bag 3, Wits 2050, South Africa; jobkibii@hotmail.com

PETER SCHMID
Anthropological Institute and Museum, University of Zürich, Winterthurerstrasse 190, Zürich CH-8057, Switzerland; Evolutionary Studies Institute and Centre for Excellence in PalaeoSciences, University of the Witwatersrand, Private Bag 3, Wits 2050, South Africa; peterschmid2014@gmail.com

LEE R. BERGER
Evolutionary Studies Institute and Centre for Excellence in PalaeoSciences, University of the Witwatersrand, Private Bag 3, Wits 2050, South Africa; proffleeberger@yahoo.com

Running title: The hand of *Australopithecus sediba*

Abstract

Here we describe the functional morphology of the *Australopithecus sediba* hand, including the almost complete hand of the presumed female Malapa Hominin (MH) 2 skeleton and a single, juvenile metacarpal from the presumed male MH1 skeleton. Qualitative and quantitative comparisons with extant hominids and fossil hominins, ranging from *Ardipithecus* to early *Homo sapiens*, reveal that *Au. sediba* presents a unique suite of morphological features that have not been found in any other known hominin. Analyses of intrinsic hand proportions show that the MH2 hand has a thumb that is longer relative to its fingers than recent humans and any other known hominin. Furthermore, the morphology of the hamatometacarpal articulation suggests that the robust fifth metacarpal was positioned in a slightly more flexed and adducted posture than is typical of Neandertals and humans. Together, this morphology would have facilitated opposition of the thumb to the fingers and pad-to-pad precision gripping that is typical of later *Homo*. However, the remarkably gracile morphology of the first ray and the morphology of the lateral carpometacarpal region suggest limited force production by the thumb. The distinct scaphoid-lunate-capitate morphology in MH2 suggests a greater range of abduction at the radiocarpal joint and perhaps less central-axis loading of the radiocarpal and midcarpal joints than is interpreted for other fossil hominins, while the morphology of the hamatotriquetrum articulation suggests enhanced stability of the medial midcarpal joint in extended and/or adducted wrist postures. The MH2 proximal phalanges show moderate curvature and, unusually, both the proximal and intermediate phalanges have well-developed flexor sheath ridges that, in combination with a palmarly-projecting hamate hamulus, suggest powerful flexion and that some degree of arboreality may have been a functionally important part of the *Au. sediba* locomotor repertoire. Finally, the MH1 and MH2 third metacarpals differ remarkably in their size and degree of robusticity, but this variation fits comfortably within the sexual dimorphism documented in recent humans and other fossil hominins, and does not necessarily

reflect differences in function or hand use. Overall, the morphology of the current *Au. sediba* hand bones suggests the capability for use of the hands both for powerful gripping during locomotion and precision manipulation that is required for tool-related behaviours, but likely with more limited force production by the thumb than is inferred in humans, Neandertals and potentially *Homo naledi*.

INTRODUCTION

Hominin hand morphology has elicited great interest over the last several decades as it has the potential to reveal information about whether our fossil ancestors and extinct relatives still engaged in arboreal locomotion, and to provide insights into the evolution of tool-related behaviours and the extraordinary manipulative abilities of the human hand (e.g. Lemelin and Schmitt 2016; Marzke 1983, 1997; Napier 1962a,b; Wood Jones 1916). However, until recently, the early hominin fossil record for hand bones was relatively sparse, composed of primarily isolated and/or fragmentary hand bones that could not be associated to particular individuals or, in some cases, particular species (e.g. Bush et al. 1982; Drapeau et al. 2005; Napier 1962a; Ricklan 1987, 1990; Susman 1988, 1989). Over the last two decades, several discoveries have fortunately greatly increased our sample of fossil hominin hand bones, including associated hand skeletons that permit a greater understanding of overall hand function in certain species (Clarke 1999, 2008, 2013; Kivell et al. 2011, 2015; Lovejoy et al. 2009; Orr et al. 2013; Tocheri et al. 2007).

In 2008 two relatively complete and partially articulated skeletons were discovered at the site of Malapa, South Africa dated to 1.977 million years ago (Ma) (Berger et al. 2010; Dirks et al. 2010; Pickering et al. 2011). Malapa hominin (MH)1 is considered a juvenile male and MH2 is considered an adult female (Berger et al. 2010). The novel combination of morphologies that characterised these skeletons established these fossils as a new species, *Australopithecus sediba* (Berger et al. 2010). Included within these fossil remains was a relatively complete right hand, found in semi-articulation with the remainder of the right upper limb associated with MH2, as well as a few bones from the left hand of the same individual (Figure 1; Table 1). The MH2 right hand preserves all bones of the hand except the pisiform, trapezium, trapezoid and the distal phalanges of the fingers, while a capitate, hamate and three partial proximal phalanges

are preserved from the left hand. In addition, a juvenile third metacarpal is associated with the MH1 skeleton. Although Kivell et al. (2011) provided a basic morphological description and functional interpretation of most of these hand bones, here we provide a more detailed description and morphological analysis of each bone in a comparative context with extant humans and African apes, as well as other australopiths, *Ardipithecus*, and early and later *Homo* fossils, including *Homo naledi*.

[INSERT Figure 1 and Table 1 about here]

MATERIALS AND METHODS

The *Au. sediba* MH1 and MH2 hand bones were compared qualitatively and quantitatively to those of extant African apes, recent humans, and a large sample of fossil hominins. The extant comparative sample is composed of *Gorilla* spp., including *Gorilla gorilla* and *Gorilla beringei*, *Pan troglodytes* spp., *Pan paniscus*, and recent *Homo sapiens*, including 19th-20th century African, European and Tierra del Fuegian populations, 6th-11th century Nubian Egyptians (Strouhal 1992), and small-bodied Khoisan individuals.

The comparative fossil sample includes data taken from original fossils of *Ardipithecus ramidus, Australopithecus* sp. StW 618*, Australopithecus afarensis, Australopithecus africanus, Australopithecus (Paranthropus) robustus* TM 1517, the Swartkrans hominin fossils attributed to either *Au. robustus* or early *Homo*, *Homo habilis* OH 7, *H. naledi*, *Homo neanderthalensis* (Kebara 2, Amud 1, Tabun 1) and early *H. sapiens* (Qafzeh 8 and 9, Ohalo II H2, Arene Candide 2, Barma Grande 2). For *Ar. ramidus* specimens, data were either derived from published values in Lovejoy et al. (2009) or collected on original specimens by TLK and Gen Suwa. Additional comparative samples include data derived from casts and 3D surface models, in comparison with published data, on *Australopithecus anamensis* (Ward et al. 2001), cf.

Australopithecus KNM-WT 22944 (Ward et al. 1999, 2012), *Homo floresiensis* (Larson et al. 2009; Orr et al. 2013; Tocheri et al. 2007), *H. neanderthalensis*, including Shanidar 3 (Trinkaus 1982, 1983), La Ferrassie 1, Regourdou 1, La Chapelle-aux-Staints, and Neandertal 1, and early *H. sapiens* Tianyuan 1 (Niewoehner 2006; Niewoehner et al. 1997; Trinkaus 1983).

The *Au. sediba* fossils were also compared with published data on *Au. afarensis* A.L. 288-1w (Johanson et al. 1982), possible *Homo erectus* specimens including the KNM-WT 51260 third metacarpal (Ward et al. 2013) and OH 86 fifth proximal phalanx (Domínguez-Rodrigo et al. 2015), *Homo* sp. ATE9-2 fifth proximal phalanx (Lorenzo et al. 2015), *Homo antecessor* isolated hand bones (Lorenzo et al. 1999), *H. neanderthalensis* Shanidar individuals (Trinkaus 1982, 1983), La Ferrassie 1 and 2, Regourdou 1, La Chapelle-aux-Saints (Heim 1982; Niewoehner et al. 1997; Niewoehner 2006), Moula-Guercy (Mersey et al. 2013), Krapina (Heim 1982) and Spy (Crevecoeur 2011), and early *H. sapiens*, including Skhul (Kimura 1976), Dolní Věstonice (Sladek et al. 2000; Trinkaus et al. 2010) and Pavlov (Trinkaus et al. 2010) individuals. Finally, the fossils were also compared to published images and/or descriptions of *Orrorin tugenensis* pollical distal phalanx and proximal phalanx (Almecija et al. 2010; Gommery and Senut 2006; Senut et al. 2001), *Australopithecus prometheus* articulated hand (Clarke 1999, 2008, 2013), *H. erectus* lunate (Weidenreich 1941), KNM-WT 15000 juvenile pollical proximal phalanx, an intermediate phalanx, and two possible first metacarpals (Walker and Leakey 1993) and two distal phalanges from Dmanisi (Lordkipanidze et al. 2007), and *H. antecessor* isolated wrist and hand bones from both juveniles and adults (Lorenzo et al. 1999; Trinkaus 2016).

Measurements for the metacarpals and phalanges follow standard metrics described by Green and Gordon (2008) and Begun (1993), respectively. Linear measurements of the carpal bones are described in Kivell and Begun (2009), Begun and Kivell (2011), and Kivell et al.

(2013a, b). Additional images of how carpal metrics were measured are depicted in box-and-whisker plots below.

Comparisons of size and shape differences across extant and fossil taxa were assessed via box-and-whisker plots. Most aspects of morphology were assessed as shape ratios, usually as a ratio of the total length of the bone. For the triquetrum, capitate and hamate, some metrics were analysed as a shape ratio against a geometric mean of the maximum proximodistal length, dorsopalmar height and mediolateral breadth of the carpal bone (Jungers et al. 1995; Mosimann 1970). All analyses were conducted in PAST.3.14 (Hammer et al. 2001).

Curvature of the dorsal surface of the non-pollical proximal phalanges was quantified using high-resolution polynomial curve fitting (HR-PCF), following the methods Deane and colleagues (Deane et al. 2005; Deane and Begun 2008). The HR-PCF method differs from that of the more traditional included angle measure (Stern et al. 1995) by modelling the surface curvature and fitting a polynomial function to the dorsal surface of the phalanx. Using standardised lateral-view photographs of each phalanx, the dorsal surface was digitised and, from selected end points and a best-fit second order polynomial function, the first polynomial coefficient was used to describe the nature and degree of longitudinal curvature (Deane et al. 2005).

Specimens and sample sizes for comparative analyses varied for each hand element. Therefore information on the specific sample is provided in the figure legend of each comparative analysis. In instances where both the left and right sides are preserved for a particular element for the same individual, the mean value was used.

ANATOMICAL DESCRIPTION OF *AU. SEDIBA* HAND FOSSILS

All specimens described below are associated with the adult MH2 skeleton, apart from U.W. 88-112, a juvenile left third metacarpal that is associated with MH1. All of the MH2 hand bones

appear externally as adult due to full fusion of epiphyses, complete ossification of carpals (Kivell 2007) and well-defined articular facets. In addition to the MH2 right hand bones being found in semi-articulation *in situ* (Figure 1), they articulate well together and with the distal radius and ulna based on the preserved morphology (Figure 2). Metric data for all MH1 and MH2 hand bones are provided in Tables 2-5. A taphonomic analysis of the MH1 and MH2 skeletons has revealed numerous perimortem fractures, including several throughout the MH2 upper limb, that are consistent with falling from a height and bracing with the arm against impact (L'Abbé et al. 2015). Among these perimortem palaeopathologies are two fractures within the MH2 hand; one on the scaphoid and one on the triquetrum (L'Abbé et al. 2015), which are noted below.

A 3D model of the articulated MH2 hand as well as separate 3D data for some of MH2 hand specimens are available on MorphoSource (https://www.morphosource.org/). The following abbreviations are used throughout the morphological descriptions below: proximodistal (PD), dorsopalmar (DP) and mediolateral (ML).

U.W. 88-158 RIGHT SCAPHOID (MH2)

Preservation This bone is complete apart from fragments missing from the tip of the tubercle and the dorsomedial edge of the capitate facet (Figure 3). There are fine cracks running along the approximate PD midline of the trapezium-trapezoid facet and the DP midline of the capitate facet, but neither crack distorts the morphology. These cracks have been previously interpreted as Class II fractures, consistent with a perimortem injury to the wrist (L'Abbé et al. 2015).

Morphology The U.W. 88-158 scaphoid has a fused os centrale (Figure 3). The tubercle is robust, conical-shaped, and proximally-oriented. The radial facet is not continuously convex but instead the point of strongest curvature is proximally-positioned, such that the facet is divided into a larger distal portion and smaller proximal portion, both of which are mildly convex. A dorsal ridge at the distal edge of the radial facet is not present. The lunate facet is generally flat,

half-moon-shaped, and is confined to the proximodorsal edge of the scaphoid. The capitate facet is oval-shaped and relatively shallow in its concavity (Table 2). Although a fragment is missing from the distomedial edge, the capitate facet appears to be “closed” (i.e., there is no excavation of the distomedial edge of the facet) (Tocheri 2007). The trapezoid and trapezium facets form a single, continuous facet that is strongly convex both the DP and ML dimensions. The trapezoid-trapezium facet appears “raised”, divided on the lateral side from the remainder of the bone by a deep sulcus that extends onto the tubercle. The trapezium facet extends onto the tubercle, reaching to roughly 3mm from the estimated tip of the scaphoid’s tubercle (as this region is not well-preserved) (Figure 3).

[INSERT Figures 2 & 3 and Table 2 about here]

U.W. 88-159 RIGHT LUNATE (MH2)

Preservation This bone is complete apart from a large fragment missing from the palmar-medial edge of lunate body, and a small fragment from the distodorsal edge of the triquetrum facet (Figure 4). All articular facets are well-defined.

Morphology The U.W. 88-159 lunate is small and narrow, although the fragment missing from the palmar-medial corner over-accentuates its narrowness (Figures 2 and 4; Table 2). The capitate and radial facets sit roughly parallel to each other. The capitate facet is remarkably ML narrow relative to its DP height. The palmar portion of the capitate facet (and lunate body) is more distally extended than the dorsal portion. A separate articulation for the hamate is not present. The radial facet occupies most of the proximal surface and extends onto the palmar surface to approximately 5.5mm from the most distal edge of lunate body. The radial facet is ML broad relative to the breadth of the lunate body and its convexity shows a similar division as seen in the scaphoid’s radial facet, such that point of peak curvature is proximally-positioned.

The scaphoid facet is flat and confined mostly to the dorsal half of the lunate's lateral side. The scaphoid facet is distolaterally oriented, such that it is positioned more acutely (i.e. less than 90 degrees) to the capitate facet, and can be clearly seen in distal view (Figures 2 and 4). The triquetrum facet is dorsally-position and generally flat. The dorsal non-articular surface is deeply excavated for attachment of the dorsal intercarpal and radiotriquetrum liagments (Taleisnik 1976). No foramina or ligamentous attachment sites can be seen on the non-articular palmar portion of the lunate body.

U.W. 88-157 RIGHT TRIQUETRUM (MH2)

Preservation This bone is complete and undistorted. There are two thin cracks on the medial surface running dorsopalmarly around the triquetrum body (Figure 5). These cracks have been previously interpreted as Class II fractures, consistent with a perimortem injury to the wrist (L'Abbé et al. 2015).

Morphology The overall shape of the MH2 triquetrum is ML broad and PD narrow, with a palmar-medially-extended tip (Figure 5; Table 2). The lunate facet is flat, roughly square-shaped, and is oriented at an approximate right angle to the hamate facet. The hamate facet has a complex concavoconvex surface; the middle of the facet has the deepest concavity that extends to a convex surface at the dorsolateral, palmar-lateral and medial borders. The hamate articulation extends to the dorsal edge of the triquetrum body and to roughly 4.7mm from the body's most medial extent. The pisiform facet is small (*contra* Kivell et al. 2011) and oval-shaped. It is positioned on the palmar-medially-projecting extension of the triquetrum body and, as such, is oriented proximopalmarly. The non-articular palmar portion of the triquetrum body is deeply excavated by a sulcus running roughly ML across the lateral half of the body (Figure 5).

[INSERT Figures 4 & 5 about here]

U.W. 88-105 LEFT CAPITATE (MH2)

Preservation This bone is complete and perfectly preserved (Figure 6).

Morphology The overall shape of the capitate appears DP tall relative to its PD length (Figure 6; Table 2). The proximal facet is relatively equal in its DP height and ML breadth (Table 2). There is no clear demarcation between the lunate and scaphoid articular areas on the proximal surface and both end distally in a small dorsal ridge. On the lateral surface, the dorsal portion of the scaphoid facet extends further distally than its palmar portion, touching the tip of the dorsal trapezoid facet. The capitate body is deeply excavated between the distal portion of the scaphoid facet and the dorsal trapezoid facet. The capitate body appears moderately “waisted” in palmar view (Figure 6).

There are two trapezoid facets on the lateral side of the capitate; a smaller triangular-shaped facet positioned dorsally and a larger, well-defined, oval-shaped facet placed palmarly (each measuring 4.1 and 3.5mm in PD length and 4.2 and 6mm in DP height, respectively). The capitate’s second metacarpal (Mc2) facet is continuous running most of the DP height of the capitate body. It is slightly concave, especially at its palmar end. The Mc2 articulation is oriented primarily laterally, with only a slight distal orientation. The Mc3 facet occupies the distal surface of the capitate body and is generally flat, with a slight concavity at dorsomedial border. The distodorsolateral border is not excavated to accommodate a Mc3 styloid process (Figure 6). The hamate facet is continuous along the complete dorsal border of the capitate’s medial surface. Most of the hamate articulation is flat apart from the distal 1/3 that curves proximally and palmarly. There is no separate articulation on the capitate for the Mc4.

U.W. 88-156 RIGHT CAPITATE (MH2)

Preservation This bone is complete and well-preserved, apart from small surface fragments missing from the distopalmar surface of the capitate body, just palmar to the border of the Mc3 facet and the distopalmar surface of the Mc2 facet (Figure 6). There is some abrasion on the palmar half of the lateral side that obscures the presence of a trapezoid facet and the full dorsal extent of the Mc2 facet. Although a portion of the distodorsolateral corner of the capitate body appears to be missing when compared with the left MH2 capitate, the dorsal non-articular surface appears continuous and undamaged. The capitometacarpal articular surfaces articulate well with the Mc2 and Mc3, suggesting that the right capitate is generally complete (Figure 7). Thus, this variation may simply reflect asymmetry between the right and left capitates in MH2.

Morphology This bone is similar in morphology to that described in the U.W. 88-105 left capitate, apart from the dorsolateral portion of the capitate body described above (Figure 6; Table 2). The overall size of the bone and facets are slightly smaller than that of the left capitate, consistent with bilateral asymmetry within one individual. Due to the preservation of the lateral side of the capitate, it is unclear if this specimen had both palmar and dorsal trapezoid facets as in U.W. 88-105. If the absence of distodorsolateral corner of capitate body is not taphonomical, than is likely that a dorsal trapezoid facet was not present.

[INSERT Figures 6 and 7 about here]

U.W. 88-106 LEFT HAMATE (MH2)

Preservation This bone is complete and perfectly preserved, except for a small pit at the distal edge of the dorsal surface (Figure 8).

Morphology The body of the hamate (excluding the hamulus) appears DP tall relative to PD length (Figure 8, Table 2). The hamulus projects palmarly much further than it does distally, such that the hamulus alone measures 7.6mm in DP height but projects distally only 0.2mm

from the hamate body. The hamulus is widest in the PD plane and is mediolaterally narrow (Figures 7 and 8). The triquetrum facet is proximomedially-oriented and extends to the distal end of the hamate body. The proximal half is convex in both the PD and DP dimensions, while the distal half is concave and more proximally-oriented. In medial view, the proximal half of the facet is inclined dorsally, such that the triquetrum would rotate dorsally during extension and/or adduction of the midcarpal joint.

The capitate facet is generally flat, but slightly curved in dorsal view to match the opposing concavity on the capitate's hamate facet (Figures 6 and 7). The Mc4 facet is absolutely larger than the Mc5 facet in both the DP and ML dimensions (Table 2). The Mc5 facet is oriented distomedially relative to the Mc4 facet and extends to the dorsal border of the hamulus (Figure 7). The Mc4 facet is generally flat while the Mc5 facet is strongly concave dorsopalmarly and slightly concave mediolaterally. There is a space between the palmar border of the Mc5 facet and the strongest curvature of the hamulus that could potentially accommodate extension of the pisometacarpal ligament to the Mc3, although no clear groove is present (Lewis 1977).

U.W. 88-95 RIGHT HAMATE (MH2)

Preservation This bone is complete except for a small fragment missing from the distopalmar tip of the hamulus (Figure 8).

Morphology The morphology of the right hamate is identical to that of left side, U.W. 88-106 (Figure 8; Table 2). The overall size of the hamate and its facets are generally slightly smaller than that of U.W. 88-106, consistent with pattern seen in the MH2 capitates and bilateral asymmetry within an individual.

[INSERT Figure 8 about here]

U.W. 88-119 RIGHT FIRST METACARPAL (MH2)

Preservation This bone is complete and well-preserved (Figure 9). There is a fracture around the approximate midshaft and a smaller crack in the distal half of the shaft, both of which run the circumference of the bone.

Morphology The first metacarpal (Mc1) of MH2 appears long and remarkably gracile (Figure 9; Table 3). The dorsal surface of the shaft is mildly convex and the proximal and distal epiphyses project slightly dorsally beyond the shaft. Muscle attachments along the shaft are poorly defined. There is a roughened surface along the lateral shaft for the attachment of the *M. opponens pollicis* tendon, extending from the beginning of the proximal shaft 15.5mm distally, although the distal end of the enthesis is slightly obscured by the midshaft fracture line. The attachment is proximally-positioned and there is no indication of tendon insertion along the distal shaft. The *M. first dorsal interosseous* attachment is equally poorly developed in U.W. 88-119, appearing as a faint ridge along proximal half of the shaft's medial border, measuring 11.8mm in PD length (Kivell et al. 2011).

Relative to interarticular length, the proximal base of U.W. 88-119 is ML narrow relative to its height (Figure 9; Table 3). The tendon attachments at the base appear robust because of the gracility of the shaft; the distolateral border of the base flares laterally with an attachment for the *M. abductor pollicis longus*. The palmar-medial portion of the base is also robust, which is the region of insertion for the *M. palmar interosseous*. A triangular-shaped fossa is found on the palmar-lateral surface between these two tendon attachment sites. The trapezium facet is saddle-shaped; the DP concavity appears slightly more pronounced than its ML convexity. There is no beak-like palmar extension of the proximal epiphysis.

The distal head of U.W. 88-119 is DP tall and ML narrow (Figure 9; Table 3). The head has a prominent beak along the midline of the palmar surface. This beak is flanked by

depressions for medial and lateral sesamoid bones, with the medial depression being more excavated than the lateral, which serve as insertion sites for *Mm. adductor pollicis oblique* and *flexor pollicis brevis*, respectively (Marzke et al. 1999). The articular surface for the first proximal phalanx is asymmetric; in palmar view, the dorsal articular surface slopes laterally and the articular surface extends further proximally on the medial side. In distal view, the dorsal half of the articular surface is ML narrower than the palmar half. The epicondyles are not prominent.

[INSERT Figure 9 and Table 3 about here]

U.W. 88-115 RIGHT SECOND METACARPAL (MH2)

Preservation This bone is complete and well-preserved. There is slight erosion on the dorsal surface of the proximal articular facet and hairline fractures running mediolaterally across the dorsal half of the proximal facet and proximodistally along the medial side of the shaft from the proximal end to roughly midshaft (Figure 10).

Morphology Like the MH2 Mc1, the shaft of U.W. 88-115 appears gracile (Figure 10; Table 3). In dorsal view, the distal shaft and head are oriented more laterally relative to the remainder of the Mc2. The dorsal shaft has a prominent crest along the sagittal midline for attachment of the first and second *Mm. dorsal interossei* that starts at the base-shaft junction and extends 15mm distally, flattening out just proximal to the midshaft. These crests are prominent on all of the MH2 medial metacarpal shafts (see below), but the crest is most well-developed on the Mc2.

The base of the Mc2 is robust relative to the gracile shaft. The dorsal surface of the proximal epiphysis has two well-developed tubercles, one dorsolateral for the attachment of the *M. extensor carpi radialis longus* tendon and one dorsomedial for the attachment of the *M. extensor carpi radialis brevis* tendon. Similarly, the palmar surface of the proximal epiphysis presents robust and distinct tubercles for the attachment of the *M. flexor carpi radialis* and

oblique tendons of the *M. adductor pollicis*. The proximal articular surface for the trapezoid is roughly triangular in outline in proximal view, although the palmar articular region is relatively ML broad (measuring 7.3mm) compared with the dorsal portion (measuring 10.2mm), giving it a somewhat “squared” appearance (Table 3). The trapezoid facet dominates the proximal surface, although the trapezium and capitate facets can also be seen in proximal view. The trapezoid facet is V-shaped, with a larger medial portion than lateral portion, that are oriented at roughly 110 degrees to each other in dorsal view.

The trapezium facet is flat and oval-shaped (measuring 4.6mm PD and 6mm DP), and oriented palmar-laterally. Relative to the long axis of the shaft, the trapezium facet is oriented approximately 35° in proximal view (Drapeau et al. 2005), and approximately 28° in dorsal view (Kivell et al. 2011). The capitate facet is rectangular in shape, measuring 5mm proximodistally and 9.6mm dorsopalmarly. It is generally flat in DP dimension but slightly convex in its PD dimension and runs most of the DP height of the medial side of the proximal epiphysis. The capitate facet is distinguished from the Mc3 facet by its more proximal orientation. The Mc3 articulation is a continuous, bilobate facet with more distinct palmar and dorsal articular areas that are connected proximally. The complete Mc3 facet measures 9.9mm dorsopalmarly but is PD longer at the dorsal end (7mm) than the palmar end (4.3mm).

The distal epiphysis of U.W. 88-115 appears ML broad and particularly DP tall (Table 3). The Mc2 head is strongly asymmetrical; the palmar articular surface is more ML expanded than the dorsal portion and the palmar articular surface extends further proximally on the lateral side. There is no ridge along the dorsal articular margin. The medial epicondyle is well-developed and more proximally positioned compared with the lateral epicondyle.

[INSERT Figure 10 about here]

U.W. 88-112 LEFT THIRD METACARPAL (MH1)

Preservation This bone is incomplete, missing its epiphyseal head, which was unfused to the distal shaft (Figure 11). The base is missing a large fragment from the dorsolateral corner and a smaller fragment from the palmar portion of the proximal articular surface. There is triangular-shaped hole running through the shaft at roughly midshaft that exposes a cross-section of the cortex. Additional small surface fragments are missing from the shaft cortex.

Morphology U.W. 88-112 is a juvenile Mc3 and is thought to be from the left side, *contra* Berger et al. (2010) and Kivell et al. (2011), which identified it as a right. Because the head and diagnostic articular surfaces of the base are not preserved, side identification is based on comparisons with the MH2 U.W. 88-116 right Mc3 and the preservation of a slight lateral torsion of the distal shaft, protuberance of the dorsolateral tubercle of the base, slight "lipping" of the mediopalmar edge of the capitate facet, and the orientation of the dorsal Mc4 facet (Figure 11) all of which suggest U.W. 88-112 is a left Mc3.

The distal surface of the metacarpal is irregular and pitted, typical of an unfused epiphyseal surface (Figure 11). In palmar view, the proximal portion of the shaft is straight but at midshaft it flares mediolaterally with slight torsion to the lateral side. In dorsal view, the distal shaft is ML broad and flat both its PD and ML dimensions (Table 3). The flaring of the distal shaft creates a ridge along the dorsomedial border that extends from the epiphyseal line proximally 15.1mm. Just palmar to this ridge is a smooth, shallowly concave fossa along the medial shaft. In lateral view, the dorsal shaft is mildly convex. Although the complete length of this bone is not preserved, the shaft appears substantially more robust, both in its ML and DP dimensions, than the Mc3 of the MH2 hand (U.W. 88-116, see below) (Figure 11; Table 3).

The preserved morphology of the U.W. 88-112 base is similar in absolute DP height (13.9mm preserved) to that of MH2 U.W. 88-116 Mc3 but is missing large fragments from its dorsolateral corner and the palmar border. With these portions preserved, the U.W. 88-112

base would be larger both dorsopalmarly and mediolaterally than U.W. 88-116. Much of the lateral surface of the base is missing and the Mc2 facet(s) is not preserved. The capitate facet, which is preserved in only the dorsomedial portion of the proximal Mc3 surface, is flat and slightly dorsally-oriented. In medial view, the slightly palmarly-oriented palmar-medial border of the capitate facet creates a small lip that is similar to the morphology found in U.W. 88-116 (Figure 11). A dorsal, oval-shaped Mc4 facet is clearly preserved, measuring 6.6mm proximodistally and 5mm dorsopalmarly, and, although the proximopalmar border of the medial side is slightly eroded, there does not appear to be a palmar Mc4 facet (unlike U.W. 88-116).

The unfused epiphyseal head of this Mc3 is consistent with the stage of juvenile development found throughout the remainder of the MH1 skeleton (Berger et al. 2010). Fusion of the Mc3 head occurs at roughly age 9-10 years in chimpanzee (Kerley 1966) and age 14-17 years in humans (Scheuer and Black 2000).

U.W. 88-116 RIGHT THIRD METACARPAL (MH2)

Preservation This bone is generally well-preserved, apart from a missing fragment at the dorsomedial edge of the proximal end, a small pit on the palmar surface of the shaft just distal to the midshaft, a large surface fracture along the palmar surface of the distal articular facet, and a thin fracture along the lateral side of the distal end, just palmar to the medial epicondyle. The fracture lines and pit do not distort the original morphology (Figure 11).

Morphology U.W. 88-116 is a gracile Mc3 that does not have a styloid process (Figure 11). In palmar view, the shaft is straight and ML narrow (Table 3). Along the proximal half of the dorsal surface of the shaft there is a small crest running PD 11.1mm along sagittal midline for the attachment of the second and third *Mm. dorsal interossei*. This crest is not as prominent as that of the MH2 Mc2 nor does it extend all the way to the base-shaft junction.

Relative to the gracile shaft, the Mc3 base appears moderately ML broad and DP tall. The palmar surface of the base is robust for the attachment for the oblique head of the *M. adductor pollicis* tendon. The proximal articular surface for the capitate is generally smooth and mildly DP convex, particularly the palmar portion such that part of the capitate facet can been seen in palmar view of the Mc3. The capitate articulation is generally rectangular in shape; it is only slightly ML broader dorsally (estimated at 9.3mm) than palmarly (8.1mm), and is approximately 12.2mm in DP height. The Mc2 articulation is a single, continuous facet measuring 10.3mm in DP height and 5.4mm in its maximum PD length. It is generally DP concave to oppose the corresponding articular convexity on the Mc2. The palmar ¾ of the Mc2 facet is oriented mostly laterally and slightly proximopalmarly, while the remaining dorsal portion is oriented more dorsally and proximally. Just distal to the dorsal portion of the Mc2 facet is a large tubercle for the attachment of *M. extensor carpi radialis brevis*. Palmar to this tubercle is a deeply excavated fossa that accentuates the prominence of the tubercle. The medial side of the base has separate dorsal and palmar articular facets for the Mc4 measuring 5.1mm and 4mm in PD length and 3.9mm and 5.1mm in DP height, respectively. The palmar facet is mildly concave and oriented primarily medially but also slightly distodorsally. The dorsal facet is flat and more distally positioned, and is oriented primarily medially and slightly proximopalmarly.

The Mc3 head is DP tall and oriented slightly laterally relative to the long axis of the shaft. The articular surface is asymmetrical with the lateral articulation extending farther proximally then the medial side. The epicondyles are prominent, with the medial one being slightly larger. There is no ridge at the dorsal edge of the articular surface (Figure 11).

[INSERT Figure 11 about here]

U.W. 88-117 RIGHT FOURTH METACARPAL (MH2)

Preservation This bone is complete and perfectly preserved, except for a small fragment missing from the lateral epicondyle and a thin fracture running the circumference of the shaft just proximal to midshaft (Figure 12). The proximal end is slightly abraded such that the lateral and dorsal borders of the hamate facet blend with the non-articular area and do not have a definitive outline.

Morphology Like the other MH2 metacarpals, the U.W. 88-117 shaft appears gracile (Figure 12; Table 3). The proximal half of the dorsal shaft presents a prominent *Mm. dorsal interossei* crest (measuring 13.5mm in PD length) that is more pronounced than that of the MH2 Mc3 but less so than the Mc2. In palmar view, there is a strong degree of medial torsion in the distal 1/3 of the shaft such that the palmar surface of the head is oriented slightly medially relative to the base. In lateral view, the dorsal shaft is slightly convex with a peak "bend" in the shaft at roughly midshaft.

The Mc4 base appears DP tall and ML broad relative to the gracile shaft (Figure 12). The proximal end is dominated by the articulation for the hamate. There is no articulation for the capitate. The lateral border of the hamate facet is not well-defined, but re-articulation with the hamate demonstrates that this facet is roughly rectangular shape, with a rounded palmar border. The hamate facet is generally flat with a mild convexity and its palmar portion of the hamate facet is estimated to be slightly ML narrower (5.7mm) than its dorsal portion (7.4mm). Mc5 facet is a single, continuous facet, measuring 8.5mm in DP height and 4.8mm in PD length. The palmar half of the facet is flat and the dorsal half is strongly concave, such that it flares medially and can been seen in palmar view. There is a deep pit at the DP centre of the medial side, just distal to the Mc5 facet. On the lateral side there are two articular facets for the Mc3 divided by a deep sulcus; the palmar facet is larger (4.4mm in PD length, 3mm in DP height), oval-shaped, flat and faces mostly laterally but also proximopalmarly, while the dorsal facet is smaller (2.8mm in PD length, 2.9mm in DP height), circular, flat and is more distally placed. The

dorsal facet is oriented primarily laterally and slightly distally. These facets correspond well with the Mc4 articulation on the Mc3 U.W. 88-116.

The Mc4 head is DP tall and ML broad relative to the shaft (Figure 12; Table 3). In palmar view, the head is relatively symmetrical in its proximal extension of the articular surface. In dorsal view, the medial epicondyle is more proximally positioned then the lateral epicondyle.

U.W. 88-118 RIGHT FIFTH METACARPAL (MH2)

Preservation This bone is complete except for a fragment (6.9mm in PD length) missing from the ridge for the *M. opponens digiti minimi* tendon attachment on the medial surface at roughly midshaft (Figure 13). There is a fracture that runs the circumference of the shaft just proximal to the head. There is also a small surface fragment missing from the palmar shaft, just proximal to midshaft.

Morphology Relative to the other MH2 metacarpals, the shaft of U.W. 88-118 appears more robust (Figure 13). In palmar view, the shaft is straight and the palmar articular surface of the head is oriented slightly medially relative to the base. In dorsal view, there is small crest for the fourth *M. dorsal interosseous* running 7.6mm along the proximal portion of the dorsal shaft, medial to the sagittal midline. This crest is less prominent than that of the MH2 Mc4 and Mc2. The medial side of the shaft has a well-developed, rugose attachment for the *M. opponens digiti minimi*, running 14.6mm in PD length. Although a large portion is missing from the center of the enthesis, it flares medially at both its proximal and distal ends suggesting that the enthesis was well-developed.

The Mc5 base is DP tall and ML broad relative to the shaft (Figure 13; Table 3). The medial side of the base flares strongly with a robust protuberance for the *M. extensor carpi ulnaris* attachment dorsally and the pisohamate ligament palmarly. The dorsal surface of the base has a prominent tubercle on the lateral side for the attachment of the dorsal metacarpal

ligament. The hamate facet dominates the proximal end of the Mc5 and is strongly DP convex and generally flat ML, corresponding to the DP concavity of the corresponding articulation on the hamate. However, the facet is also palmarly-positioned, such that it does not occupy any of the dorsal portion of Mc5 proximal surface, but instead extends onto the palmar surface of the base and can be seen clearly in palmar view (Figure 13). The hamate facet is asymmetrical such that in proximal view, the dorsal portion of the articular surface is slightly ML broader (8.5mm) than the palmar portion (8.2mm) and the articulation extends farther palmarly on the medial side than the lateral side. The Mc4 facet is a single, continuous and generally flat facet, measuring 8.1mm in DP height and 4.2mm in PD length and oriented primarily laterally. The dorsal portion of the Mc4 facet extends farther distally than the palmar portion, matching the corresponding articular morphology on the Mc4.

The Mc5 head is DP tall and ML broad relative to its shaft (Figure 13). In palmar view, the head is asymmetric, with the distal outline of the articular surface slanted proximomedially. The proximal extension of the palmar articular surface is approximately equal on the medial and lateral sides. The facet tapers strongly towards the sagittal midline as it curves dorsally, such that the dorsal articular area appears slightly “pinched” between the epicondyles. The lateral epicondyle is prominent while the medial epicondyle is comparatively small.

[INSERT Figures 12 & 13 about here]

U.W. 88-91 LEFT POLLICAL PROXIMAL PHALANX (MH2)

Preservation This bone is complete and perfectly preserved apart from a fragment missing from the palmar-medial surface of the trochlea and a small surface fragment missing from the medial side of the proximal shaft at the junction between the base and shaft (Figure 14).

Morphology The U.W. 88-91 pollical proximal phalanx (PP1) has a gracile shaft (Figure 14; Table 4). The dorsal surface of the shaft is PD convex, with greatest curvature along the distal 1/3 of the shaft. The dorsal surface of the shaft is ML broad and flat at its distal end but tapers proximally, such that the proximal half of the shaft slopes steeply on the medial and lateral sides from the flat dorsal midline. In sagittal view, the proximal 2/3 of the shaft is DP tall but narrows strongly just proximal to the trochlea (Figure 14). Most of the palmar shaft surface is generally ML flat, with a concave fossa just proximal to the trochlea, which gives U.W. 88-91 a "hollowed" appearance.

The PP1 base is strongly asymmetric, with a more proximally-extended lateral portion of the proximal articular surface and a larger, prominent lateral tubercle for the attachment of the *Mm. flexor polllicis brevis* and *abductor pollicis brevis* tendons (Figure 14). The medial side of the base also has as well-developed tubercle for the attachment of the *M. adductor pollicis* tendon. This tubercle extends distally into a well-defined ridge that is 5.4mm long PD. The proximal facet is oval-shaped, being ML broader than it is DP tall, and strongly concave, especially along its lateral border (Table 4). The distal trochlea of U.W. 88-91 is also asymmetrical; in palmar view, the medial portion of the trochlea extends further distally than the lateral portion. The articular facet extends proximally onto the dorsal surface 2.3mm.

U.W. 88-160 RIGHT POLLICAL PROXIMAL PHALANX (MH2)

Preservation This bone is less well-preserved than its left counterpart. A large fragment from the palmar and medial portion of the base and a smaller fragment of the palmar-medial trochlea are missing, and the remainder of the palmar surface of the trochlea is abraded (Figure 14).

Morphology The preserved morphology is almost identical to that described for U.W. 88-91, although most dimensions are slightly smaller, consistent with the bilateral asymmetry found in the carpal bones (Table 4).

[INSERT Figure 14 and Table 4 about here]

U.W. 88-164 RIGHT SECOND PROXIMAL PHALANX (MH2)

Preservation This bone is complete and perfectly preserved apart from a crack running ML across the distodorsal surface of the trochlea and slight erosion along the palmar-lateral edge of the lateral trochlea (Figure 15).

Morphology U.W. 88-164 is considered to be a PP2 based on its overall length and slightly greater robusticity and asymmetry at the base compared with the other proximal phalanges of the right hand (Figure 15; Table 4). The dorsal surface of this bone is moderately curved, especially at the distal end. The shaft is DP taller at the proximal end and tapers distally and, in palmar view, the medial and lateral sides of the shaft are straight. The palmar surface is PD and ML concave. There is a prominent flexor sheath ridge measuring 8.2mm in PD length, with its centre just distal to midshaft, on the medial edge that extends roughly 1.3mm above the palmar surface of the remaining shaft. The flexor sheath ridge on the lateral side is not distinct.

At the proximal end of U.W. 88-164 both basal tubercles are pronounced, but the lateral basal tubercle is more prominent. In palmar view, the proximolateral border extends farther proximally than that of the medial side. The proximal articular facet is concave, oriented proximally and is oval-shaped, being ML broader than it is tall (Table 4). The head of U.W. 88-164 is generally symmetrical in palmar view, with the medial and lateral trochlear head extending proximally to an equal extent. However, the medial trochlear surface is slightly more ML expanded than that of the lateral side. The dorsal articular surface of the trochlea is ML narrow and expands palmarly.

[INSERT Figure 15 about here]

U.W. 88-109 LEFT SECOND PROXIMAL PHALANX (MH2)

Preservation This bone preserves the full PD length of the medial half of the phalanx, broken roughly at the sagittal midline (Figure 15). There are two thin fractures; one just distal to the base-shaft junction and the other distal to the midshaft. The palmar-medial border of the proximal shaft and flexor sheath ridge is also missing.

Morphology The preserved morphology is identical to the medial side of PP2 of the right hand. The flexor sheath ridge measures roughly 7mm PD and appears equally developed and similarly positioned to that of the medial flexor sheath ridge of U.W. 88-164. The medial trochlea is better preserved than that of U.W. 88-164 and demonstrates that the distodorsal portion of the articular surface is more rounded in sagittal view than what is preserved on the right PP2. The sagittal break along the midline reveals cortical bone in the proximal shaft that is approximately 2.3mm thick on dorsal and palmar sides and the trabecular structure, although filled with matrix, appears to extend distally into the shaft roughly 7.2mm.

U.W. 88-120 RIGHT THIRD PROXIMAL PHALANX (MH2)

Preservation This bone is complete and perfectly preserved except for small fragments missing from the palmar side of the medial trochlea and the dorsolateral edge of the proximal facet, and erosion of the palmar-lateral edge of the shaft and flexor sheath ridge (Figure 15).

Morphology The overall morphology of this bone is similar to that described for U.W. 88-164 right PP2. U.W. 88-120 is considered a PP3 based on its long length and reduced asymmetry relative to the remaining proximal phalanges of the MH2 right hand (Figure 15; Table 4). In palmar view, the shaft is PD concave, ML concave at midshaft, but ML flat at the proximal and distal ends. Both the medial and lateral flexor sheath ridges appear to be well-defined, although the proximal half of the lateral ridge is eroded. Both ridges extend roughly 1.4mm beyond the

palmar surface of the remaining shaft. The PD length of the medial ridge is 14.4mm and the lateral ridge is roughly 11.4mm. At the PP3 base the lateral basal tubercle is much more prominent than the medial tubercle. The proximal articular surface is more circular than that of the PP2, but is still ML broader than it is DP tall. The trochlea is generally symmetrical.

U.W. 88-182 LEFT THIRD PROXIMAL PHALANX (MH2)

Preservation This specimen is the proximal half of a proximal phalanx. The proximal end is perfectly preserved and it broken at an angle just distal to the midshaft (Figure 15).

Morphology This bone is identified as a left PP3 based on it similar size and morphology to the right PP3, U.W. 88-120 (Figure 15; Table 4). In palmar view, the flexor sheath ridges are well-developed on both sides. The medial ridge is completely preserved and measures 11.5mm PD length. The portion of the lateral ridge that is preserved (7.6mm in PD length) is similar in its development to that of the medial ridge. The basal tubercles are less asymmetrical than those of the right PP3.

U.W. 88-108 RIGHT FOURTH PROXIMAL PHALANX (MH2)

Preservation This bone is complete and well-preserved apart from erosion to the palmar portion of the basal tubercles and fragments missing from the palmar-lateral and palmar-medial surfaces of the trochlea (Figure 15).

Morphology This bone is identified as the PP4 based on its relative length, slightly less robust base and slight asymmetry of the trochlea compared with the other proximal phalanges (Figure 15; Table 4). Its overall morphology is generally similar to that described for the PP2 and PP3. The palmar surface of the shaft is PD concave and is ML concave at the proximal end and, especially, at midshaft, while the distal portion is ML flat. The flexor sheath ridges are very well-developed on both sides, more so than in any other ray. The lateral flexor ridge is more palmarly

and PD extended than the medial ridge, measuring 14.9mm in PD length and extending roughly 2.2mm above the remainder of the palmar surface of the shaft. The medial flexor ridge is 8.9mm in PD length and 1.9mm extended above the palmar surface of the shaft. The base is slightly asymmetric; the medial side of the proximal facet and base extend more proximally than the lateral side and the preserved morphology suggests that the medial tubercle was slightly more prominent. The preserved morphology of the trochlea displays slight asymmetry with the lateral articular surface extending more distally than the medial side.

U.W. 88-110 LEFT FOURTH PROXIMAL PHALANX (MH2)

Preservation This bone preserves only the dorsolateral portion of the proximal end of a proximal phalanx, including the dorsal half of the proximal facet and the dorsolateral side of the base (Figure 15).

Morphology The bone is identified as a likely left PP4 based on its similarity in size and morphology with the complete right PP4 U.W. 88-108 (Figure 15; Table 4). The DP height of the preserved portion of the proximal shaft as well as the curvature, size and proximal orientation of the articular surface are all comparable to that of U.W. 88-108.

U.W. 88-121 RIGHT FIFTH PROXIMAL PHALANX (MH2)

Preservation This bone is complete apart from strong erosion of the trochlea, a small surface fragment missing from the palmar-medial edge of the proximal border of the base, and fragments missing from both flexor sheath ridges. There is small, square piece of sediment still attached to the dorsal surface of the shaft, just proximal to the trochlea (Figure 15).

Morphology This bone is identified as a PP5 based on its small size and morphology relative to the other proximal phalanges (Figure 15; Table 4). The overall morphology is generally similar to the other MH2 proximal phalanges with a few distinct differences; the palmar surface is

largely convex ML with a well-developed “bar” that extends from the medial basal tubercle proximally to roughly 3mm from the sagittal midline of the distal articular surface. Along the palmar surface of the medial tubercle, the convex bar turns into a prominent ridge. There is an outline of white exposed cortex where the flexor sheath ridges have eroded on both the medial and lateral sides. The lateral flexor ridge extends an estimated 12.3mm distally from the lateral tubercle. At the tubercle the ridge appears to curve proximally and medially around the palmar surface of the shaft to form a teardrop-shaped concavity lateral to the convex “bar” described above (Figure 15). Compared with the lateral ridge, the medial flexor ridge appears not to extend as far distally (estimated at 7.7mm in PD length), although erosion of the surface makes this difficult to determine with certainty. The PP5 base is asymmetric with the medial tubercle being more prominent and medial portion of the articular surface being more proximally extended than on the lateral side. Much of the distal trochlea is eroded and thus the degree of asymmetry cannot be assessed.

U.W. 88-123 RIGHT SECOND INTERMEDIATE PHALANX (MH2)

Preservation The bone is largely complete but the dorsal portion of the proximal half is still encased in sediment (to preserve the remaining morphology), and the dorsal portion of the distal half is missing. The trochlea is eroded on the distal and palmar surfaces. The bone is broken ML just distal to the base such that the distal 2/3 of the bone is shifted slightly proximally and palmarly, resting just on the edge the remaining proximal 1/3 of the bone. This orientation makes the bone appear slightly shorter than its true overall length (Figure 16).

Morphology This bone is considered a second intermediate phalanx (IP2) based on its relatively short estimated length compared to the remaining intermediate phalanges of the MH2 right hand (Figure 16; Table 5). Given the preservation and degree of preparation of U.W. 88-123, only the morphology the palmar surface can be described. Like the other intermediate

phalanges of the MH2 right hand (see below), the morphology of U.W. 88-123 is best described as a smaller version of a proximal phalanx. The palmar surface is mildly concave in both the PD and ML dimensions. There is a thick flexor sheath ridge along the lateral shaft and a thinner, shorter (though slightly obscured) ridge along the medial shaft. A median bar or lateral fossae are not present. The proximal palmar surface appears hollowed, with a concave area just distal to a thick ridge along the proximal border of the phalanx.

[INSERT Figure 16 and Table 5 about here]

U.W. 88-161 RIGHT THIRD INTERMEDIATE PHALANX (MH2)

Preservation The bone is complete and perfectly preserved, except for small surface fragments missing from the dorsal surface of the trochlea and the medial border of the proximal facet. There are thin fractures along the sagittal midline of the medial trochlea and running ML along the dorsal surface of the proximal shaft (Figure 16).

Morphology This bone is considered an IP3 based on its long length and large overall size relative to the other MH2 intermediate phalanges (Figure 16; Table 5). Its morphology is similar to that described above for U.W. 88-123, although this specimen is much better preserved. The dorsal surface is mildly convex longitudinally, with stronger convexity at the distal end, and in dorsal or palmar view, the sides of the shaft are straight. Both flexor sheath ridges are well-developed; the lateral ridge is larger than that of the medial side, extending 8.8mm distally from the base and extending approximately 2mm from the palmar surface. The medial flexor ridge is smaller, extending 4mm from the base and extending approximately 1mm from the palmar surface of the shaft. A palmar median bar and lateral fossae are not present.

The proximal end of the bone appears “scooped”, such that the palmar surface is ML concave and then slanted palmarly up to a thick proximal border (Figure 16). In sagittal view,

the dorsal border of the base flares dorsally in sagittal view. The proximal articular surface extends onto the palmar and dorsal flaring portions, creating a PD tall but still ML broad facet (Table 5). The condyles of the proximal facet are roughly equal in size and DP concave. The trochlea is more ML expanded than the distal shaft. The articular surface extends just to the distal edge of the dorsal surface. The medial trochlea appears slightly more distally and palmarly extended than the lateral trochlea, although this asymmetry may be accentuated by the eroded dorsal surface of the articular facet.

U.W. 88-122 RIGHT FOURTH INTERMEDIATE PHALANX (MH2)

Preservation This bone is complete and well-preserved except for a fragment missing from palmar surface of the proximal border of the base and a small surface fragment missing from the palmar surface of the trochlea (Figure 16).

Morphology This bone is considered to be from the fourth ray based on its large size and being only slightly smaller than U.W. 88-161 (Figure 16; Table 5). The preserved morphology of this bone is virtually identical to that of U.W. 88-161.The lateral flexor sheath ridge is slightly more pronounced, extending 8.4mm distally from the base and roughly 1.5mm from the palmar surface of the shaft. The medial flexor ridge extends 8mm distally from the base and is roughly the same height as the lateral ridge. The dorsal border of the base is dorsally flaring, but less so than that of U.W. 88-161. The condyles of the distal trochlea are symmetrical and the articular surface extends onto the dorsum 3.1mm.

U.W. 88-162 RIGHT FIFTH INTERMEDIATE PHALANX (MH2)

Preservation This bone is complete apart from a fragment missing from the palmar surface of the base, and small fragments from the dorsomedial surface and palmar-medial border of the trochlea (Figure 16).

Morphology This bone is identified as an IP5 because of its small size and morphology compared with the other MH2 intermediate phalanges (Figure 16; Table 5). Its morphology is similar to that described for the other intermediate phalanges. The flexor sheath ridges are not as pronounced; both are 4.4mm in PD length and extend only slightly above the palmar surface in sagittal view. In palmar view, the short ridges slope medially toward the midline, such that the palmar surface of the midshaft is only mildly concave. The dorsal surface of the proximal end flares less than that of U.W. 88-122 and U.W. 88-161.

U.W. 88-124 RIGHT POLLICAL DISTAL PHALANX

Preservation This bone is approximately half complete, preserving most of the PD length of the bone and its lateral side. Much of the medial half is missing as well as lateral corner of the proximal end (Figure 17).

Morphology This bone is identified as a distal pollical phalanx (DP1) based on the presence of well-developed proximal and distal fossae, a *M. flexor pollicis longus* (FPL) tendon attachment, and its ML broad apical tuft (Figure 17). The dorsal shaft is longitudinally straight with slight dorsal flaring at the proximal end. In palmar view, the proximal portion of the palmar surface is dominated by a deeply concave proximal fossa, measuring approximately 4.6mm in PD length. The distal border of this fossa is palmarly extended well above the remainder of the shaft, creating a ridge roughly 1.8mm PD for the attachment of the FPL tendon. The distal half of the bone is dominated by what appears to be a ML broad apical tuft that is DP thick (Table 5). Just proximal to the apical tuft is a concave distal fossa, measuring 3mm in PD length and roughly 3.4mm in ML breadth, for the palmar ungual pulp.

[INSERT Figure 17 about here]

COMPARATIVE MORPHOLOGY

SCAPHOID

The U.W. 88-158 scaphoid is smaller in absolute size than the *Australopthecus* sp. StW 618 and *H. habilis* OH 7 scaphoids, but slightly DP taller than that of *H. naledi*. The tubercle is much shorter and less robust than that of *Ar. ramidus* but longer and more robust than that of *H. naledi*. The U.W. 88-158 tubercle is most similar in morphology to that of StW 618, apart from the tubercle being more proximally-oriented and the base being slightly less robust (Figure 3). The relative size and shape of the radial facet is generally most similar to *Homo*; it is DP tall relative to the DP height of the scaphoid body and relative to the PD length of the facet (Figure 18). In contrast, *Ar. ramidus,* StW 618 and African apes tend to have relatively short radial facets, making them more round, rather than oval, in their overall shape. The lunate facet of U.W. 88-158 is confined to the proximodorsal corner of the scaphoid body, which is most similar to *H. naledi* and typical of humans and some Neandertals. This morphology is unlike the more distally-extended lunate facet of OH 7 and StW 618 (Figure 3).

The shape of the *Au. sediba* capitate facet falls out as intermediate among the comparative sample, being most similar to the median values of *P. troglodytes*, early *Homo* and recent humans, although there is substantial overlap across all taxa (Figure 18). StW 618 and *H. naledi* have a relatively long PD length of the capitate facet, whereas OH 7 is relatively short. The shallow concavity of the capitate facet in U.W. 88-158 is unlike the deeply concave, circular capitate facet of *Ar. ramidus* and StW 618, or the more rectangular-shaped facet of OH 7 (Figure 3). The distomedial edge of the capitate facet appears more “closed”, which is most similar to StW 618, OH 7 and *H. naledi*, rather than the “open” border of humans and Neandertals (Tocheri 2007).

Finally, the trapezium-trapezoid facet of U.W. 88-158 is highly convex in both the DP and ML dimensions, and appears “raised” off of the bone due to deep sulcus running parallel to its proximdorsal border (Figure 3). This morphology is similar to what is preserved in OH 7, and unlike the flatter facet of *Ar. ramidus* and StW 618. The trapezium facet also extends much further onto the tubercle than that of *Ar. ramidus* and StW 618, but is less extended than that of *H. naledi*, Neandertals and *H. sapiens*. The trapezoid facet is more extensive distomedially, reflecting the more “closed” border of the capitate facet, than that typically found in humans and Neandertals, and in this way appears most similar to OH 7 and *H. naledi.*

LUNATE

The MH2 lunate is remarkably ML narrow both in the overall size of the lunate body and its capitate facet (Figures 4 and 19). In this way, U.W. 88-159 is distinctly different from the spherical lunates of cf. *Australopithecus* KNM WT 22944-J (Ward et al. 1999) and *Au. afarensis* (Ward et al. 2012), and the generally broader lunates of African apes, humans and most other fossil hominins (Figure 19). The narrowness of the U.W. 88-159, although accentuated by the missing fragment from the palmar-medial portion of the lunate (Figure 4), is more reminiscent of Miocene apes like *Proconsul* (Schön and Ziemer 1973) and *Afropithecus* (Leakey et al. 1988). The lack of a separate articulation for the hamate in MH2 is shared with KNM WT 22944-J and *H. naledi*, and is common in African apes (Marzke et al. 1994), while a lunatohamate articulation is present in *Ar. ramidus*, *Au. afarensis* and most Neandertals and recent humans (Marzke et al. 1994).

The U.W. 88-159 radial facet is ML broad relative to its DP height and to the breadth of the lunate body (Figure 19). This morphology is similar to other extant and fossil hominins, and different from the relatively narrow radial facet of African apes. The scaphoid facet of U.W. 88-159 lunate is notably more distally-oriented than the typically laterally-facing scaphoid facets

(i.e. oriented at approximately 90° angle to the capitate facet) of African apes, *Ar. ramidus*, *Au. afarensis*, most Neandertals, and humans.

[INSERT Figures 18 & 19 about here]

TRIQUETRUM

The MH2 triquetrum presents a distinct morphology that is not seen in other known hominin triquetra. The U.W. 88-157 triquetrum body is relatively (i.e. divided by a geometric mean) PD narrow and ML broad compared with the more blocky triquetra typical of extant humans and African apes (Figure 20). In this way, the overall shape of U.W. 88-157 is similar to other fossil hominins, particularly *Ar. ramidus*, SKX 3498 and Neandertals. Its hamate facet is also DP tall relative to its ML breadth and in this way is more similar to Neandertals and *H. sapiens,* rather than the ML broader hamate facets of SKX 3498 and *H. naledi* (Figure 20). The concavoconvex complexity of the hamate facet is more accentuated than that of SKX 3498 (Kivell 2011), *H. naledi* and Neandertals, and is consistent with the opposing morphology of the triquetrum facet on the MH2 hamate (Figure 8).

U.W. 88-157 is distinct in having an almost tubercle-like palmar-medial extension to the triquetrum body that is not known in any other hominin (Figure 5). This extension orients the small pisiform facet in a proximopalmar direction. As such, this morphology suggests, especially when the ulna is in anatomical position (Figure 2), that the pisiform was small, unlike the rod-shaped pisiform of African apes and *Au. afarensis* (Bush et al. 1982). However, any correlation that might exist between the size of the pisiform and the size and shape of the pisiform's articular facet on the triquetrum is unknown.

CAPITATE

The MH2 capitates are larger in absolute size than *Au. afarensis* A.L. 288-1w but smaller than cf. *Australopithecus* KNM-WT 22944-H and *Au. afarensis* A.L. 333-40. The absolute length is similar to *Au. africanus* TM 1526 but the MH2 capitates are ML broader at both the proximal and distal ends. The MH2 capitate body is DP tall relative to its PD length and overall size (i.e. a geometric mean), compared with other australopiths and the particularly short capitates of *H. floresiensis* and *H. naledi* (Figure 21). Like other australopiths, *H. naledi* and *H. floresiensis*, the distodorsolateral border is not excavated to accommodate a Mc3 styloid process, which is found in the KNM-WT 51260 Mc3 possibly attributed to *H. erectus* (Ward et al. 2013) and later *Homo* (Lorenzo et al. 1999; Trinkaus 1983). The capitate body is "waisted" in palmar view to a similar degree as that found in *Ar. ramidus*, other australopiths and *H. naledi*, being less waisted than that of KNM-WT 22944-H and African apes but more so than is typical for recent humans (Figures 6 and 21). The proximal facet is ML expanded to the same degree as most other hominins and extant humans (Figure 21), but does not have the bulbous appearance of KNM-WT 22944-H, which is accentuated by its strong degree of waisting. The capitate body is deeply excavated between the distal portion of the scaphoid facet and the dorsal trapezoid facet, and unlike the continuous articulation found in humans (Figure 6). However, the scaphoid facet does not have a well-developed, concave J-hook morphology at its distal border, as is found in *Pan*, *Au. afarensis* and *H. floresiensis* (Orr et al. 2013).

The presence of both a dorsal and palmar trapezoid facet on the lateral side of the capitate (at least in the better preserved left capitate, U.W. 88-105) is similar to the condition described in *H. antecessor* (Lorenzo et al. 1999) and that is found in some Neandertals (e.g. Tabun 1) and rarely in humans (Lewis 1989; Tocheri 2007). KNM-WT 22944-H, *Au. afarensis* A.L. 333-40 and possibly *Ar. ramidus* demonstrate similar morphology, suggesting that a dual trapezoid articulation may be primitive for the hominin clade (although *Au. africanus* TM 1526 does not have a palmar capitate-trapezoid articulation).

The primarily lateral orientation of the Mc2 facet on the MH2 capitates is similar to African apes, *Ar. ramidus* (Lovejoy et al. 2009), *Au. anamensis* KNM-KP 31724 (Ward et al. 2001), *H. floresiensis* (Orr et al. 2013; Tocheri et al. 2007), and what has been inferred for OH 7 (Tocheri et al. 2003). It is less distally-orientated than A.L. 333-40, TM 1526 and *H. naledi* (Kivell et al. 2011, 2015). The generally flat morphology of the capitate's Mc3 articulation is similar to that of humans and Neandertals, and is less concavoconvex than African apes, *Ar. ramidus*, *Au. afarensis*, TM 1526, or what is preserved in KNM-WT 22944-H.

The U.W 88-95 right capitate differs from the left in missing a portion of the capitate body at the distodorsolateral border (Figure 6). Although taphonomic damage for this missing portion cannot be ruled out, the morphology of this region appears to be complete. This is the same region that is truncated in humans and Neandertals to accommodate the Mc3 styloid process, however the preserved morphology in U.W. 88-95 capitate is not similar. Instead, the dorsal surface of U.W. 88-95 appears non-articular rather than the dorsally-extended articular surface of the Mc3 facet that is typical of humans and Neandertals. Furthermore, the MH2 Mc3 U.W. 88-116 does not have a styloid process (Figure 11). If this morphology is not due to taphonomic damage, it is possible that a separate ossification centre between the capitate and Mc3 (O'Rahilly 1953) was present on the right side only. Either way, there was likely little difference in overall function of this carpometacarpal joint between the left and right hands.

[INSERT Figures 20 & 21 about here]

HAMATE

The hamate body of MH2 is DP taller relative to its PD length than that of *Au. afarensis* and Neandertals, falling within upper range of variation of *H. sapiens* and *Pan*. In this way, MH2 is most similar to cf. *Australopithecus* KNM-WT 22944-I and *Gorilla* (Figure 22). The hamulus

projects primarily palmarly and to a similar degree found in *H. naledi*, *H. sapiens* and *Gorilla*. Relative to hamate size (i.e. a geometric mean), it is more palmarly-projecting than that of *Au. afarensis* and KNM-WT 22944-1, but less so than Neandertals. However, distal projection of the MH2 hamulus is minimal like that of *H. sapiens*, while all other fossil hominins are more distally extended (Figure 22). Similarily, the PD long but ML narrow shape of the hamulus, creating an oval-shaped cross-section, is most similar to the human condition and unlike the ML broader hamuli of African apes, *Au. afarensis,* KNM-WT 22944-I, *H. naledi* and *H. floresiensis* (Orr et al. 2013; Figure 8).

Although the Mc4 facet is absolutely larger than the Mc5 facet in the MH2 hamates, a ratio of Mc5/Mc4 facet ML breadth reveals that MH2 has a relatively broader Mc5 facet than *Pan*, KNM-WT 22944-I and *Au. afarensis* (Figure 22). In this way, MH2 is most similar to condition found in *H. naledi* and Neandertals, but also overlaps with that of *Gorilla*. The MH2 hamatometacarpal articulation differs from *Ar. ramidus*, KNM-WT 22944-I and *Au. afarensis* in having a generally flat, rather than concave, Mc4 facet and an Mc5 facet that does not extend onto the hamulus. In this way, MH2 is more similar to *H. naledi* and later *Homo*. MH2 does not show a saddle-shaped Mc5 facet as in *H. naledi* or typically found in recent humans (Kivell et al. 2015; Marzke and Marzke 2000). There is a space between the palmar border of the Mc5 facet and the most dorsal edge of the hamulus (which is particularly marked on the left hamate with a more well-preserved hamulus) that could accommodate the extension of the pisometacarpal ligament to the Mc3, as is found in humans (Lewis 1977) and has been described in *Au. afarensis* (Marzke and Marzke 1987; Figure 7). In medial view, the proximal half of the triquetrum facet is inclined dorsally, such that proximal border of the hamate appears somewhat pointed (Figure 8). This differs from the rounded profile of the more proximally-oriented triquetrum facets of *Ar. ramidus*, KNM-WT 22944-I, *Au. afarensis, H. naledi* and that is typical of *H. sapiens*.

[INSERT Figure 22 about here]

FIRST METACARPAL

The MH2 first metacarpal is remarkably long in its PD length. Relative to the length of the Mc3, U.W. 88-119 falls outside the range of variation and well-above the regression lines for recent humans (including smaller-bodied individuals), with a much longer Mc1 for its size (Kivell et al. 2011) (Figure 23). The same pattern holds true for thumb length (i.e. including the PP1) relative to PD length of the third ray (Figure 23). The Mc1 and thumb of MH2 are longer relative to the Mc3 and third ray, respectively, than the estimated proportions of the *Au. afarensis* composite hand, Neandertals and early *H. sapiens*. The only fossil hominin (for which associated hand bones are known) to come close to the same relative Mc1 or thumb length as MH2 is *H. naledi*.

The Mc1 shaft is also remarkably gracile; relative to interarticular length, the midshaft ML breadth and DP height are smaller than all other fossil hominins and falling only within the lower range of variation in *Pan* (Figure 24). The poorly-developed muscle attachments along the shaft are similar to that of *Ar. ramidus* ARA-VP-6/500-15 and *Au. afarensis* A.L. 333-39w. The U.W. 88-119 enthesis morphology contrasts the more robust or flaring flanges for the *M. opponens pollicis* insertion found in *Ar. ramidus* ARA-VP 6/1638, *Au. africanus* StW 418, the *Au. robustus*/early *Homo* SKX 5020 and SK 84 specimens from Swartkans, *H. naledi* and Neandertals. Furthermore, the *M. opponens pollicis* insertion is proximally-positioned in U.W. 88-119, with no indication of attachment along the distal shaft. This is distinctly different from the distally-placed attachment in *Ar. ramidus, Au. afarensis, Au. africanus*, SK 84, SKX 5020 and *H. naledi*, which is similar to the positioning found in *Pan* (although the enthesis is not nearly as rugose in *Pan*), or the larger insertion of humans, which extends the entire PD length of the Mc1's lateral shaft (Jacofsky 2009). The first *M. dorsal interosseous* attachment is equally

poorly developed in U.W. 88-119, however this enthesis is also not well-defined in humans and most early fossil hominins (e.g. A.L. 333-39w, StW 418 or SKX 5020). Swartkrans specimen SK 84, with a rugose *M. first dorsal interosseous* insertion, is a notable exception. The positioning of the *M. first dorsal interosseous* enthesis in MH2 is similar to that of other hominins (e.g. StW 418, SK 84, SKX 5020) and humans, being distally extended and distinct from the localized proximo-medial insertion of *Pan* (Jacofsky 2009).

Relative to interarticular length, the base of U.W. 88-119 is more ML narrow than all other fossil hominins except *H. naledi* (Kivell et al. 2015) (Figure 24). However, the relative DP height of the base is taller than *Au*. *africanus* and most similar to SKX 5020, extant humans and *Pan*. The DP curvature of the trapezium facet appears similar to that of *Ar. ramidus, Au. africanus*, and SK 84, and is more curved than SKX 5020 or humans. The U.W. 88-119 proximal articulation also appears to be distinct from the strongly DP concave and "V-shaped" articulation described for *Au. prometheus* (Clarke 1999), although a formal description of the StW 573 Mc1 morphology has not been published. U.W. 88-119 does not have a beak-like extension of the palmar base as is found in *Au. afarensis* A.L. 333-58 (Bush et al. 1982).

U.W. 88-119 has a relatively ML narrower breadth of the Mc1 head than all other fossil hominins except *Au. afarensis*, falling closest to the mean values of African apes, although still within the lower range of variation found in recent humans (Figure 24). The DP height of the head is comparatively taller, being most similar to *Au. afarensis*, Neandertals and *H. sapiens*, although also falling within the upper range of variation in African apes (Figure 24). The prominent palmar beak that characterises the U.W. 88-119 Mc1 head is also present in SK 84 (Susman 1988b, 1989, 1994; Trinkaus and Long 1990). It has been suggested that the KNM-WT 15000 *H. erectus* juvenile Mc1s and SKX 5020 also have this beak (Walker and Leakey 1993; Susman 1988b, 1989), however all of these specimens are missing the majority of the

proximal epiphysis. A beak is not present in *Ar. ramidus*, *Au. afarensis* (A.L. 333w-39), *Au. africanus* (StW 418 and StW 583), *H. naledi* or Neandertals.

[INSERT Figures 23 & 24 about here]

SECOND METACARPAL

The MH2 Mc2 shaft is gracile compared with other fossil hominins and modern humans. Relative to interarticular length, the ML breadth at midshaft in U.W. 88-115 is much narrower than that of *Au. afarensis, Au. africanus,* and especially *H. naledi*, although it falls within the lower range of variation in Neandertals and *H. sapiens* (Figure 25). The proximal portion of the shaft is also absolutely more gracile than what is preserved in the OH 7 Mc2. The Mc2 has a particularly prominent *M. dorsal interossei* crest compared to the other MH2 metacarpals, in which two *Mm. dorsal interossei* attachments joint to form a single crest. This morphology is similar to *Pan* and is occasionally found in muscularly robust humans (Drapeau et al. 2005), but is not seen in other known australopiths (*Au. afarensis* or *Au. africanus*) or *H. naledi*.

Despite the gracility of the shaft, the base of U.W. 88-115 is robust relative to its interarticular length. It is ML broader than *Au. afarensis* and *Au. africanus*, and DP taller than *Au. afarensis*, being most similar to Neandertals and *H. sapiens* (Figure 25). The dorsal muscle attachments on the proximal epiphysis appear more well-developed than in *Au. afarensis, Au. africanus* and *H. naledi*. The trapezoid facet is more “squared” (i.e. ML broad) at its palmar portion than that of *Au. afarensis*. The orientation of the U.W. 88-115 trapezium facet (relative to the long axis of the shaft) in proximal view (35 degrees) is more palmarly oriented than that of *Au. africanus* StW 382, but more laterally oriented than that of *H. naledi*, and is most similar to *Au. afarensis*, recent humans and *Gorilla* (Drapeau et al. 2005). When viewed dorsally, the U.W. 88-115 trapezium facet is more proximally-oriented (28 degrees) than *Au. afarensis* but

less so than *H. naledi*, and falls out as intermediate between the more laterally-facing facet of African apes and more proximally-oriented facet of humans (Drapeau et al. 2005). The capitate and Mc3 articulation is similar to that of *Au. afarensis*, being intermediate between the African ape condition and the typically continuous and dorsopalmarly-convex capitate-Mc3 articulation of humans and *H. naledi.*

Relative to its interarticular length, the U.W. 88-115 head is as ML broad as that of all other fossil hominins and recent humans, but is DP taller than all other hominins, falling only within the upper range of variation of Neandertals (Figure 25). The Mc2 head is strongly asymmetrical, slightly more so than the *Au. afarensis* Mc2s from A.L. 333 but similar to the A.L. 438-1 specimens, *Au. africanus* and *H. naledi*.

THIRD METACARPAL

The Mc3 is the only bone that is preserved for both MH1 and MH2 (Figure 11). The Mc3 of MH1, U.W. 88-112, is juvenile, with an unfused epiphyseal head that is consistent with the stage of juvenile development (estimated to be 12-13 years old by human standards) found throughout the remainder of the MH1 skeleton (Berger et al. 2010). Fusion of the Mc3 head occurs at roughly 9-10 years of age in chimpanzee (Kerley 1966) and 14-17 years of age in humans (Scheuer and Black 2000). Although U.W. 88-112 is missing its proximal epiphysis, the total preserved length is similar to the complete adult Mc3, U.W. 88-116, of MH2 (Figure 11; Table 3). For comparative analyses, the complete length of the U.W. 88-112 (i.e., including a proximal epiphysis) was estimated to be 53mm (preserved length is 44.7mm). This estimate is based on the fact that the metacarpal proximal epiphysis is in the process of fusing with the diaphysis in 12-13 year-old human males and thus the overall length of the metacarpal shaft is generally adult-like (Greulich et al. 1971; Gilsanz and Ratib 2005). Although this is just an estimation, comparative analyses reveal sexual dimorphism between MH1 and MH2.

Qualitative comparisons between MH1 U.W. 88-112 and MH2 U.W. 88-116 Mc3s clearly show a substantial difference in shaft robusticity. Indeed, relative to (estimated) interarticular length, ML breadth at midshaft in MH2 is narrower than all other hominins, including *Au. afarensis*, *Au. africanus, H. naledi* and most Neandertals and is slightly narrower than *H. erectus* KNM-WT 51260. In contrast, MH1 is ML broader than *Au. afarensis*, KNM-WT 51260, and the average breadth of Neandertals and *H. sapiens*. However, both Mc3 specimens fall within the lower (MH2) and upper (MH1) ranges of variation of Neandertals and *H. sapiens* (Figure 26).

A styloid process is not present at the proximal end of either Mc3 specimen, which is similar to morphology found in other australopiths (Bush et al. 1982; Tocheri et al. 2008; Ward et al. 2012; *contra* Susman 1988b; Ricklan 1987), and unlike the possibly *H. erectus* specimen KNM-WT 51260 (Ward et al. 2013) and later *Homo* (Lorenzo et al. 1999; Trinkaus 2016). Comparison of the relative size of the Mc3 base shows that the MH1 and MH2 Mc3s share a similar ML breadth, which is intermediate between *Au. afarensis* and all other fossil hominins and most similar to the median values of *H. sapiens* (Figure 26). The DP height of the base is relatively larger in MH1 compared with MH2, but both specimens are taller than *Au. afarensis*, *H. naledi* and *H. erectus*. The smooth and mildly convex capitate articular surface in both specimens is unlike the more concavoconvex topography of the *Au. afarensis* A.L. 333 specimens or SKX 3646 from Swartkrans. The MH1 and MH2 Mc3s differ in their Mc4 articular morphology, such that MH1 is missing a palmar Mc4 facet that is present in MH2. This articular variation is common within the hominin fossil record; *Au. afarensis* A.L. 438-1d and A.L. 333-122, Swartkrans SKX 3646 and *H. naledi* U.W. 101-1319 have a dorsal Mc4 facet only, while both dorsal and palmar facets are found in *Ar. ramidus* ARA-VP-6/500-6, *Au. afarensis* A.L. 333-16 and A.L. 333w-6, and *Au. africanus* StW 64 and StW 68.

MH2 also demonstrates a remarkably tall DP height of the Mc3 head, being taller than all other fossil hominins and falling only within the upper range of variation in *H. sapiens* and *Gorilla* (Figure 26).

[INSERT Figures 25 & 26 about here]

FOURTH METACARPAL

Like the other MH2 metacarpals, the U.W. 88-117 Mc4 shaft is gracile (Figure 12). However, relative to its interarticular length, the Mc4 is comparatively more robust in most dimensions than the MH2 Mc2 and Mc3 (Figure 27). Relative ML breadth at midshaft is similar to (rather than narrower than, as in the Mc2 and Mc3) all other fossil hominins and modern humans, apart from *H. naledi* and, especially, SKX 2954 from Swartkrans. The prominent *Mm. dorsal interossei* crest on the dorsal shaft of U.W. 88-117 is more developed than that of *Au. afarensis*, SKX 2954 and later hominins. The dorsal "bend" in the Mc4 shaft is similar to that seen in StW 330 and not as accentuated as that of SKX 2954.

Relative to interarticular length, the U.W. 88-117 base is as ML broad as Neandertals and *H. sapiens* and broader than all other fossil hominins (Figure 27). The base is relatively taller than all other fossil hominins in DP height, falling only within the extreme upper range of variation in recent humans. The mildly convex morphology of the hamate articulation is similar to SKX 2954, *H. naledi* and *H. sapiens* and unlike the more concavoconvex morphology of *Au. afarensis, Au. africanus* StW 65, and *Pan*. The U.W. 88-117 head is remarkably ML broad and DP tall, particularly in contrast to its relatively narrow shaft (Figure 12). For example, in absolute dimensions, U.W. 88-117 is almost identical in head size (10mm in ML breadth, 10.9mm in DP height) to that of SK 85 (10.2mm and 10.8mm, respectively) and SKX 2954 (10.1mm and 10.5mm, respectively) despite having a much more gracile shaft (5.2mm in ML breadth, 6.6mm

in DP height, compared with 7.3mm and 7.8mm, respectively, in SK 85 and 6mm and 8.1mm, respectively, in SKX 2954). Relative to interarticular length, the MH2 Mc4 head is broader (and DP taller) than all other fossil hominins apart from *H. naledi* and falling only within the extreme upper range of variation of recent humans (Figure 27).

FIFTH METACARPAL

The U.W. 88-118 Mc5 is the most robust metacarpal for its length compared with the other MH2 metacarpals. Compared with other hominins, the U.W. 88-118 ML midshaft breadth is similar to that of Neandertals and *H. sapiens*, broader than *Au. afarensis* and *Ar. ramidus*, but narrower than *Au. africanus* StW 63 and SK(W)14147 from Swartkrans (Figure 28). The *M. opponens digiti minimi* enthesis along the medial side of U.W. 88-118 is more well-developed and proximally-extended than that of *Au. africanus* StW 63, but it is less developed than that of *Au. afarensis*, SK(W) 14147, and *H. naledi* (Figure 13).

The MH2 Mc5 base is ML broader than that of all other hominins, including Neandertals and early *H. sapiens*, and is most similar to *Au. africanus* and SK(W) 14147 (Figure 28). The DP height of the U.W. 88-118 base is also taller than all other hominins except SK(W) 14147 and falls only within the upper range of variation in recent humans. This robusticity is largely due to an extremely well-developed medial protuberance for the *M. extensor carpi ulnaris* dorsally and the pisohamate ligament palmarly, which is most similar to *Au. africanus* StW 63, and more protruding than that of *Ar. ramidus*, *Au. afarensis,* SK(W) 14147 and *H. naledi*. The strongly convex, palmarly-extended and asymmetrical hamate facet is most similar to articular morphology found in SK(W) 14147. In *Ar. ramidus* and *Au. afarensis* the hamate articular surface also extends onto the palmar Mc5 surface, but the palmar border of the facet is more symmetrical. The hamate facet of U.W. 88-118 is unlike the saddle-shaped articulation found in *H. naledi*, Neandertals and *H. sapiens*.

Relative to interarticular length, U.W. 88-118 head is DP taller than all other hominins, falling outside even the upper range of variation in recent humans (Figure 28). The ML head breadth is also relatively broad, being similar to that of Neandertals and *H. sapiens* and broader than all other hominins except SK(W) 14147. The distal articular outline of U.W. 88-118 head in palmar view is most similar to SK(W) 14147, being more asymmetrical than *Au. afarensis*, but less so than that of *Au. africanus* StW 63, *H. naledi* and other later *Homo*.

[INSERT Figures 27 & 28 about here]

POLLICAL PROXIMAL PHALANX

The MH2 proximal pollical phalanx (PP1) appears more gracile, curved and asymmetrical compared with many other fossil hominins (Figure 14). Relative to total PP1 length, the ML breadth at midshaft in both MH2 PP1s is narrower than that of all other fossil hominins, apart from *Ar. ramidus*, and is almost identical to that of *Au. afarensis* A.L. 333-69 (although it differs substantially from the more robust, but incomplete, A.L. 438-4) (Figure 29). The dorsal surface of the MH2 PP1s is mildly PD convex, especially at the distal end, like that of *Ar. ramidus*, *Au. afarensis*, *Au. africanus* StW 575, and is more curved than that of *H. naledi* and other *Homo* specimens. In sagittal view, the palmar surface is strongly PD concave due to a dramatic narrowing in the DP height of the shaft just proximal to the trochlea; this narrowing and curvature is more accentuated than that of all other known fossil hominin PP1s. The “hollowed” appearance of the palmar shaft surface differs from slightly convex surface in *Au. afarensis* and *H. naledi* and strongly convex surface of *Au. africanus*.

Despite a gracile shaft, the relative ML breadth of the MH2 PP1 base is similar to all other hominins, apart from *Ar. ramidus*, which is narrower, and Neandertals, which are much broader (**Figure 29**). In relative DP basal height, U.W. 88-91 is also taller than all other fossil

hominins, apart from Neandertals, although all early hominins fall within range of recent human and *Pan* variation. The basal asymmetry of the MH2 PP1s is much more pronounced than that of *Ar. ramidus, Au. afarensis* and *Au. africanus,* both in the development of the tubercles and, especially, the proximal extension of the metacarpal facet (Figure 14). Relative to total PP1 length, ML breadth and DP height of the MH2 PP1 trochlea are smaller than all other fossil hominins, being most similar to *Au. afarensis* (Figure 29).

Comparison of the intrinsic proportions within the thumb shows that, relative to the length of the Mc1, MH2 has a short PP1 that is most similar to Neandertals, particularly the Shanidar 4 specimen (Table 6). The MH2 PP1 is shorter than the estimate for *Au. afarensis* (A.L. 333-69 and A.L. 333w-39; Marzke 1983), *H. naledi*, and *H. sapiens.*

[INSERT Figure 29 & Table 6 about here]

NON-POLLICAL PROXIMAL PHALANGES

Overall, the MH2 non-pollical proximal phalanges show moderate PD curvature of the dorsal surface, and are relatively gracile and short in absolute length compared with most other hominins (**Figure 30**). Although there is substantial overlap in the degree of curvature across the comparative sample, *Au. sediba* curvature is less than the median value of *Ar. ramidus*, *Au. afarensis, H. naledi* and OH 7, but greater than that of *Au. africanus* and hominins from Swartkrans (Figure 30). Phalangeal curvature in *Au. prometheus* is also reportedly “strong” (Clarke 2013:116) and similar to *Au. afarensis* (Clarke 1999:479), but measurements of the curvature have not yet been published. Relative to metacarpal length, the MH2 proximal phalanges are of similar length to those of modern humans: the PP3 is 71.7% of the Mc3 interarticular length and the PP4 is 75.5% the Mc4 total length, compared with mean values of 71.5% and 74.7% in recent humans, respectively (Table 6). In comparison, *Ar. ramdius* (ray 4

only), *H. naledi* and *H. sapiens* specimen Qafzeh 9 have relatively longer proximal phalanges than MH2, while African apes and the *Au. afarensis* composite hand have relatively shorter proximal phalanges.

Relative to PP total length, the MH2 bases fall out as intermediate in ML breadth (and DP height), being most similar to *Au. africanus*, the PPs from Swartkrans, *H. naledi*, *H. floresiensis*, *H. sapiens* and *Gorilla*. In contrast, *Ar. ramidus* and *Au. afarensis* have ML narrow PP bases for their length, while OH 86 (Domínguez-Rodrigo et al. 2015), ATE9-2 (Lorenzo et al. 2015) and Neandertals are relatively broader (Figure 31). In relative ML breadth at midshaft, the MH2 proximal phalanges, again, fall out as intermediate, being most similar to *H. naledi*, the Swartkrans specimens, and ATE9-2, and relatively broader than *Ar. ramidus*, *Au. afarensis* and recent *H. sapiens*, but narrower than *Au. africanus*, OH 86 and Neandertals (Figure 31). However, the palmar surfaces of the MH2 PP2-PP4 shafts are concave both ML and PD, making them appear gracile compared to the ML flat or mildly convex palmar surfaces of the *Ar. ramidus* (e.g. ARA-VP-6/500-30 and -69), *Au. afarensis* (e.g. A.L. 1044-1, A.L. 444-4), *Au. africanus* (e.g. StW 28 and - 293), the Swartkrans specimens (e.g. SKX 5018 and -15468), *H. habilis* (OH 7) and *H. naledi*, and the strongly convex palmar surface of the *H. floresiensis* proximal phalanges (Larson et al. 2009). The concave palmar surface morphology of the MH2 proximal phalanges makes the flexor sheath ridges particularly prominent (especially on the PP4) relative to most *Au. afarensis*, *Au. africanus*, Swartkrans, *H. naledi* and *H. floresiensis* specimens. The MH2 PP5 (U.W. 88-121) morphology differs from that of the other proximal phalanges, in having a ML flatter palmar surface that is more similar to other fossil hominins, and a well-developed convex “bar” extending from the medial basal tubercle (Figure 15). This morphology is not seen in other potential PP5s from *Au. afarensis* (A.L. 333-62) and OH 86 (Domínguez-Rodrigo et al. 2015), or *H. naledi*.

The relative ML breadth and DP height of the MH2 PP trochlea are generally similar to all other fossil hominins and recent humans, apart from *Ar. ramidus* and *Au. afarensis*, which are relatively smaller in both dimensions, and Neandertals, which are relatively bigger (Figure 31).

[INSERT Figures 30 & 31 about here]

INTERMEDIATE PHALANGES

Overall, the morphology of the MH2 intermediate phalanges is unique among hominins; the palmar surface is generally concave, both ML and PD, and the flexor sheath ridges are well-developed, with no indication of median bar and lateral fossae (Figure 16). In this way, MH2 looks superficially most similar to the Miocene hominoid *Sivapithecus* (Madar et al. 2002) rather than other hominins. Although Marzke et al. (2007) demonstrated a high degree of variability in primate intermediate phalanx morphology and *M. flexor digitorum superficialis* tendon attachment, all of the fossil hominin middle phalanges recovered to date demonstrate a palmar median bar and lateral fossae that is typical of human intermediate phalanges, including *Ar. kadabba*, *Ar. ramidus, Au. afarensis, Au. africanus*, Swartkrans specimens, *H. habilis*, *H. erectus*, *H. naledi*, *H. floresiensis*, and other later *Homo* (e.g. Bush et al. 1982; Larson et al. 2009; Lorenzo et al. 1999; Susman and Creel 1979; Walker and Leakey 1993). The concave palmar morphology and tall flexor ridges of the MH2 intermediate phalanges – described by Marzke et al. (2007) as a “palmar median fossa” – was found in only two humans and one adult chimpanzee in their hominoid sample. The FDS tendons attach primarily to the lateral margins of the middle phalanx (i.e., not to the lateral fossa, *contra* Susman and Creel 1979; Susman and Stern 1979). Furthermore, in palmar or dorsal view, the sides of the MH2 intermediate phalanx shafts are relatively straight, which is more similar to typical proximal phalanx morphology.

Instead, in all other known hominin specimens the shaft sides taper distally, such that the distal shaft is ML narrower than the proximal shaft in *Ar. ramidus, Au. afarensis, Au. africanus*, Swartkrans specimens, *H. naledi* and *H. floresiensis* (Larson et al. 2009). The MH2 intermediate phalanges are distinctly different from the bottle-shaped shaft (Susman and Creel 1979: 391) of the OH 7 *H. habilis* intermediate phalanges.

Quantitatively, the relative length of IP3 to Mc3 is similar to that of *H. sapiens*, as well as *H. naledi*, while the *Au. afarensis* composite hand and Neandertals have a relatively shorter IP3 (Table 6). Relative to total length of the IP, the MH2 IP bases fall out as intermediate in their ML breadth, being most similar to *H. naledi*, *H. sapiens* and *Gorilla* (Figure 32). *Ar. ramidus, Au. afarensis, Au. africanus*, and *H. floresiensis* have relatively ML narrower bases, while most specimens from Swartkrans and Neandertals are relatively broader. The MH2 IP relative ML breadth at midshaft is most similar to *Au. afarensis, Au. africanus*, and *H. sapiens*, while all other hominins, apart from *Ar. ramidus*, are broader. Comparative analysis of the distal trochlea reveals limited variation in trochlea DP height across all hominins (only *Ar. ramidus* and *H. floresiensis* are relatively short), while the MH2 IPs have relatively ML broad trochlea compared with earlier hominins, being most similar to the Swartkrans specimens, *H. naledi* and *H. sapiens* (Figure 32).

DISTAL POLLICAL PHALANX

Although the MH2 distal pollical phalanx is not complete, enough of the lateral proportion and its total length are preserved to confidently estimate its overall size and to identify key morphological features that can be compared with other hominins (Figure 17). Relative to the total estimated DP1 length, U.W. 88-124 has a ML expanded apical tuft that is most similar to *Au. africanus* StW 294 and Swartkrans specimen SKX 5016 (Figure 33). The MH2 DP1 apical tuft is more ML expanded than that of *Ar. ramidus, Au. afarensis*, Neandertals and *H. sapiens*,

but less expanded than *Au. robustus* TM 1517k, *H. habilis* OH 7 and *H. naledi*. This is generally consistent with the qualitative comparisons in which the relative ML narrow but DP tall shaft of U.W. 88-124 is more similar to morphology to StW 294 than the ML broader and DP flatter DP1 morphology typical of OH 7, TM 1517k and *H. naledi* (although SKX 5016 would fall into the latter category as well). MH2, however, differs from StW 294, as well as TM 1517k, OH 7 and SKX 5016, in having both a well-developed proximal and distal (ungual) fossae and a more well-developed gable for the FPL tendon attachment on its palmar surface. MH2 shares a similar palmar morphology with that described in *Orrorin tugenensis*, although the apical tuft is less ML expanded in the latter (Almecija et al. 2010).

[INSERT Figures 32 & 33 about here]

DISCUSSION AND CONCLUSION

The rare occurrence of semi-articulated hand skeleton in association with a relatively complete skeleton affords a unique opportunity to investigate potential hand function within an australopith individual. The MH2 hand presents morphological features that are similar to both earlier and later hominins, as well as some features that are distinct to *Au. sediba* (Table 7). Together, the combination of features found in the MH2 hand skeleton is not found in any other known hominin. Below, we describe some of the potential functional implications of the MH2 hand, divided by anatomical region.

The thumb and lateral carpometacarpal articulations

Although the trapezium and trapezoid are not yet known for *Au. sediba*, some functional inferences can be drawn from the lateral carpometacarpal articulations and thumb morphology.

The mosaic morphology of the MH2 scaphoid, capitate and Mc1-Mc3 suggest a unique pattern of load transmission through the thumb, lateral wrist and palm compared with that of other fossil hominins and humans. Features that are shared typically with *Pan*, *Ar. ramidus,* and the preserved elements of early australopiths (*Australopithecus* sp.*, Au. anamensis*, *Au. afarensis* and/or *Au. africanus*), as well as *H. floresiensis,* include a relatively large trapezoid facet on the scaphoid (associated with a "closed" distal border of the scaphoid's capitate facet), a small trapezium-Mc1 articulation, a gracile Mc1 shaft, absence of a large, palmarly-positioned trapezoid-capitate articulation, a Mc2-capitate articulation that is more laterally facing, and the absence of a Mc3 styloid process (Bush et al. 1982; Kibii et al. 2011; Lovejoy et al. 2009; Marzke 1983; Marzke et al. 1992; McHenry 1983; Tocheri 2007; Tocheri et al. 2007, 2008; Ward et al. 1999, 2001, 2012). The *Au. sediba* MH2 hand shares all of these morphological features with other early fossil hominins (and *H. floresiensis*) that together suggest relatively small force production by the thumb and limited ability to pronate the Mc2, both of which are considered important for forceful precision gripping in humans (Marzke 1983, 1997; Marzke et al. 1992, 1998; Marzke and Marzke 2000; Tocheri 2007; Tocheri et al. 2008). In fact, the MH2 Mc1 shaft is the most gracile shaft for its length of all known fossil hominins (Figure 24), strongly supporting an interpretation of limited force production by the thumb.

The MH2 hand, however, also shows morphological features that indicate a mosaic evolution of the lateral carpometacarpal region and suggest that function of this region was somewhat different from that of other australopiths. Although MH2 has a dorsal capitate-trapezoid articulation as in African apes, it also has a small palmar trapezoid facet like that of some other early and later hominins, including cf. *Australopithecus* sp. KNM-WT 22944-H, *Au. afarensis* A.L. 333-40*, H. antecessor* (Lorenzo et al. 1999) and possibly *Ar. ramidus*. This morphology is intermediate between the single dorsally-positioned facet of *Pan* and some australopiths (*Au. africanus* TM 1526, *Au. afarensis* A.L. 288-1w) and the single, expanded

palmar capitate-trapezoid articulation typical of recent humans and Neandertals (Lewis 1989; Tocheri 2007). Furthermore, MH2 lacks a J-hook scaphoid facet on the capitate that is found in *Pan*, *Au. afarensis*, and *H. floresiensis* (Orr et al. 2013) and the trapezium facet extends further onto the scaphoid tubercle than in *Australopithecus* sp. StW 618, OH 7 and *H. floresiensis* (Kibii et al. 2011; Tocheri et al. 2007). The MH2 Mc1 shaft is uniquely gracile (Figure 24) and the entheses are poorly developed (but see below). MH2 is similar to most other hominins in the weak expression of the *M. first dorsal interosseous* enthesis (SK 84, *H. naledi*, and Neandertals being notable exceptions) that is distally-extended, which provides a longer moment arm for adduction of the thumb than that of African apes (Jacofsky 2009; Tocheri et al. 2008). However, the MH2 *M. opponens pollicis* (OP) insertion is distinct in being proximally-positioned and poorly developed. The MH2 insertion differs from the distally-positioned OP enthesis of *Pan*, *Ar. ramdius*, other australopiths and *H. naledi*, and from the more extended enthesis of humans that runs the entire length of the Mc1 lateral shaft (Jacofsky 2009). Jacofsky (2009:128) noted that the proximal portion of the human OP insertion had a larger abduction moment arm when the thumb was extended, while the distal OP insertion had a larger abduction moment arm when the thumb was flexed. This may suggest subtle differences in OP muscle efficiency and thumb function in MH2 relative to other fossil hominins. It is important to note, however, that no consistent relationship has been found between OP enthesis morphology and several aspects of the muscle size and architecture in human cadaveric specimens (Williams-Hatala et al. 2016), and that several recent studies have highlighted the complexity of inferring muscle size, function and even presence/absence from enthesis morphology (Eliot and Jungers 2000; Marzke et al. 2007; Rabey et al. 2015; Zumwalt 2006; but see Karakostis et al. 2017).

The MH2 Mc1 also has a prominent intersesamoid beak on the palmar surface of the head that is not preserved in any other known hominin Mc1 specimens (*contra* Susman 1988a, b), apart from SK 84 from Swartkrans (Napier 1959; Trinkaus and Long 1990). If the

prominence of the beak is correlated with an increased size of the medial and lateral sesamoids, then the morphology of the MH2 (and SK 84) Mc1 may suggest well-developed pullies for the *Mm. adductor pollicis oblique* and *flexor pollicis brevis* and thus enhanced adduction and flexion of the thumb (Marzke et al. 1999).

Finally, and perhaps most notably, the MH2 thumb, and particularly the Mc1, is exceptionally long relative to the length of the fingers, being relatively longer than that of recent humans (i.e. outside the range of variation in our sample) and all known fossil hominins (Figure 23; Kivell et al. 2011). Intrinsic hand proportions are strongly linked with precision grip capability (Feix et al. 2015; Lui et al. 2016) and, indeed, the relatively long thumb in humans has long been considered key to pad-to-pad precision abilities (e.g Marzke 1997; Napier 1960, 1962b; Susman 1998). Thus, despite the gracility of the MH2 PP1 and, particularly, the Mc1, such a relatively long thumb would have facilitated precision opposition of the thumb to the fingers. Indeed, kinematic modelling as shown that if range of motion at the MH2 trapezium-Mc1 joint is assumed to be more limited, like chimpanzees, or more mobile, like humans, the manipulative "workspace" between the thumb and index finger is similar to or greater than that of recent humans (Feix et al. 2015).

Together, the morphology found in MH2 suggests at least some repositioning of the trapezoid-trapezium within the lateral carpometacarpal complex (which was also likely occurring in earlier hominins as well; Tocheri et al. 2008), perhaps with some degree of palmar expansion of the trapezoid (compared with the wedge-shaped trapezoid of African apes and *H. floresiensis*), and an enhanced ability to perform precision grips between the thumb and fingers. However, the small trapezium-Mc1 joint, extremely gracile Mc1 (and PP1) shafts, and absence of a Mc3 styloid process, strongly suggest that the manipulative capabilities of MH2 had limited force production. The full expression of the lateral carpometacarpal features in humans and Neandertals, and to a large extent in *H. naledi* (Kivell et al. 2015) results in a more proximodistal

alignment of the joint surfaces, that is thought to facilitate better transmission of high transverse loads from the thumb during manipulative activities (Marzke et al. 2010; Tocheri 2007). The combination of morphological features in MH2 lateral carpometarcarpal region suggest that *Au. sediba* was clearly not capable of forceful precision manipulation to the same degree as humans, Neandertals, and potentially *H. naledi*, but that its precision abilities were enhanced relative to African apes, *H. floresiensis*, and what is currently known from most other australopiths.

Radiocarpal and midcarpal joints

Associated wrist bones are rare in the early fossil hominin record (Clarke 1999; Lovejoy et al. 2009). As such, MH2 provides the first opportunity to investigate wrist function in an australopith. The MH2 scaphoid incorporates a fused os centrale, as in humans, African apes (Kivell and Begun 2007) and all other known fossil hominins (e.g. Kibii et al. 2011; Kivell et al. 2015; Lovejoy et al. 2009; Napier 1962a) (Figure 3). Similarly, MH2 has a relatively larger radial facet on the lunate than that of the scaphoid, which is similar to the pattern found in humans, Neandertals, *H. naledi* and the unassociated carpal and radial remains of other australopiths (Heinrich et al. 1993; Johanson et al. 1982; Kibii et al. 2011; Ward et al. 2001, 2012). This morphology in MH2 is consistent with the radiocarpal articulation of the associated MH2 distal radius (Churchill et al. 2013; this volume). The opposite relationship is typical of African apes, in which they have a relatively larger scaphoid-radial articulation (Heinrich et al. 1993; Ward et al. 1999, 2012). The radiocarpal articular pattern in humans and fossil hominins is thought to reflect loading along a more central axis of the wrist rather than then the more radial loading of African apes (Ward et al. 2012).

However, in MH2 this central-axis loading does not appear to translate through to the midcarpal joint in same way as other australopiths or *Ar. ramidus* given its ML narrow lunate

body, remarkably small (in both ML and DP dimensions) lunate-capitate articulation, and more distally-oriented scapholunate articulation. The narrow lunate morphology in MH2 differs from the ML broad lunates of *Ar. ramidus*, KNM-WT 22944-J, *Au. afarensis* and *H. erectus* (Lovejoy et al. 2009; Ward et al. 1999, 2012; Weidenrich 1941). Although the distinction between the lunate and scaphoid articular surfaces of the capitate is not well-defined, rearticulation of the midcarpal joint (**Figure 2**; see also Fig. 5 in Kivell et al. 2011) suggests that the articulation for the lunate was relatively small compared with that of the scaphoid. This differs from the larger capitate facets of *Ar. ramdius*, *Au. afarensis*, and *H. naledi* lunates (Figure 19), as well as the articular morphology of the ML broad capitate heads of other australopiths (KNM-WT 22944-H, A.L. 333-40, TM 1526) in which the lunate facet is relatively larger than that of the scaphoid, while the opposite relationship is typical of African apes (Jenkins and Fleagle 1975; Corruccini 1978). Furthermore, the more distally-oriented scaphoid facet positions the scaphoid in a more distomedially-rotated position relative to the lunate, which is distinct from the more laterally-facing scapholunate articulation found in *Ar. ramidus* and *Au. afarensis*. This scapholunate articulation in MH2 is consistent with a more medially-facing radiocarpal articulation of the MH2 distal radius relative to the human condition (Churchill et al. this volume). Altogether, the scaphoid-lunate-capitate morphology in MH2 might allow for a greater range of abduction at the radiocarpal joint and suggests less central-axis loading of the radiocarpal and midcarpal joints than that of other australopiths.

Within the medial aspect of the MH2 carpus, MH2 has a DP tall and strongly concavoconvex articulation between the triquetrum and hamate (Figures 5 and 8), which differs from the less complex articular morphology seen in SKX 3498, *H. naledi* and Neandertals. Furthermore, the proximal half of the hamate's triquetrum facet is inclined dorsally, which differs from the more proximally-oriented triquetrum facets of *Ar. ramidus*, KNM-WT 22944-I, *Au. afarensis, H. naledi* and that is typical of *H. sapiens*. As such, the MH2 triquetrum would rotate

dorsally onto the hamate during extension and/or adduction of the midcarpal joint, suggesting enhanced stability in the medial midcarpal joint in extended and/or adducted wrist postures relative to other hominins.

Flexor apparatus

The tubercles of the scaphoid and trapezium laterally, and the pisiform and hamate hamulus medially form the "walls" of the carpal tunnel. In African apes, all of these morphological features are palmarly extended (e.g. large tubercles, rod-shaped pisiform) to create a deep carpal tunnel that accommodates well-developed flexor tendons, while the opposite condition is typical of humans (Corruccini 1978; Kivell 2016; Lewis 1989; Niewoehner 2006; Sarmiento 1988; Tuttle 1969). In the MH2 hand, although the trapezium is not preserved, the size of the scaphoid tubercle is smaller and less palmarly-oriented than that of *Ar. ramidus*, StW 618 and some Neandertals, but larger than *H. naledi* and *H. sapiens* (Kivell et al. 2011; Trinkaus 1983) (Figure 3; Table 2). The MH2 triquetrum is unusual in having a tubercle-like mediopalmar projection that is not found in any of known fossil hominin triquetra, although there are few preserved (i.e. *Ar*. *ramidus*, SKX 3498, *H. naledi* and Neandertals). This projection orients the small pisiform facet proximopalmarly. When the MH2 carpus is articulated with the associated ulna, there is minimal space between the ulnar styloid process and the triquetum, suggesting the pisiform was smaller than the rod-shaped pisiform of *Au. afarensis* (Bush et al. 1982) and African apes. Finally, the hamate hamulus projects strongly palmarly, but its distal projection and oval-shaped cross-section is most similar to the human and Neandertal condition (Figure 22) (although KNM-WT 22994-H also has an oval-shaped cross-section; Orr et al. 2013). Its greater palmar projection may enhance the capacity of the *M. flexor carpi ulnaris* to act as a flexor and increase the moment arm of the *Mm. opponens digiti minimi* and *flexor digiti minimi* (Niewoehner 2006; Ward et al. 1999), although more research is needed to understand the

relationship, if any, between hamulus shape and extrinsic and intrinsic flexor muscle morphology (Orr et al. 2013). Together, the preserved morphology of the MH2 carpus suggests a moderately developed carpal tunnel, intermediate between the deep carpal tunnels of *Ar. ramidus*, *Au. afarensis*, and Neandertals, the shallow morphology of *H. naledi* and *H. sapiens*.

That being said, there appear to be potential trade-offs in the bony morphology of the carpal tunnel among hominins that, without a complete and associated carpus, make functional interpretations difficult. For example, *Ar. ramidus* has large, projecting tubercles on the scaphoid, trapezium and hamate (Lovejoy et al. 2009); unassociated specimens of *Au. afarensis* show a rod-shaped pisiform but a less palmarly-projecting hamulus relative to hamate size (the A.L. 333-80 trapezium does not preserve its tubercle); the *H. naledi* Hand 1 has a relatively small scaphoid tubercle and hamate hamulus, but a large, projecting tubercle on the trapezium; while most Neandertals generally have large, projecting tubercles on scaphoid, trapezium and hamate, but a pea-shaped pisiform (McCown and Keith 1939; Trinkaus 1982, 1983; but see Kivell et al. 2018). Thus it is unclear how the different combinations of morphology across the four bones of the carpal tunnel might translate into potential functional differences, if any, of the flexor apparatus at the hominin wrist joint.

The proximal and, unusually, the intermediate phalanges of the MH2 hand have well-developed flexor sheath ridges, indicating strong flexion of all of the fingers, and particularly the fourth and fifth digits. The proximal and intermediate phalanges are also moderately curved, suggesting some degree of arboreality was still a functionally important part of the MH2 locomotor repertoire (Jungers et al. 1995b; Kivell et al. 2015; Nguyen et al. 2014; Richmond 1998). However, although there is a large degree of overlap in the degree of phalangeal curvature across extant and fossil taxa, the MH2 phalanges are less curved than those *Au. afarensis* and *Ar. kadaba*, suggesting less dependence on arboreality than in earlier hominins. Furthermore, the proximal phalanges are absolutely short and, relative to the length of the palm,

similar in length to modern humans and Neandertals (Kebara 2) (and actually shorter than early *H. sapiens* Qafzeh 9). Finally, although the distinct flexor sheath ridges of the MH2 intermediate phalanges suggests enhanced flexion at the interphalangeal joints, it is the DP thickening of the shaft created by a palmar median bar that likely reflects high dorsopalmarly-directed bending stress of the phalanges (Begun et al. 1994; Marzke et al. 2007). The absence of the median bar in MH2 suggests lower loading/bending stress during grasping (either during locomotor or manipulative behaviours) than in other hominins. The MH2 morphology is particularly distinct from the robust phalanges –both proximal and, especially, intermediate— of the OH 7 *H. habilis* hand (Napier 1962a) and the strongly curved phalanges of *H. naledi* (Kivell et al. 2015). Together, the few associated fossil hominin hand skeletons reveal varied mosaics of morphologies that suggest potentially different selective pressures on finger morphology, or different morphological solutions to similar selective pressures, across australopiths and *Homo*.

The medial metacarpus

Like the Mc1, the MH2 medial metacarpal shafts appear remarkably gracile (Figures 10-13). Indeed, relative to their lengths, the medial metacarpal midshaft breadths are ML narrow compared to other australopiths and *H. naledi* (Figs. 25-28). However, the MH2 relative midshaft breadths fall close to the median values or within the range of variation found in Neandertals and *H. sapiens*. Furthermore, the proximal bases and distal heads of the medial metacarpals are among the largest in our comparative sample; for example, the relative DP height of the Mc2-Mc5 heads are taller than all other hominins, apart from *H. naledi*, and fall only within the extreme upper range of variation found in recent humans. The dorsal surface of the MH2 medial metacarpal shafts also have prominent attachments for the *Mm. dorsal interossei*. These entheses may be accentuated due to the relatively gracile shafts and/or indicate powerful abduction of the fingers.

The MH2 Mc2 and Mc3 are comparatively more gracile than its Mc4 and Mc5 and the overall morphology of both metacarpals is generally similar to other australopiths (Figures 25-28). The strongly asymmetrical Mc2 head would facilitate opposition of the index finger to the thumb as in other australopiths (Drapeau et al. 2005; Marzke 1983). The more laterally-facing Mc2-capitate articulation than that of humans suggests that MH2 may have had more limited pronation of the second digit, which is considered particularly important for cupping the palm during precision grasping in humans (Marzke 1997). The same functional interpretation has been made for the relatively laterally-facing Mc2 facet typical of Neandertals (Niewoehner 2006; Niewoehner et al. 1997). The Mc3 lacks a styloid process as in all other australopiths and *H. naledi* (Bush et al. 1982; Drapeau et al. 2005; Kivell et al. 2015; Marzke and Marzke 2000) and the capitometacarpal articulation is ML broad like that of other South African hominins (*Au. africanus* and SKX 3646 from Swartkrans) and humans (Rein and Harvati 2013). The generally flat morphology of the Mc3-capitate articulation is similar to that of humans and Neandertals, and distinct from the more concavoconvex morphology of African apes, *Ar. ramidus*, A.L. 333-40, TM 1526, and what is preserved in KNM-WT 22944-H, which is interpreted as reducing sliding and rotation at the capitometacarpal joint (Lovejoy et al. 2009; Marzke and Marzke 1987; Selby et al. 2016). Altogether, the MH2 morphology suggests greater mobility at the capitometacarpal articulation than the concavoconvex joints of earlier hominins, but also greater mobility than what is found in humans and Neandertals (and possibly *H. erectus*; Ward et al. 2013), in which their joints are further stabilized via the styloid process (Marzke and Marzke 1987, 2000).

The MH2 Mc5 is particularly robust (Figure 28). The ML broad and DP tall Mc5 base suggests well-developed extrinsic and intrinsic musculature to the fifth digit, including the *Mm. extensor carpi ulnaris* and *flexor carpi ulnaris*, via the pisohamate ligament, while the rugose enthesis along the medial shaft may suggests a well-developed *M. opponens digiti minimi*. This

morphology is consistent with the robust insertion for the *M. flexor carpi ulnaris* on the proximal ulna (Churchill et al. 2013, this volume). The Mc5-hamate articulation is DP convex and extends onto the palmar surface of the shaft, while the corresponding facet of the hamate is constrained to the hamate body (i.e. does not extend onto the hamulus) and is distomedially oriented. This morphology differs from the proximally-oriented and saddle-shaped Mc5 hamate facet that is typical of humans and Neandertals (Marzke and Marzke 2000) and *H. naledi* (Kivell et al. 2015). The articular morphology of MH2 suggests that the Mc5 was positioned in a slightly more flexed and abducted position on the hamate than is typical of humans and Neandertals. This is consistent with the limited distal- but strong palmar projection of the hamulus found in the MH2 hamate. Altogether, this morphology in combination with an asymmetric Mc5 head, suggests substantial mobility at the hamatometacarpal joint with strong flexion of the wrist and strong flexion and opposition of the fifth digit, but without the Mc5 rotation that is possible with a saddle-shaped hamatometacarpal articulation.

Comparison between MH1 and MH2 third metacarpals

Although the MH1 juvenile individual preserves only an incomplete Mc3, its association with a relatively complete skeleton that can be identified as presumably male provides a rare opportunity to investigate variation in hand morphology between sexes in early hominins. The MH1 Mc3 is missing its distal epiphysis but its absolute length is just slightly shorter than the fully adult Mc3 of MH2. Given the estimated age of MH1, the adult length of the Mc3 can be reasonably estimated and is approximately 8% longer than that of the MH2 Mc3. For comparison, there are only two complete Mc3s each known for the following hominin taxa, although, unlike *Au. sediba*, none is associated with other skeletal remains from which sex can be confidently estimated: *Au. afarensis*, in which A.L. 438-1d (64.8mm) is 7.1% longer than A.L. 333-16 (60.2mm), *Au. africanus*, in which the total length of StW 64 (55.8mm) is 2.9% longer

than StW 68 (54.2mm), and *H. naledi*, in which U.W. 101-1319 (49mm) is approximately 6% longer than U.W. 101-1651+1628 (estimated at 46mm). Within our human samples, the total (and interarticular) length of male Mc3s are, on average, 3.6% longer than females, and within small-bodied humans, male Mc3s are, on average, 7.5% longer than females. Thus, the sexual dimorphism in Mc3 length between MH1 and MH2 is consistent with that of small-bodied recent humans and potentially other fossil hominins.

The MH1 Mc3 shaft is notably more robust than that of MH2 (Figures 11 and 26). Relative to length, the MH1 Mc3 midshaft breadth is among the broadest in our comparative sample, being similar to *Au. africanus* and *H. naledi*, while the MH2 Mc3 is among the narrowest, but similar to the absolutely long KNM-WT 51260. However, importantly, both Mc3 specimens fall within the range of variation documented in Neandertals and *H. sapiens*. Therefore, although the two *Au. sediba* Mc3 specimens appear remarkably different in their robusticity, their variation comfortably fits within the sexual dimorphism documented in other fossil hominins and recent humans and does not necessarily reflect differences in function or hand use. This morphological variability between sexes is important to consider when drawing functional or taxonomic interpretations from isolated specimens (Trinkaus and Long 1990).

ACKNOWLEDGEMENTS

For this study, we are grateful to the institutions and curators that have provided access to specimens in their care, including: F. Mayer and S. Jancke (Berlin Natural History Museum), C. Boesch (Max Planck Institute for Evolutionary Anthropology), M. Teschler-Nicola and R. Muehl (Vienna Natural History Museum), E. Gilissen, M. Louette and W. Wendelin (Royal Museum for Central Africa), J. Moggi Cecchi and S. Bortoluzzi (University of Florence), M. Harman (Powell-Cotton Museum), L. Gordon and D. Hunt (Smithsonian Institution), Y. Haile-Selassie and L. Jellema (Cleveland Museum of Natural History), P. Reed (University of Toronto), J. Eger and S.

Woodward (Royal Ontario Museum), B. Zipfel (University of the Witwatersrand), S. Potze and L. Kgasi (Ditsong National Museum of Natural History), A. Kweka and A. Gidna (National Museum of Tanzania), B. Kimbel, T. White, B. Asfaw, G. Suwa and G. Shimelies (National Museum of Ethiopia), Y. Rak and I. Hershkovitz (Tel Aviv University). We thank Nick Stephens for sharing comparative data of Barma Grande 2 and Arene Candide 2 and Matt Tocheri for sharing surface models for several Neandertal and early *H. sapiens* carpal bones. We are grateful to Andrew Deane for his comparative analysis of phalangeal curvature. This research was funded by Natural Science and Engineering Research Council of Canada (TLK), General Motors Women and Mathematics and Sciences Award (TLK), Max Planck Society (TLK) and the European Research Council Starting Grant 336301 (TLK). For the Malapa project in general, we thank the South African Heritage Resources Agency for the permits to work at the Malapa site; the Nash family for granting access to the Malapa site and continued support of research on the Malapa and John Nash nature reserves; the South African National Centre of Excellence in PalaeoSciences, the Lyda Hill Foundation, South African Department of Science and Technology, the South African National Research Foundation, the Evolutionary Studies Institute, University of the Witwatersrand, the University of the Witwatersrand's Vice Chancellor's Discretionary Fund, the National Geographic Society, the Palaeontological Scientific Trust, the Andrew W. Mellon Foundation, the Ford Foundation, the U.S. Diplomatic Mission to South Africa, the French embassy of South Africa, the Oppenheimer and Ackerman families, and Sir Richard Branson for funding; the University of the Witwatersrand's Schools of Geosciences and Anatomical Sciences and the Bernard Price Institute for Palaeontology for support and facilities; the Gauteng Government, Gauteng Department of Agriculture, Conservation and Environment and the Cradle of Humankind Management Authority; the University of Zurich 2010 Field School. Numerous individuals have been involved in the ongoing preparation and excavation of these fossils, including C. Dube, C. Kemp, M. Kgasi, M.

Languza, J. Malaza, G. Mokoma, P. Mukanela, T. Nemvhundi, M. Ngcamphalala, S. Jirah, S. Tshabalala, and C. Yates. Other individuals who have given significant support to this project include B. de Klerk, W. Lawrence, C. Steininger, B. Kuhn, L. Pollarolo, J. Kretzen, D. Conforti, C. Dlamini, H. Visser, B. Nkosi, B. Louw, L. Backwell, F. Thackeray, and M. Peltier. Finally, we thank Scott Williams and Jeremy DeSilva for co-editing this special issue and Jeremy DeSilva and two anonymous reviewers for helpful comments that have greatly improved this manuscript.

REFERENCES

Alba, D.M., Moyà-Solà, S., Köhler, M., 2003. Morphological affinities of the *Australopithecus afarensis* hand on the basis of manual proportions and relative thumb length. *Journal of Human Evolution* 44, 225-254.

Almécija, S., Moyà-Solà, S., Alba, D., 2010. Early origin for human-like precision grasping: A comparative study of pollical distal phalanges in fossil hominins. *PLoS ONE* 5, e11727.

Berger, L.R., de Ruiter, D.J., Churchill, S.E., Schmid, P., Carlson, K.J., Dirks, P.H.G.M., Kibii, J.M., 2010. *Australopithecus sediba*: a new species of *Homo*-like australopith from South Africa. *Science* 328, 195-204.

Begun, D.R., 1993. New catarrhine phalanges from Rudabánya (northeastern Hungary) and the problem of parallelism and convergence in hominoid postcranial morphology. *Journal of Human Evolution* 24, 373-402.

Begun, D.R., Kivell T.L., 2011. Knuckle-walking in *Sivapithecus*? The combined effects of homology and homoplasy with possible implications for pongine dispersals. *Journal of Human Evolution* 60, 158-170.

Bush, M.E., Lovejoy, C.O., Johanson, D.C., Coppens, Y., 1982. Hominid carpal, metacarpal, and phalangeal bones recovered from the Hadar Formation: 1974-1977 collections. *American Journal of Physical Anthropology* 57, 651-677.

Clarke, R.J., 1999. Discovery of complete arm and hand of the 3.3 million-year-old *Australopithecus* skeleton from Sterkfontein. *South African Journal of Science* 95, 477-480.

Clarke, R.J. 2008. Latest information on Sterkfontein's *Australopithecus* skeleton and a new look at *Australopithecus*. *South African Journal of Science* 104, 443-449.

Clarke, R.J. 2013. *Australopithecus* from Sterkfontein Caves, South Africa. In: Reed, K.E., Fleagle, J.G., Leakey, R.E. (Eds.) *The Paleobiology of* Australopithecus. Springer, Dordrecht, pp.105-123.

Churchill, S.E., D.J. Green, E.M. Feuerriegel, M.E. Macias, S. Mathews, K.J. Carlson, P. Schmid and L.R. Berger., (this volume) The shoulder, arm, and forearm of Malapa Hominins 1 and 2. *PaleoAnthropology*

Churchill, S.E., Holliday, T.W., Carlson, K.J., Jashashvili, T., Macias, M.E., Matthews, S., Sparling, T.L., Schmid, P., de Ruiter, D.J., Berger, L.R., 2013. The upper limb of *Australopithecus sediba*. *Science* 340,1233477-1-5.

Corruccini, R.S., 1978. Comparative osteometrics of the hominoid wrist joint, with special reference to knuckle-walking. *Journal of Human Evolution* 7, 307-321.

Deane, A.S., Kremer, E.P., Begun, D.R. 2005. A new approach to quantifying anatomical curvatures using high resolution polynomial curve fitting (HR-PCF). *American Journal of Physical Anthropology* 128, 630-638.

Deane, A.S., Begun, D.R., 2008. Broken fingers: retesting locomotor hypotheses for fossil hominoids using fragmentary proximal phalanges and high-resolution polynomial curve fitting (HR-PCF). *Journal of Human Evolution* 55, 691-701.

DeSilva, J.M., Sylvester, A.D., Churchill, S.E., Harcourt-Smith, W.E.H., Carlson, K.J., Walker, C., McNutt, E.J., Claxton, A., Zipfel, B., Berger, L.R., (this volume) The anatomy of the lower limb skeleton of *Australopithecus sediba*. *PaleoAnthropology*

Dirks, P.H.G.M., Kibii, J.M., Kuhn, B.F., Steininger, C., Churchill, S.E., Kramers, J.D., Pickering, R., Farber, D.L., Mériaux, A.-S., Herries, A.I.R., King, G.C.P., Berger, L.R., 2010. *Science* 328, 205-208.

Domínguez-Rodrigo, M., Pickering, T. R., Almécija, S., Heaton, J. L., Baquedano, E., Mabulla, A., Uribelarrea, D., 2015. Earliest modern human-like hand bone from a new >1.84-million-year-old site at Olduvai in Tanzania. *Nature Communications* 6, 7987.

Drapeau, M.S.M., Ward, C.V., Kimbel, W.H., Johanson, D.C., Rak, Y., 2005. Associated cranial and forelimb remains attributed to *Australopithecus afarensis* from Hadar, Ethiopia. *Journal of Human Evolution* 48, 593-642.

Eliot, D. J., Jungers, W. L., 2000. Fifth metatarsal morphology does not predict presence or absence of fibularis tertius muscle in hominids. *Journal of Human Evolution* 38, 333–342.

Feix, T., Kivell, T.L., Pouydebat, E., Dollar, A.M., 2015. Estimating thumb-index finger precision grip and manipulation potential in extant and fossil primates. *Journal of the Royal Society Interface* 12, 20150176.

Gilsanz, V., Ratib, O., 2005. *Hand Bone Age: A Digital Atlas of Skeletal Maturity*. Springer-Verlag, Berlin.

Gommery, D., Senut, B., 2006. La phalange distale du pouce d'*Orrorin tugenensis* (Miocène supérieur du Kenya). *Geobios* 39, 372-384.

Green, D.J., Gordon, A.D., 2008. Metacarpal proportions in *Australopithecus africanus*. *Journal of Human Evolution* 54, 705-719.

Greulich, W.W., Pyle, S.I., Waterhouse, A.M., 1971. *A Radiographic Standard of Reference for the Growing Hand and Wrist*. Case Western Reserve University, Chicago.

Hammer, Ř., Harper, D.A.T., Ryan, P.D., 2001. PAST: Paleontological statistics software package for education and data analysis. *Palaeontologia Electronica* 4, 1-9.

Heim, J.L., 1982. *Les hommes fossils de La Ferrassie II*. Archives de l'Institut de Paléontologie Humaine 38, 1-272.

Heinrich, R.E., Rose, M.D., Leakey, R.E., Walker, A.C., 1993. Hominid radius from the Middle Pleistocene of Lake Turkana, Kenya. *American Journal of Physical Anthropology* 92, 139-148.

Jacofsky, M.C., 2009. *Comparative muscle moment arms of the primate thumb:* Homo*,* Pan*,* Pongo*, and* Papio. Ph.D. Thesis, Arizona State University, Tempe, AZ.

Jenkins, F.A., Jr., Fleagle, J.G., 1975. Knuckle-walking and the functional anatomy of the wrists in living apes. In: Tuttle, R.H. (Ed.) *Primate Functional Morphology and Evolution*. Mouton, The Hague, pp. 213-231.

Johanson, D.C., Lovejoy, C.O., Kimbel, W.H., White, T.D., Ward, S.C., Bush, M.E., Latimer, B.M., Coppens, Y., 1982. Morphology of the Pliocene partial hominid skeleton (A.L. 288-1) from Hadar Formation, Ethiopia. *American Journal of Physical Anthropology* 57, 403-451.

Jungers, W.L., Falsetti, A.B., Wall, C.E., 1995a. Shape, relative size and size-adjustments in morphometrics. *Yearbook of Physical Anthropology* 38, 137–161.

Jungers, W.L., Godfrey, L.R., Simons, E.L., Chatrath, P.S., 1995b. Phalangeal curvature and positional behaviour in extinct sloth lemurs (Primates, Palaeopropithecidae). *Proceedings of the National Academy of Sciences USA* 94, 11998-1001.

Karakostis, F.A., Hotz, G., Scherf, H., Wahl, J., Harvati K., 2017. Occupational manual activity is reflected on the patterns among hand entheses. *American Journal of Physical Anthropology* 164,30-40.

Kerley, E.R., 1966. Skeletal age changes in the chimpanzee. *Tulane Studies in Zoology*, Tulane University, New Orleans, pp. 71-82.

Kibii, J.M., Clarke, R.J., Tocheri, M.W., 2011. A hominin scaphoid from Sterkfontein, Member 4: Morphological description and first comparative phenetic 3D analyses. *Journal of Human Evolution* 61, 510-517.

Kimura, T., 1976. Correction to the metacarpale I of the Amud man: a new description especially on the insertion area of the M. opponens pollicis. *Journal of the Anthropological Society of Nippon* 84, 48-54.

Kivell, T.L., 2007. *Ontogeny of the hominoid midcarpal joint and implications for the origin of hominin bipedalism*. Ph.D. Thesis, University of Toronto, Toronto, ON.

Kivell, T.L., 2011. A comparative analysis of the hominin triquetrum (SKX 3498) from Swartkrans, South Africa. *South African Journal of Science* 107, 1-10.

Kivell, T.L., Begun, D.R., 2007. Frequency and timing of scaphoid-centrale fusion in hominoids. *Journal of Human Evolution* 52, 321-340.

Kivell, T.L., Begun, D.R., 2009. New primate carpal bone from Rudabánya (late Miocene, Hungary): taxonomic and functional implications. *Journal of Human Evolution*. 57, 697-709.

Kivell, T.L., Barros, A.P., Smaers, J.B., 2013a. Different evolutionary pathways underlie the morphology of the wrist bones in hominoids. *BMC Evolutionary Biology* 13, 229.

Kivell, T.L., Guimont, I., Wall, C.E., 2103b. Sex-related shape dimorphism in the human radiocarpal and midcarpal joints. *Anatomical Record* 296, 19-30.

Kivell, T.L., Kibii, J.M., Churchill, S.E., Schmid, P., Berger, L.R., 2011. *Australopithecus sediba* hand demonstrates mosaic evolution of locomotor and manipulative abilities. *Science* 333, 1411-1417.

Kivell, T.L., Deane, A.S., Tocheri, M.W., Orr, C.M., Schmid, P., Hawks, J., Berger, L.R., Churchill, S.E., 2015. The hand of *Homo naledi*. *Nature Communications* 6, 8431.

Kivell, T.L., Rosas, A., Estalrrich, A., Huguet, R., García-Tabernero, A., Ríos, L., de la Rasilla, M. 2018. New Neandertal wrist bones from El Sidrón, Spain (1994-2009). *Journal of Human Evolution* 11, 45-75.

L'Abbé, E.N., Symes, S.A., Pokines, J.T., Cabo, L.L., Stull, K.E., Kuo, S., Raymond, D.E., Randolph-Quinney, P.S., Berger, L.R. 2015. Evidence of fatal skeletal injuries on Malapa Hominins 1 and 2. *Scientific Reports* 5, 15120.

Larson, S.G., Jungers, W.L., Tocheri, M.W., Orr, C.M., Morwood, M.J., Sutikna, T., Rokhus Due Awe, Djubiantono, T., 2009. Descriptions of the upper limb skeleton of *Homo floresiensis*. *Journal of Human Evolution* 57, 555-570.

Leakey, R.E., Leakey, M.G., Walker, A.C., 1988. Morphology of *Afropithecus turkanensis* from Kenya. *American Journal of Physical Anthropology* 76, 289-307.

Lemelin, P., Schmitt, D., 2016. On primitiveness, prehensility, and opposability of the primate hand: the contributions of Frederic Wood Jones and John Russell Napier. In: Kivell, T.L., Lemelin, P., Richmond, B.G., Schmitt, D. (Eds.), *The Evolution of the Primate Hand: Anatomical, Developmental, Functional and Paleontological Evidence*. Springer, New York, pp. 5-13.

Lewis, O.J., 1977. Joint remodelling and the evolution of the human hand. *Journal of Anatomy* 123, 157-201.

Lewis, O. J., 1989. *Functional Morphology of the Evolving Hand and Foot*. Clarendon Press, Oxford.

Liu, M.-J., Xiong, C.-H., Hu, D. 2016. Assessing the manipulative potentials of monkeys, apes and humans from hand proportions: implications for hand evolution. *Proceedings of the Royal Society B* 283, 20161923.

Lordkipanidze, D., Jashashvili, T., Vekua, A., de León, M.S.P., Zollikofer, C.P.E., Rightmire, G. P., Pontzer, H., Ferring, R., Oms, O., Tappen, M., Bukhsianidze, M., Agusti, J., Kahlke, R., Kiladze, G., Martinez-Navarro, B., Mouskhelishvili, A., Nioradze, M., Rook, L., 2007. Postcranial evidence from early *Homo* from Dmanisi, Georgia. *Nature* 449, 305-310.

Lorenzo, C., Arsuaga, J.L.. Carretero, J.M., 1999. Hand and foot remains from the Gran Dolina Early Pleistocene site (Sierra de Atapuerca, Spain). *Journal of Human Evolution* 37, 501-522.

Lorenzo, C., Pablos, A., Carretero, J.M., Huguet, R., Valverdú, J., Martinón-Torres, M., Arsuaga, J.L., Carbonell, E., Bermúdez de Castro, J.M., 2015. Early Pleistocene human hand phalanx from the Sima del Elefante (TE) cave site in Sierra de Atapuerca (Spain). *Journal of Human Evolution* 78, 114-121.

Lovejoy, C.O., Simpson, S.W., White, T.D., Asfaw, B., Suwa, G., 2009. Careful climbing in the Miocene: the forelimbs of *Ardipithecus ramidus* and humans are primitive. *Science* 326, 70e1-70e8.

Madar, S.I., Rose, M.D., Kelley, J., MacLatchy, L., Pilbeam, D., 2002. New *Sivapithecus* postcranial specimens from the Siwaliks of Pakistan. *Journal of Human Evolution* 42, 705-752.

Marzke, M.W., 1983. Joint functions and grips of the *Australopithecus afarensis* hand, with special reference to the region of the capitate. *Journal of Human Evolution* 12, 197-211.

Marzke, M.W., 1997. Precision grips, hand morphology, and tools. *American Journal of Physical Anthropology* 102, 91-110.

Marzke, M.W., Marzke, R.F., 1987. The third metacarpal styloid process in humans: origin and function. *American Journal of Physical Anthropology* 73, 415-431.

Marzke, M.W., Marzke, R.F., 2000. Evolution of the human hand: approaches to acquiring, analysing and interpreting the anatomical evidence. *Journal of Anatomy* 197, 121-140.

Marzke, M.W., Marzke, R.F., Linscheid, R.L., Smutz, P., Steinberg, B., Reece, S., An, K. N., 1999. Chimpanzee thumb muscle cross sections, moment arms and potential torques, and comparisons with humans. *American Journal of Physical Anthropology* 110, 163-178.

Marzke, M.W., Shrewsbury, M.M., Horner, K.E., 2007. Middle phalanx skeletal morphology in the hand: can it predict flexor tendon size and attachments? *American Journal of Physical Anthropology* 134, 141–151.

Marzke, M.W., Toth, N., Schick, K., Reece, S., Steinberg, B., Hunt, K., Linscheid, R.L., An, K. N., 1998. EMG study of hand muscle recruitment during hard hammer percussion manufacture of Oldowan tools. *American Journal of Physical Anthropology* 105, 315-332.

Marzke, M.W., Wullstein, K.L., Viegas, S.F., 1992. Evolution of the power ("squeeze") grip and its morphological correlates in hominids. *American Journal of Physical Anthropology*. 89, 283-298.

Marzke, M.W., Wullstein, K.L., Viegas, S.F., 1994. Variability at the carpometacarpal and midcarpal joints involving the fourth metacarpal, hamate and lunate in Catarrhini. *American Journal of Physical Anthropology* 93, 229-240.

Marzke, M.W., Tocheri, M.W., Steinberg, B., Femiani, J.D., Reece, S.P., Linscheid, R.L., Orr, C.M., Marzke, R.F., 2010. Comparative 3D quantitative analyses of trapeziometacarpal joint surface curvatures among living catarrhines and fossil hominins. *American Journal of Physical Anthropology* 141. 38-51.

McCown, T.D., Keith, A., 1939. *The Stone Age of Mt. Carmel Vol.II: The Fossil Remains from the Levalloiso-Mousterian*. Clarendon Press, Oxford.

McHenry, H.M., 1983. The capitate of *Australopithecus afarensis* and *A. africanus*. *American Journal of Physical Anthropology* 62, 187-198.

Mersey, B., Jabbour, R.S., Brudvik, K., Defleur, A., 2013. Neanderthal hand and foot remains from Moula-Guercy, Ardèche, France. *American Journal of Physical Anthropology* 152, 516-529.

Mosimann, J.E., 1970. Size allometry: size and shape variables with characterizations of the log- normal and gamma distributions. *Journal of the American Statistical Association* 56, 930-945.

Napier, J.R., 1962a. Fossil hand bones from Olduvai Gorge. *Nature* 196, 409-411.

Napier, J.R., 1962b. The evolution of the human hand. *Scientific American* 207, 56-62.

Napier, J.R., 1993. *Hands*. Revised by R.H. Tuttle. Princeton University Press, Princeton.

Niewoehner, W.A., 2006. Neandertal hands in their proper perspective. In: Harvati, K., Harrison, T. (Eds.), *Neanderthals Revisited: New Approaches and Perspectives*. Springer, Netherlands, pp. 157-190.

Niewoehner, W.A.,Weaver, A.H., Trinkaus, E., 1997.Neandertal capitate-metacarpal articular morphology. *American Journal of Physical Anthropology* 103, 219‐223.

O'Rahilly, R., 1953. A survey of carpal and tarsal anomalies. *Journal of Bone and Joint Surgery* 35, 626-642.

Orr, C.M., Tocheri, M.W., Burnett, S.E., Awe, R.D., Saptomo, E.W., Sutikna, T., Jatmiko, Wasisto, S., Morwood, M.J., Jungers, W.L., 2013. New wrist bones of *Homo floresiensis* from Liang Bua (Flores, Indonesia). *Journal of Human Evolution* 64, 109-129.

Pickering, R., Dirks, P.H.G.M., Jinnah, Z., de Ruiter, D.J., Churchill, S.E., Herries, A.I.R., Woodhead, J.D., Hellstrom, J.C., Berger, L.R., 2011. *Science* 333, 1421-1423.

Rabey, K.N., Green, D.J., Taylor, A.B., Begun, D.R., Richmond, B.G., McFarlin, S.C., 2015. Locomotor activity influences muscle architecture and bone growth but not muscle attachment site morphology. *Journal of Human Evolution* 78, 91–102.

Rein, T.R., Harvati, K., 2012. Exploring third metacarpal capitate facet shape in early hominins. *Anatomical Record* 296, 240-249.

Ricklan, D.E., 1987. Functional anatomy of the hand of *Australopithecus africanus*. *Journal of Human Evolution* 16, 643-664.

Ricklan, D.E., 1990. The precision grip in *Australopithecus africanus*: anatomical and behavioural correlates. In: Tobias, P.V., Sperber, G.H. (Eds), *From Apes to Angels: Essays in Anthropology in Honor of Phillip V. Tobias*. Wiley-Liss, New York, pp. 171-183.

Scheuer, L., Black, S., 2000. *Developmental Juvenile Osteology*. Academic Press, San Diego.

Schön, M.A., Ziemer, L.K., 1973. Wrist mechanism and locomotor behavior of *Dryopithecus* (*Proconsul*) *africanus*. *Folia Primatologica* 20, 1-11.

Selby, M.S., Simpson, S.W., Lovejoy C.O., 2016. The functional anatomy of the carpometacarpal complex in anthropoids and its implications for the evolution of the hominoid hand. *Anatomical Record* 299, 583-600.

Senut, B., Pickford, M., Gommery, D., Mein, P., Cheboi, K., Coppens, Y., 2001. First hominid from the Miocene (Lukeino formation, Kenya). *Comptes rendus de l'Académie des Sciences Paris* 332, 137-144.

Sládek, V., Trinkaus, E., Hillson, S.W., Holliday, T.W., 2000. *The People of the Pavlovian: Skeletal Catalogue and Osteometrics of the Gravettian Fossil Hominids from Dolní Věstonice and Pavlov, Dolní Věstonice Studies 5*. Archeologicky ústav AV ČR, Brno.

Strouhal, E., 1992. Anthropological and archaeological identification of an ancient Egyptian royal family (5th dynasty). *International Journal of Anthropology* 7, 43-63.

Stern, J.T., Jr., Jungers, W.L., Susman, R.L., 1995. Quantifying phalangeal curvature: an empirical comparison of alternative methods. *American Journal of Physical Anthropology* 97, 1-10.

Susman, R.L., 1988a. Hand of *Paranthropus robustus* from Member 1, Swartkrans: Fossil evidence for tool behaviour. *Science* 240, 781-784.

Susman, R.L., 1988b. New postcranial remains from Swartkrans and their bearing on the functional morphology and behavior of *Paranthropus robustus*. In: Grine, F.E. (Ed), *Evolutionary History of the "Robust" Australopithecines*. Aldine de Gruyter, New York, pp. 149-172.

Susman, R.L., 1989. New hominid fossils from the Swartkrans Formation (1979-1986 excavations): postcranial specimens. *American Journal of Physical Anthropology* 79, 451-474.

Susman, R.L., 1994. Fossil evidence for early hominid tool use. *Science* 265, 1570-1573.

Susman, R.L., 1998. Hand function and tool behaviour in early homininds. *Journal of Human Evolution*. 53, 23-46.

Susman, R.L., Creel, N., 1979. Functional and morphological affinities of the subadult hand (OH 7) from Olduvai Gorge. *American Journal of Physical Anthropology* 51, 311-331.

Susman, R.L., Stern Jr, J.T., 1979. Telemetered electromyography of flexor digitorum profundus and flexor digitorum superficialis in *Pan troglodytes* and implications for interpretation of the OH 7 hand. *American Journal of Physical Anthropology* 50, 565-574.

Taleisnik, J., 1976. The ligaments of the wrist. *Journal of Hand Surgery* 1, 110-118.

Tocheri, M.W., 2007. *Three-dimensional riddles of the radial wrist: derived carpal and carpometacarpal joint morphology in the genus Homo and the implications for understanding the evolution of stone tool-related behaviours in hominins*. Ph.D. Thesis, Arizona State University, Tempe, AZ.

Tocheri, M.W., Marzke, M.W., Liu, D., Bae, M., Jones, G.P., Williams, R.C., Razdan, A., 2003. Functional capabilities of modern and fossil hominid hands: three-dimensional analysis of trapezia. *American Journal of Physical Anthropology* 122, 101-112.

Tocheri, M. W., Orr, C. M., Larson, S. G., Sutikna, T., Saptomo, E. W., Due, R. A., Jungers, W. L., 2007. The primitive wrist of *Homo floresiensis* and its implications for hominin evolution. *Science* 317, 1743-1745.

Tocheri, M. W., Orr, C. M., Jacofsky, M. C., Marzke, M. W., 2008. The evolutionary history of the hominin hand since the last common ancestor of *Pan* and *Homo*. *Journal of Anatomy* 212, 544-562.

Trinkaus, E., 1982. The Shanidar 3 Neandertal. *American Journal of Physical Anthropology* 57, 37-60.

Trinkaus, E., 1983. *The Shanidar Neandertals*. Academic Press, New York.

Trinkaus, E., 2016. The evolution of the hand in Pleistocene *Homo*. In: Kivell, T.L., Lemelin, P., Richmond, B.G., Schmitt, D. (Eds.), *The Evolution of the Primate Hand: Anatomical, Developmental, Functional and Paleontological Evidence*. Springer, New York, pp. 545-571.

Trinkaus, E., Long, J.C., 1990. Species attribution of the Swartkrans Member 1 first metacarpals: SK 84 and SKX 5020. *American Journal of Physical Anthropology* 83, 419-424.

Trinkaus, E., Svoboda, J.A., Wojtal, P., Nývltová Fišákova, M., Wilczynski, J., 2010. Human remains from the Moravian Gravettian: morphology and taphonomy of additional elements from Dolní Věstonice II and Pavlov I. *International Journal of Osteoarchaeology* 20, 645-669.

Walker, A., Leakey, R.E. (Eds.)., 1993. *The Nariokotome* Homo erectus *skeleton*. Harvard University Press, Cambridge.

Ward, C.V., Leakey, M.G., Brown, B., Brown, F., Harris, J., Walker, A., 1999. South Turkwel: a new Pliocene hominid site in Kenya. *Journal of Human Evolution*. 36, 69-95.

Ward, C.V., Leakey, M.G., Walker, A., 2001. Morphology of *Australopithecus anamensis* from Kanapoi and Allia Bay, Kenya. *Journal of Human Evolution* 41, 255-368.

Ward, C.V., Kimbel, W.H., Harmon, E.H., Johanson, D.C., 2012. New postcranial fossils of *Australopithecus afarensis* from Hadar, Ethiopia (1990-2007). *Journal of Human Evolution* 63, 1-51.

Ward, C.V., Tocheri, M.W., Plavcan, J.M., Brown, F.H., Manthi, F.K., 2013. Early Pleistocene third metacarpal from Kenya and the evolution of modern human-like hand morphology. *Proceedings of the National Academy of Sciences* USA 111, 121-124.

Williams-Hatala, E.M., Hatala, K.G., Hiles,S., Rabey, K. N., 2016. Morphology of muscle attachment sites in the modern human hand does not reflect muscle architecture. *Scientific Reports* 6, 28353.

Weidenreich, F., 1941. *The extremity bones of* Sinanthropus pekinensis. Paleontol. Sinica New Series D 5.

Wood Jones, F., 1916. *Arboreal man*. Edward Arnold, London.

Zumwalt, A., 2006. The effect of endurance exercise on the morphology of muscle attachment sites. *Journal of Experimental Biology* 209, 444–454.

FIGURE

Figure 1. MH2 right hand bones in situ*, showing the scaphoid, lunate, metacarpals (Mc), proximal phalanges (PP), intermediate phalanges (IP) and the distal pollical phalanx (DP1). Originally published in Kivell et al. (2011).*

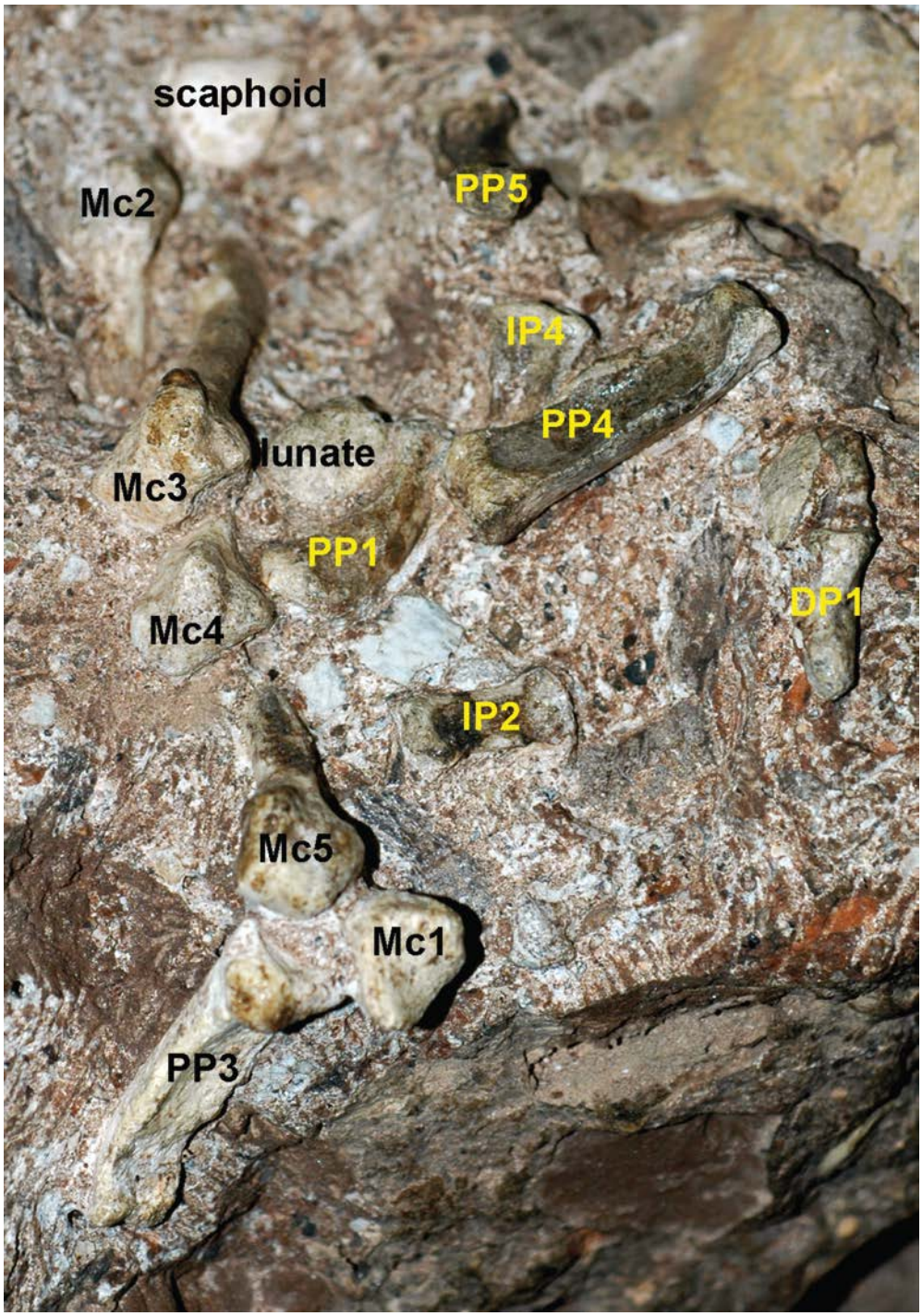

Figure 2. Articulated MH2 carpus with the associated radius (U.W. 88-85) and ulna (U.W. 88-62) in palmar (left) and dorsal (right) views. See also Churchill et al. (this volume).

Figure 3. MH2 right scaphoid U.W. 88-158 in, from left to right, approximate dorsal view, showing most of radial facet, palmar view showing trapezium facet, distal view of trapezium-trapezoid facet, medial view of capitate and lunate facets, proximal view of non-articular surface, and lateral view showing radial and trapezium-trapezoid facets. In the first two images on the left, proximal is towards the top; in the latter four images, palmar is towards the top.

Figure 4. MH2 right lunate U.W. 88-159 in, from left to right in the top row, lateral view of scaphoid facet, distomedial view of capitate and triquetrum facets, medial view of triquetrum facet, and in the bottom row, proximal view of the radial facet, and palmar and dorsal views of non-articular surface.

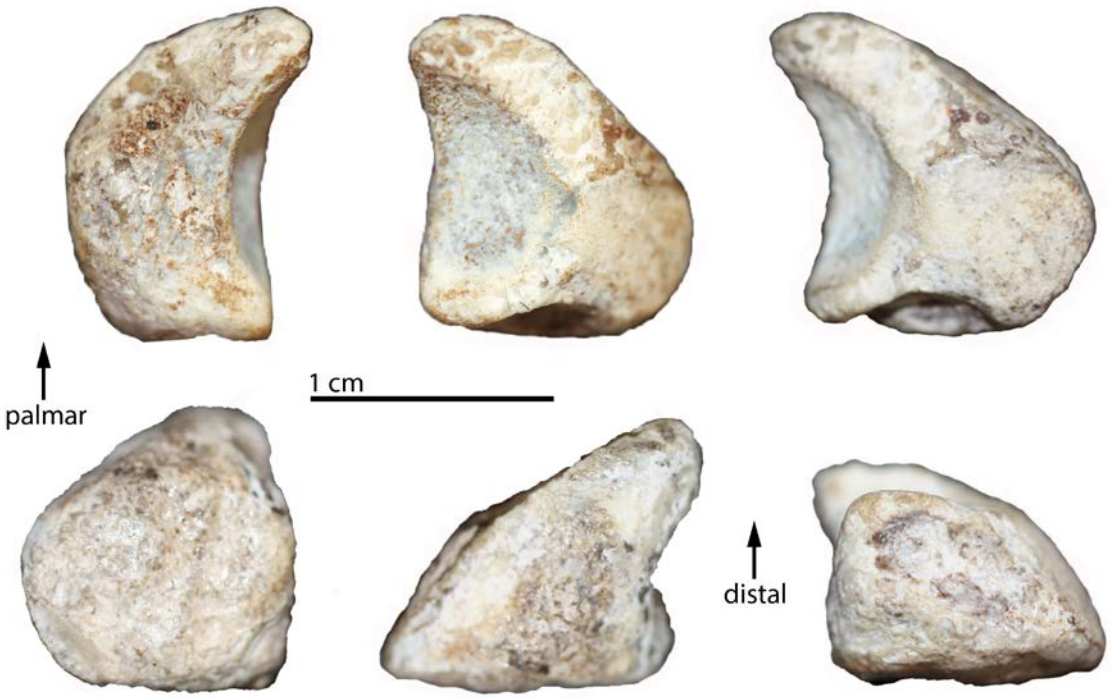

Figure 5. MH2 right triquetrum U.W. 88-157 in, from left to right, lateral view of lunate facet, distal view of hamate facet, medial view of non-articular surface, and palmar view of the pisiform facet.

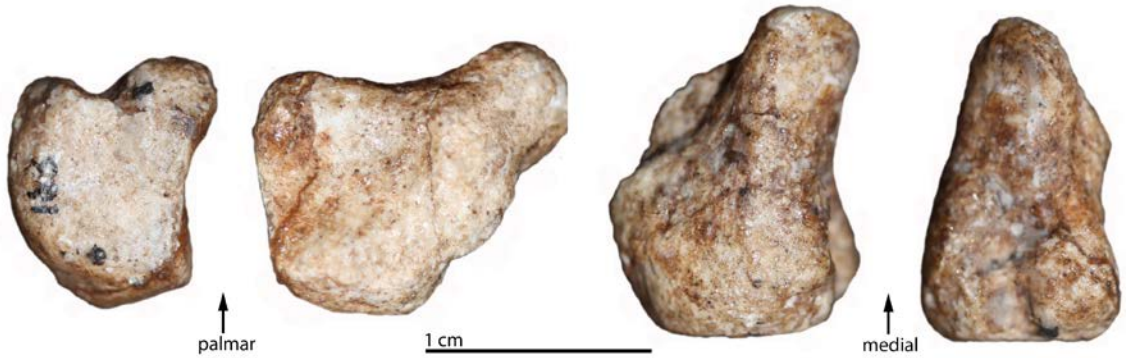

Figure 6. MH2 left (U.W. 88-105) and right (U.W. 88-156) capitates. Top, from left to right, U.W. 88-105 shown in lateral view of the scaphoid and second metacarpal facets, proximal view of the scapholunate facet, medial view of hamate facet, palmar view of non-articular surface. Bottom, U.W. 88-105 shown in distal view of third metacarpal facet (far left) and dorsal view of non-articular surface (far right). In box, U.W. 88-156 shown in distal and dorsal views, missing a portion of the distodorsolateral corner of the capitate body.

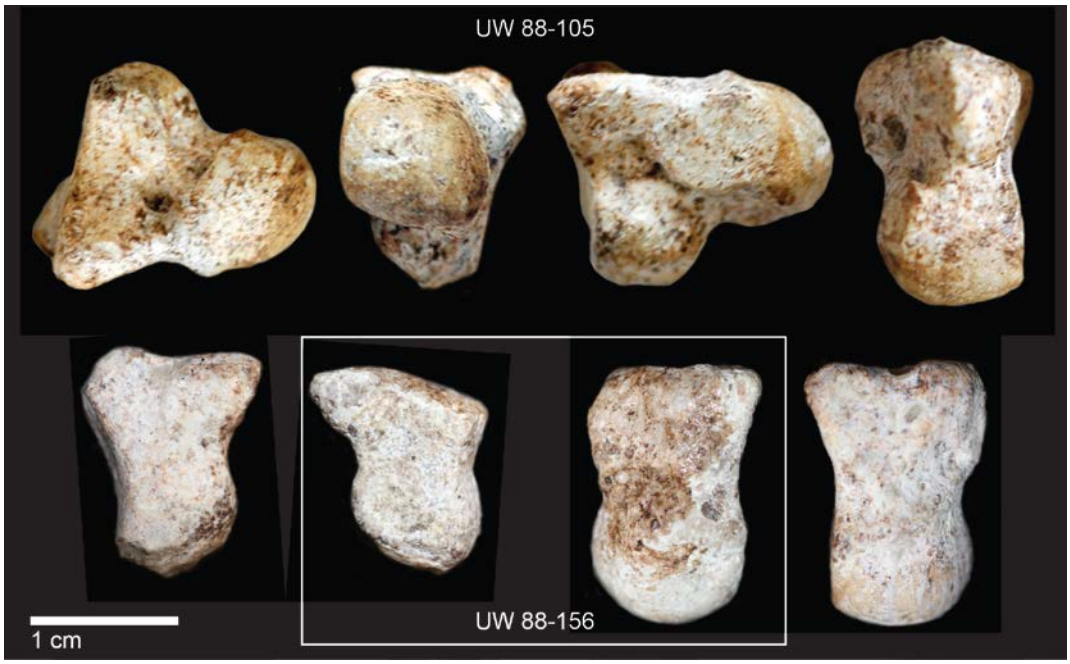

Figure 7. Carpometacarpal articulations in the MH2 right hand. Above, capitate-third metacarpal (Mc3) articulation in medial (left), lateral (middle) and dorsal (right) views. Below, hamate-metacarpal articulations, showing, from left to right, hamate-Mc5 in medial view, hamate-Mc4 articulation in lateral view, and hamate-Mc4-Mc5 articulation in palmar and dorsal views. The arrow points to the space between palmar edge of the Mc5 facet and the dorsal curvature of the hamulus that could accommodate the pisometacarpal ligament.

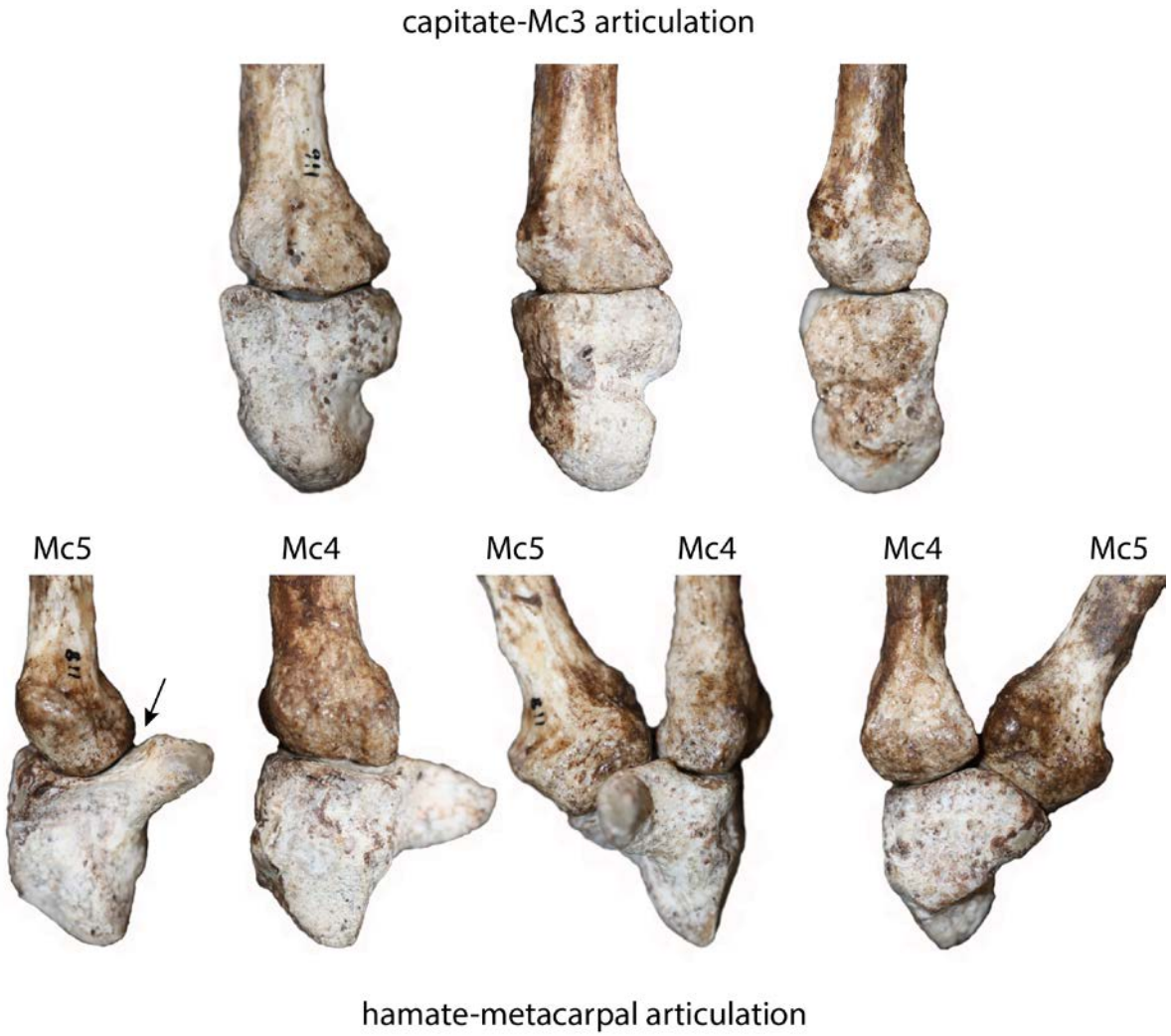

Figure 8. MH2 left (U.W. 88-106) and right (U.W. 88-95) hamates, above, shown in dorsal view of the non-articular surface, in which proximal is towards the top; middle, shown in medial view of triquetrum facet, and, below, lateral view of hamate facet, in which palmar is towards the top.

Figure 9. MH2 right first metacarpal U.W. 88-119, shown in, from left to right, dorsal, palmar, lateral, medial, distal (far right, above) and proximal (far right, below) views. Extent of muscle insertions are highlighted with lines for the M. first dorsal interosseous *(A) and* M. opponens pollicis *(B). Note the prominent palmar beak on the head of the Mc1 (C). Arrows highlight depressions flanking the palmar beak for the medial and lateral sesamoid bones.*

Figure 10. MH2 right second metacarpal U.W. 88-115 shown in, from left to right, palmar, medial, lateral and dorsal views.

Figure 11. MH1 U.W. 88-112 left and MH2 U.W. 88-116 right third metacarpals, both shown in, from left to right, lateral, palmar, medial, and dorsal views. At the far right, distal view of epiphyseal surface in U.W. 88-112 (top) and proximal view of base (bottom).

Figure 12. MH2 right fourth metacarpal U.W. 88-117 shown in, from left to right, palmar, medial, lateral and dorsal views.

Figure 13. MH2 right fifth metacarpal U.W. 88-118 shown in, from left to right, palmar, medial, lateral, dorsal, distal (far right, above) and proximal (far right, below) views. The extent of the M. opponens digiti minimii *insertion is highlighted in the palmar view and the arrow points to a crest along the dorsal surface for the fourth* M. dorsal interosseous *insertion.*

Figure 14. MH2 left (U.W. 88-91) and right (U.W. 88-160) pollical proximal phalanges shown in palmar (top, left), dorsal (top, right), lateral (middle, left), medial (middle, right), and proximal (bottom) views. The left first proximal phalanx (left side of each set of images) is better preserved than the right, particularly at the articular ends.

Figure 15. MH2 non-pollical proximal phalanges, including U.W. 88-109 left PP2, U.W. 88-164 right PP2, U.W. 88-182 left PP3, U.W. 88-120 right PP3, U.W. 88-110 left PP4, U.W. 88-108 right PP4, and U.W. 88-121 right PP5. Extent of complete flexor sheath ridges are highlighted by black lines in palmar and medial views.

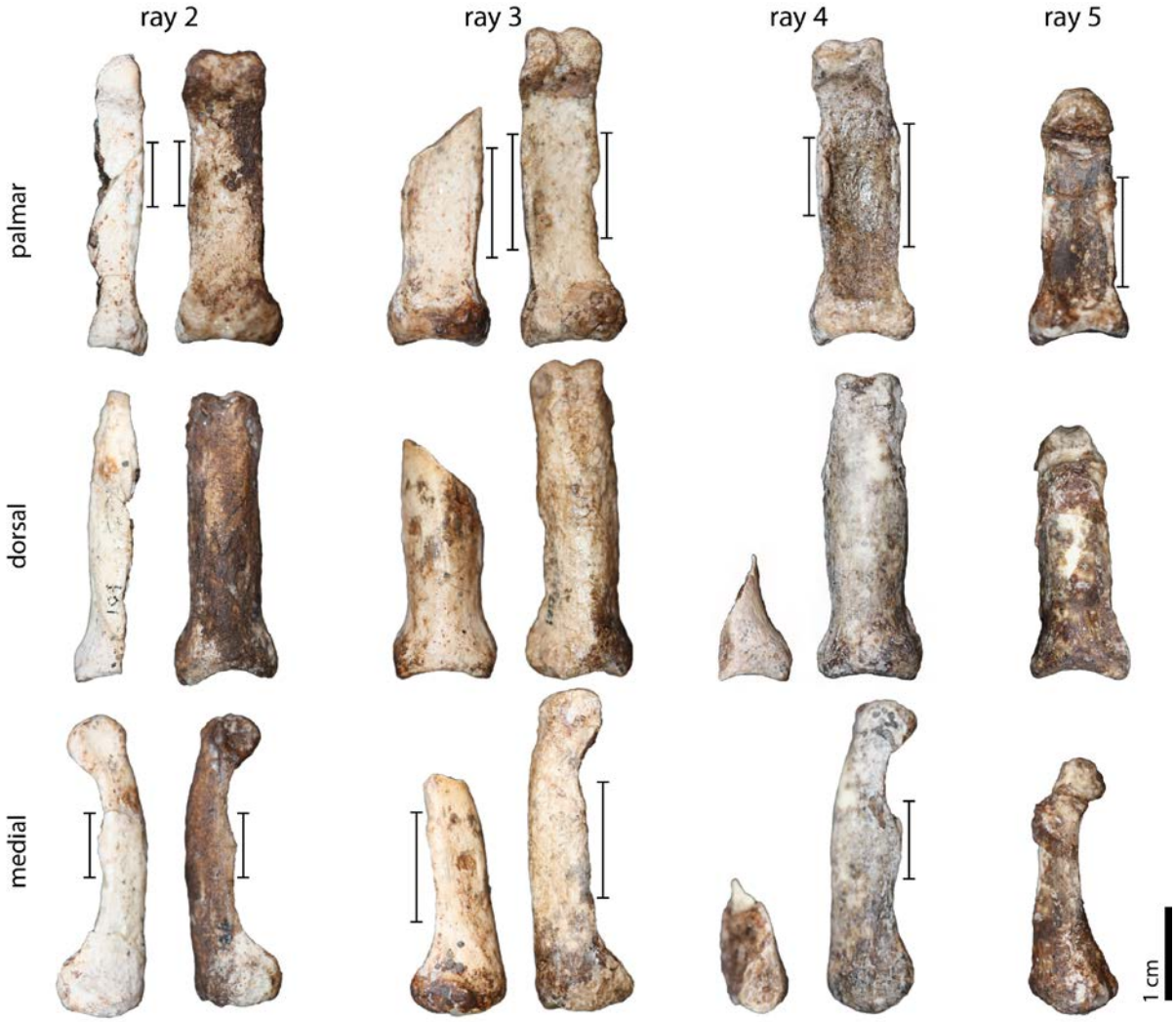

Figure 16. MH2 intermediate phalanges, shown in palmar (above) and medial (below) views, except for U.W. 88-123, which is shown in lateral view due to matrix. Extent of complete flexor sheath ridges are highlighted by black lines in palmar and medial views.

Figure 17. MH2 right distal pollical phalanx U.W. 88-124, shown in, from left to right, medial, dorsal, lateral and palmar views. Morphological features highlighted by arrows are the ridge for the attachment of the M. flexor pollicis longus *(A), the proximal fossa (B), and the distal or ungual fossa (C).*

Figure 18. Comparative analysis of the MH2 U.W. 88-158 scaphoid morphology. Box-and-whisker plots of scaphoid shape showing dorsopalmar (DP) height of the radial facet relative to DP height of the scaphoid body (top), proximodistal (PD) length relative to DP height of the radial facet (bottom left) and capitate facet (bottom right). Comparative extant sample includes Gorilla *sp. (n=56),* P. troglodytes *ssp. (n=46),* P. paniscus *(n=23), recent small-bodied (s-b) Khoisan humans (n=16), recent humans (n=142). Comparative fossil sample composed of in* Ar. ramidus *(n=2, ARA-VP-6/500-085 and -062),* Australopithecus *sp. StW 618,* H. habilis *FLK NN-P of OH 7 hand,* H. naledi *(n=3, including U.W. 101-807, -1639 and -1726), Neandertals (n=8, including Shanidar 3, 4, 6 and 8, Kebara 2, Tabun 1-152, La Ferrassie 1, and Regourdou 1) and early* H. sapiens *('early* Homo*') (n=7, including Dolní Věstonice 3, 14 and 16, Qafzeh 9, Ohalo II, Barma Grande 2 and Arene Candide 2). Inset image shows how measurements were taken, with palmar surface of scaphoid oriented towards the top of the page. For* Ar. ramidus *specimens, all data were measured on original fossils by TLK, apart from the published data on the DP height and PD length of the radial facet on ARA-VP-6/500-085 from Lovejoy et al. (2009).*

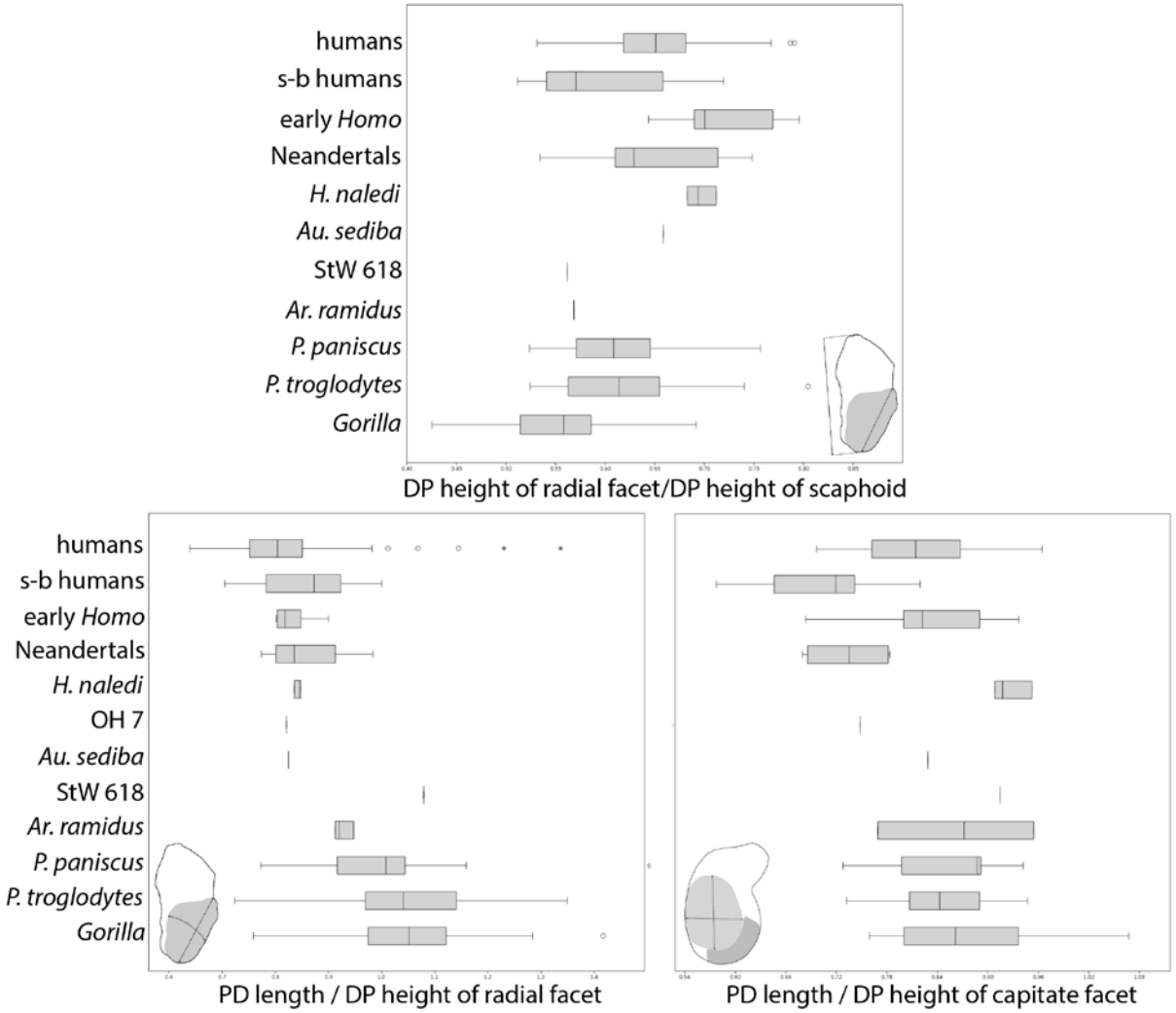

Figure 19. Comparative analysis of the MH2 U.W. 88-159 lunate morphology. Box-and-whisker plots of lunate shape, showing mediolateral (ML) breadth of the capitate facet relative to the ML breadth of the lunate body (left), ML breadth relative to dorsopalmar (DP) height of capitate facet (middle) and radial facet (right). Comparative extant sample includes Gorilla *sp. (n=51),* P. troglodytes *ssp. (n=38),* P. paniscus *(n=22), recent small-bodied (s-b) Khoisan humans (n=16), recent humans (n=136). Comparative fossil sample composed of* Ar. ramidus *ARA-VP-6/500-034, cf.* Au. afarensis *KNM-WT 22944-J,* Au. afarensis *A.L. 444-3,* H. naledi *(n=3, including U.W. 101-418B, -1546, and -1732), Neandertals (n=6, including Shanidar 3 and 4, Kebara 2, Tabun 1-162, Amud 1, and Neandertal 1), and early* H. sapiens *('early* Homo*') (n=9, including Dolní Věstonice 3, 14, 15 and 16, Qafzeh 9, Ohalo II, Barma Grande 2, Arene Candide 2, and Tianyuan 1). Inset images show how measurements were taken, with palmar surface of lunate oriented towards the top of the page. For* Ar. ramidus *ARA-VP-6/500-034, all data were measured on original fossils by TLK, and DP height (13.7mm) and ML breadth (13.2mm) of the radial facet values are adjusted from data reported from casts in Lovejoy et al. (2009).*

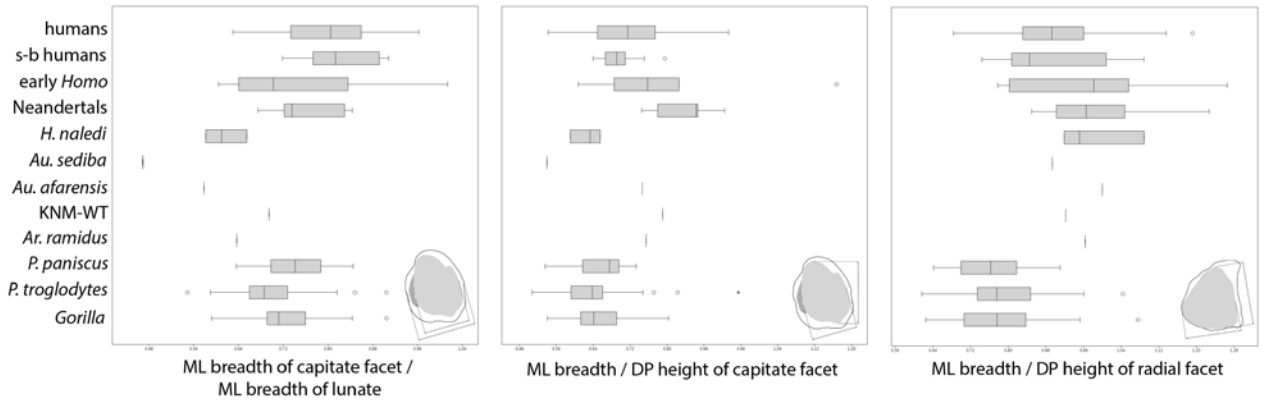

Figure 20. Comparative analysis of the MH2 U.W. 88-157 triquetrum morphology. Box-and-whisker plots of triquetrum shape, showing mediolateral (ML) breadth relative to proximodistal (PD) length of the triquetrum (top, left), ML breadth relative to dorsopalmar (DP) height of the hamate facet (top, right), and relative (i.e. divided by a geometric mean) ML breadth and PD length of the triquetrum body. Comparative extant sample includes Gorilla *sp. (n=56),* P. troglodytes *ssp. (n=45),* P. paniscus *(n=22), recent small-bodied (s-b) Khoisan humans (n=16), recent humans (n=135). Comparative fossil sample composed of* Ar. ramidus *(n=2, ARA-VP-6/500-029 and -068), Swartkrans* Au. robustus *or early* Homo *SKX 3498,* H. naledi *U.W. 101-1727, Neandertals (n=5, including Kebara 2, Tabun 1-154, Amud 1, Regourdou 1, and La Ferrassie 1), and early* H. sapiens *('early* Homo*') (n=7, including Skhul IV and V, Qafzeh 8 and 9, Ohalo II, Barma Grande 2 and Arene Candide 2). For* Ar. ramidus *specimens, all data were measured on original fossils by TLK. Inset images show how measurements were taken.*

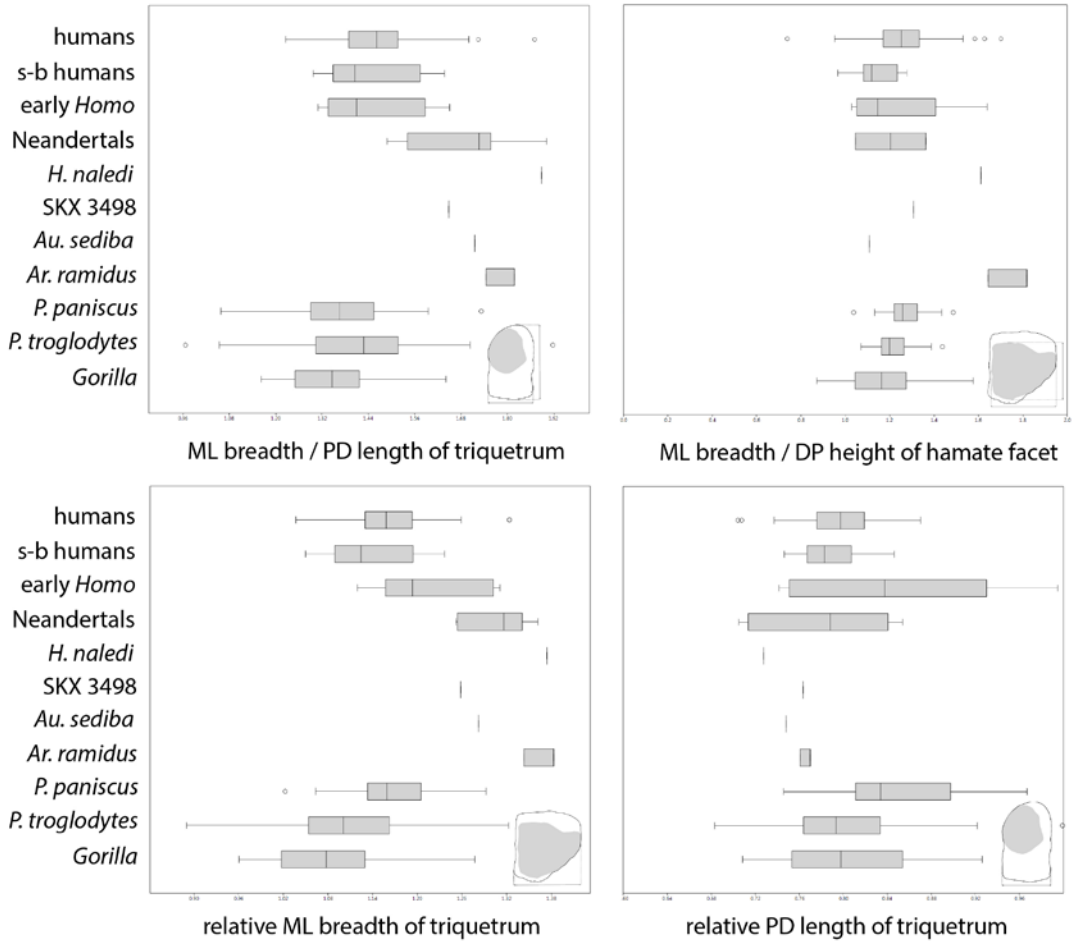

Figure 21. Comparative analysis of the MH2 U.W. 88-105 and -156 capitate morphology. Box-and-whisker plots of capitate shape, showing relative (i.e. divided by a geometric mean) dorsopalmar (DP) height of capitate body (top, left), DP height relative to proximodistal (PD length of capitate body (top, right), capitate "waisting" measured as mediolateral (ML) breadth of the capitate neck relative to ML breadth of the proximal facet (bottom, left), ML breadth relative to DP height of proximal facet. Comparative extant sample includes Gorilla *sp. (n=52),* P.

troglodytes *ssp. (n=46),* P. paniscus *(n=21), recent small-bodied (s-b) Khoisan humans (n=25), recent humans (n=167). Comparative fossil sample composed of* Ar. ramidus *ARA-VP-6/500-058 [using published values from Lovejoy et al. (2009)], cf.* Au. afarensis *KNM-WT 22944-H,* Au. afarensis *(n=2, A.L. 288-1w and 333-40,* Au. africanus *TM 1526,* H. floresiensis *(n=2, LB1-45 and LB 20),* H. naledi *(n=2, U.W. 101-930 and -1730, Neandertals (n=10, including Shanidar 4, Kebara 2, Tabun 1, Amud 1, La Ferrassie 1 and 2, Moula Guercy M-F1-461, La Chapelle, Krapina 200, and Neandertal 1), and early* H. sapiens *('early* Homo*') (n=7, including Dolní Věstonice 15 and 16, Qafzeh 9, Ohalo II, Tianyuan 1, Barma Grande 2 and Arene Candide 2). Inset images show how measurements were taken.*

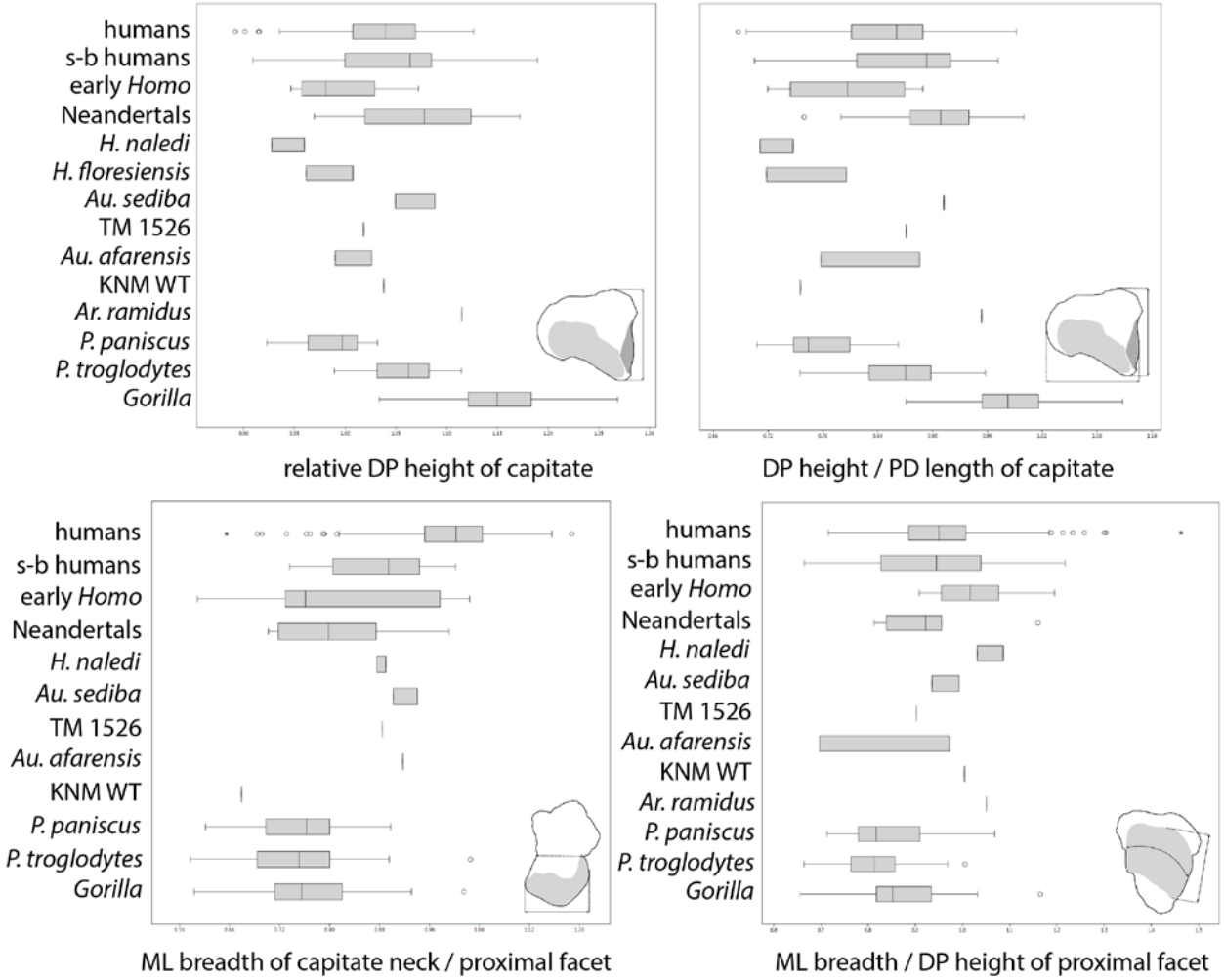

Figure 22. Comparative analysis of the MH2 U.W. 88-106 (left) and -95 (right) hamate morphology. Box-and-whisker plots of hamate shape, showing dorsopalmar (DP) height relative to proximodistal (PD) length of hamate body (excluding hamulus; top, left), mediolateral (ML) breadth of the fifth relative to the fourth metacarpal facets (top, right), relative (i.e. divided by geometric mean) palmar projection (bottom, left) and distal projection (bottom, right) of the hamulus. For the latter, several H. sapiens *specimens show no distal projection of the hamulus. Comparative extant sample includes* Gorilla *sp. (n=51),* P. troglodytes *ssp. (n=42),* P. paniscus *(n=23), recent small-bodied (s-b) Khoisan humans (n=16), recent humans (n=138). Comparative fossil sample composed of cf.* Au. afarensis *KNM-WT 22944-I,* Au. afarensis *A.L. 333-50,* H. naledi *(n=2, including U.W. 101-1640 and -1729, Neandertals (n=5, including Shanidar 3, Kebara 2, Regourdou 1, Tabun 1-154 and Tabun 3), and early* H. sapiens *('early* Homo*') (n=4, including Dolní Věstonice 3, Qafzeh 9, Ohalo II, and Arene Candide 2). Inset images show how measurements were taken.*

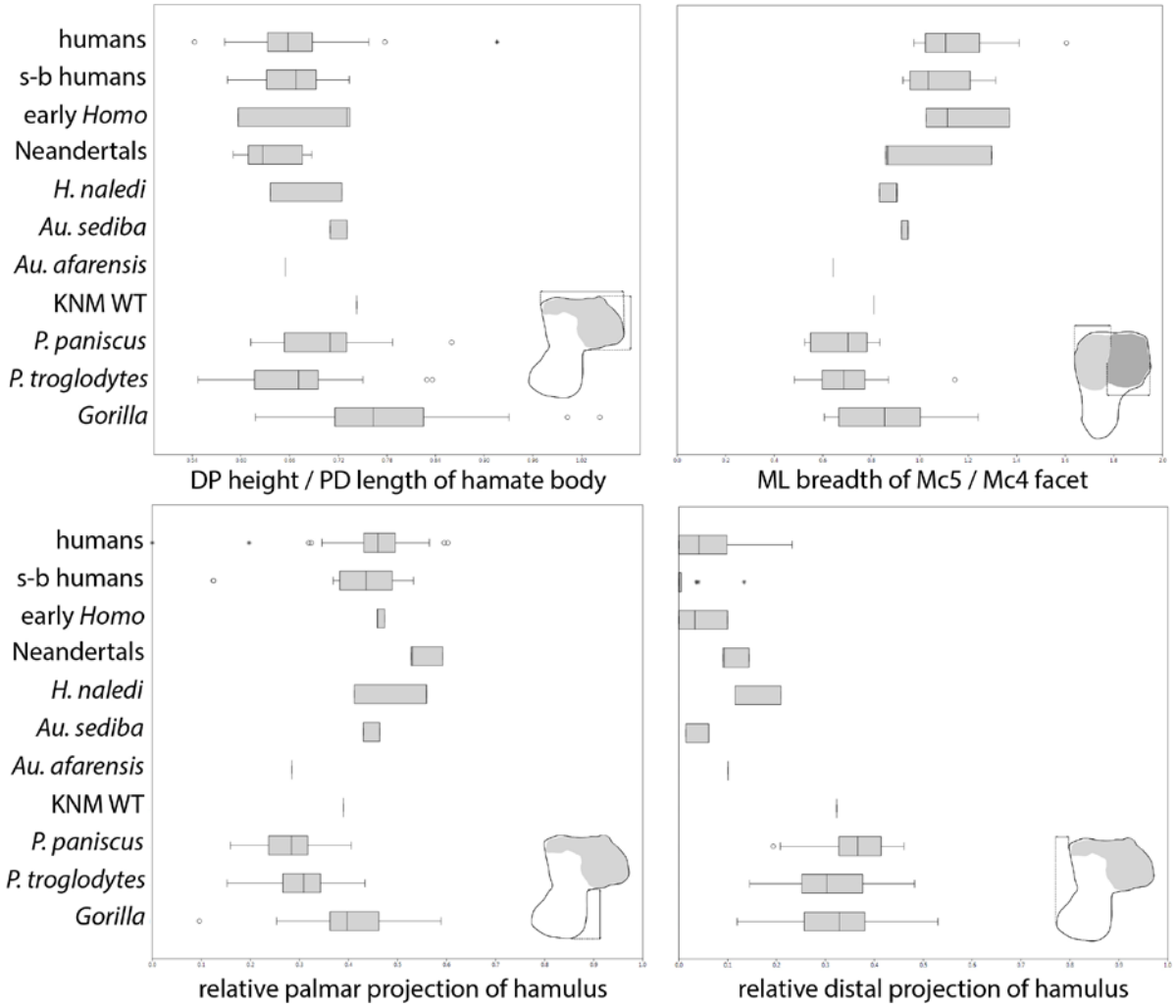

Figure 23. Relative thumb length in MH2. (A) First metacarpal (Mc1) length against third metacarpal (Mc3) length and (B) thumb length (Mc1 length + proximal phalanx (PP) 1 length) against third ray length (Mc3 length + PP3 length + intermediate phalanx (IP) 3 length), in comparison to recent humans (gray diamonds), small-bodied recent humans (black diamonds), P. paniscus *(dark triangles),* P. troglodytes *ssp. (light triangles), and* Gorilla *ssp. (crosses). All fossil values are derived from hand bones associated with a single individual apart from the* Au. afarensis*, which is a composite of several individuals (Marzke 1983; Alba et al. 2003). Linear regression lines shown for recent humans (gray) and small-bodied humans (black). The* Au. sediba *MH2 hand has a relatively long Mc1 and thumb for its small hand size, falling outside the range of variation of recent humans, and is most similar to Hand 1 of* H. naledi*.*

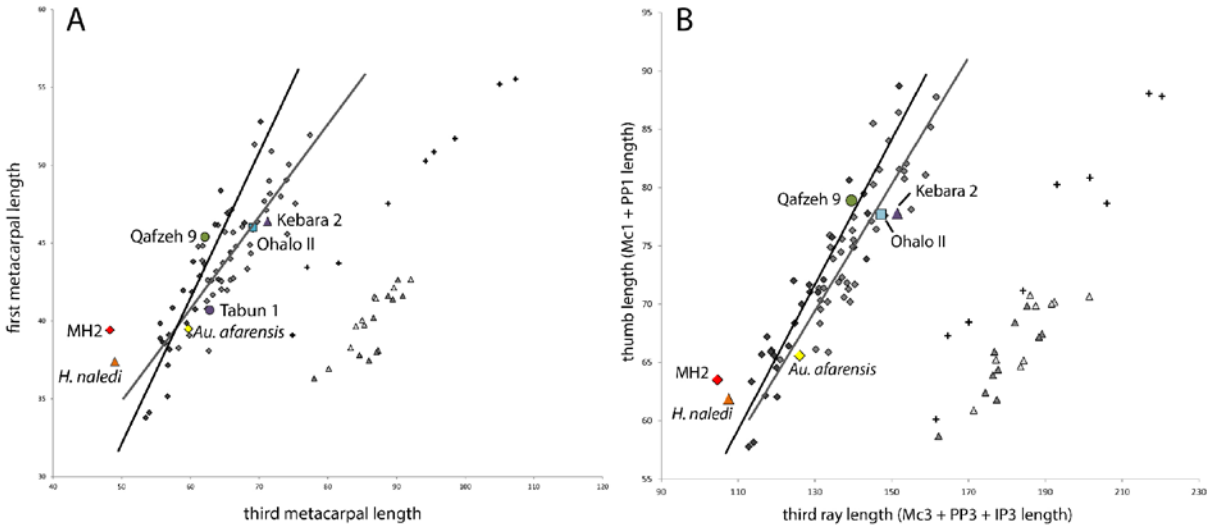

Figure 24. Comparative analysis of the MH2 U.W. 88-119 first metacarpal morphology. Box-and-whisker plots of first metacarpal (Mc1) shape, in which each variable is shown as a ratio of interarticular (IA) length: mediolateral (ML) breadth of the Mc1 base (top, left), midshaft (top, right) and Mc1 head (bottom left), as well as the dorsopalmar (DP) height of the Mc1 head (bottom, right). Comparative extant sample includes Gorilla *sp. (n=9),* P. troglodytes *ssp. (n=10),* P. paniscus *(n=11), recent small-bodied (s-b) Khoisan humans (n=25), recent humans (n=43). Comparative fossil sample composed of* Ar. ramidus *(n=2, ARA-VP-6/500-015 and ARA-VP-6/1638),* Au. afarensis *A.L. 333w-39,* Au. africanus *StW 418,* Au. robustus*/early* Homo *SK 84 and SKX 5020,* H. naledi *(n=6, including U.W. 101-007, -270, -917, -1282, -1321, and 1641), Neandertals (n=4, including Shanidar 4, Kebara 2, Amud 1 and Tabun 1), and early* H. sapiens *('early* Homo*') (n=5, including Dolní Věstonice 16, Qafzeh 9, Ohalo II, Barma Grande 2 and Arene Candide 2). Note that interarticular length is estimated for SKX 5020, as the proximal end is not preserved and thus results should be interpreted with caution. Regarding* Ar. ramidus *specimens, all data are taken published values in Lovejoy et al. (2009) apart from values for DP height of the base ([12mm] and midshaft (6.3mm) and ML breadth of the head (11mm) in ARA-VP-6/500-015 and DP height of head (12.4mm) in ARA-VP-6/1638, which have been adjusted after re-measurement on original fossils. Interarticular length of both* Ar. ramidus *specimens was measured directly on the original fossils by TLK.*

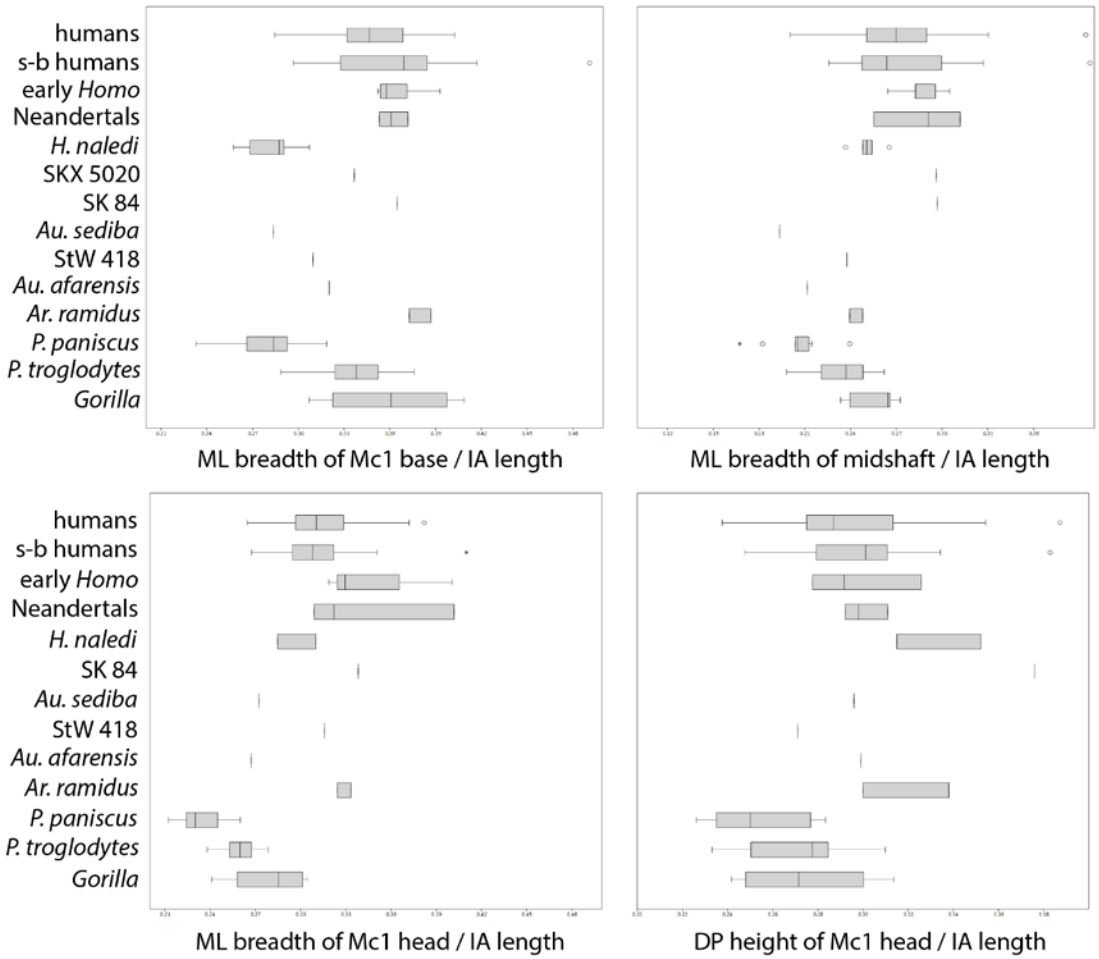

Figure 25. Comparative analysis of the MH2 U.W. 88-115 second metacarpal morphology. Box-and-whisker plots of second metacarpal (Mc2) shape, in which each variable is shown as a ratio of interarticular (IA) length: mediolateral (ML) breadth (top, left) and dorsopalmar (DP) height (top, right) of the Mc2 base, ML breadth at midshaft (bottom, left) and DP height of the head (bottom, right). Comparative extant sample includes Gorilla *sp. (n=10),* P. troglodytes *ssp. (n=11),* P. paniscus *(n=11), recent small-bodied (s-b) Khoisan humans (n=25), recent humans (n=45). Comparative fossil sample composed of* Au. afarensis *(n=3, A.L. 333-48, A.L. 438-If and –Ie,* Au. africanus *StW 382,* H. naledi *U.W. 101-1320, Neandertals (n=11, La Chapelle, La Ferrassie 1 and 2, Regourdou 1, Shandiar 4 and 5, Spy 2 and 21A, Tabun 1-160, Kebara 2, and Moula-Guercy M-G2-648), and early* H. sapiens *('early* Homo*') (n=8, Dolní Věstonice 13, 15, 16 and 59, Pavlov 31, Qafzeh 9, Ohalo II, and Arene Candide 2).*

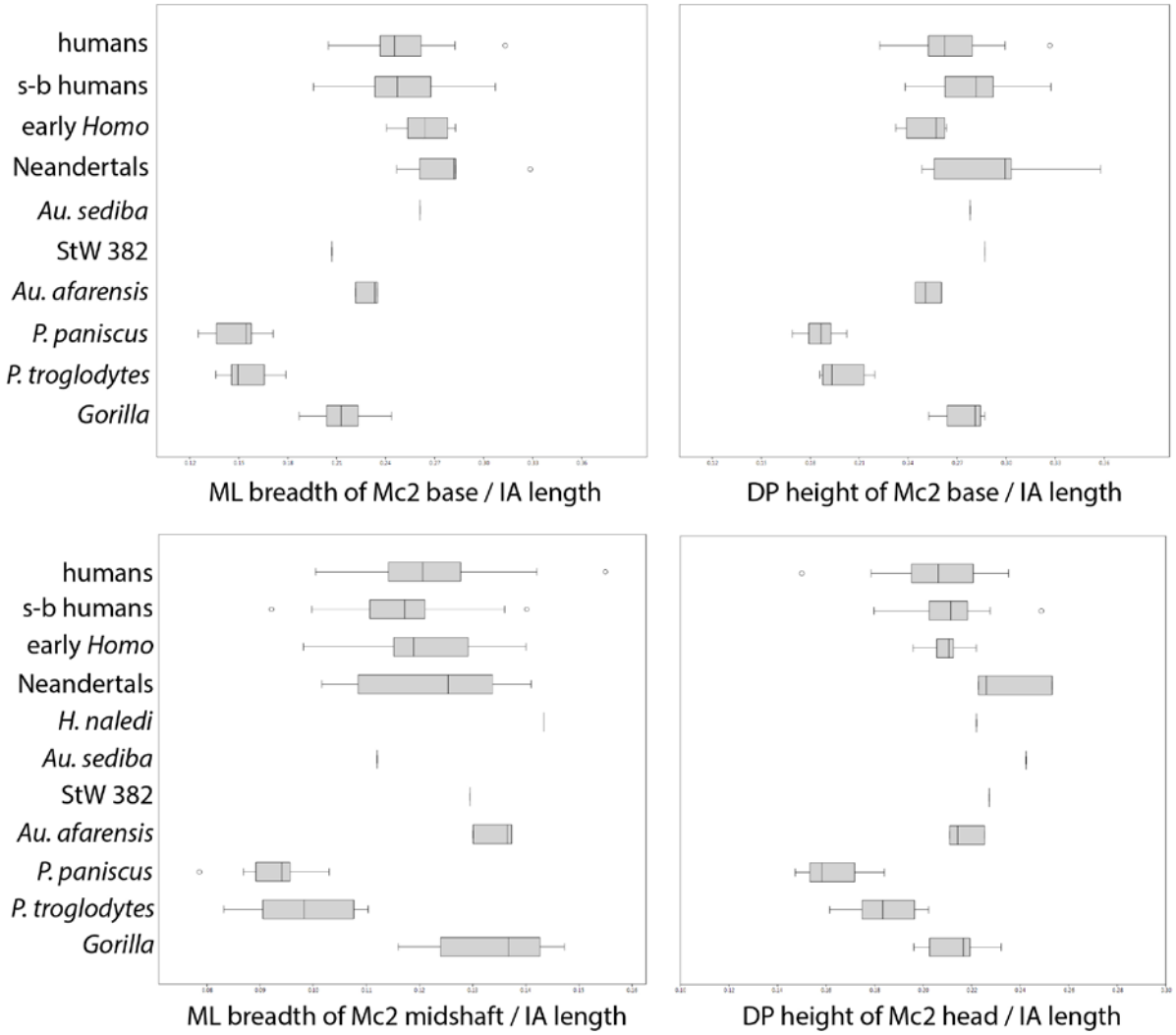

Figure 26. Comparative analysis of the MH1 U.W. 88-112 and MH2 U.W. 88-116 third metacarpal morphology. Box-and-whisker plots of third metacarpal (Mc3) shape, in which each variable is shown as a ratio of interarticular (IA) length: mediolateral (ML) breadth (top, left) and dorsopalmar (DP) height (top, right) of the Mc3 base (top, left), ML breadth at midshaft (bottom, left) and DP height of the head (bottom, right). Comparative extant sample includes Gorilla *sp. (n=11),* P. troglodytes *ssp. (n=12),* P. paniscus *(n=11), recent small-bodied (s-b) Khoisan humans (n=25), recent humans (n=42). Comparative fossil sample composed of* Au. afarensis *(n=2, A.L. 333-16 and A.L. 438-1d),* Au. africanus *(n=2, StW 64 and 68), probable* H. erectus *KNM-WT 51260 (Ward et al. 2013),* H. naledi *U.W. 101-1319, Neandertals (n=11, La Chapelle, La Ferrassie 1 and 2, Regourdou 1, Shanidar 4 and 6, Kebara 2, Amud 1, Moula-Guercy M-D3-768, Spy 22A and Tabun 1-151), and early* H. sapiens *('early* Homo*') (n=8, Dolní Věstonice 13, 16 and 58, Qafzeh 8 and 9, Ohalo II, Barma Grande 2 and Arene Candide 2). Note that interarticular length was estimated for La Chapelle and Amud 1 (Niewoehner et al. 1997), and, importantly, for MH1 U.W. 88-112, which is missing its proximal epiphysis. All variables were also analysed using total length that includes the Mc3 styloid process in* H. sapiens *and Neandertals and relative relationships among taxa did not change.*

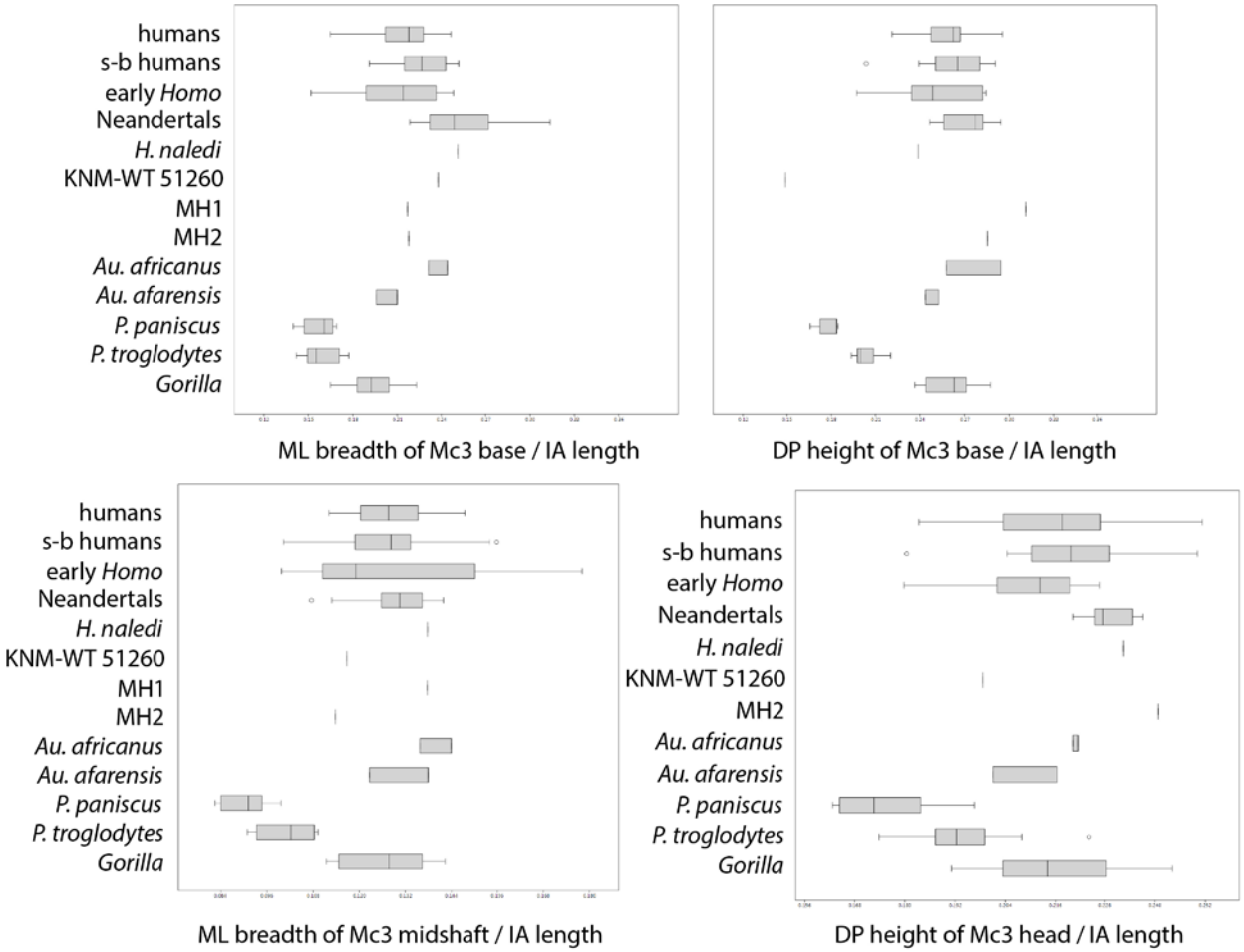

Figure 27. Comparative analysis of the MH2 U.W. 88-117 fourth metacarpal morphology. Box-and-whisker plots of fourth metacarpal (Mc4) shape, in which each variable is shown as a ratio of interarticular (IA) length: mediolateral (ML) breadth (top, left) and dorsopalmar (DP) height (top, right) of the Mc4 base (top, left), ML breadth at midshaft (bottom, left) and DP height of the head (bottom, right). Comparative extant sample includes Gorilla *sp. (n=11),* P. troglodytes *ssp. (n=12),* P. paniscus *(n=11), recent small-bodied (s-b) Khoisan humans (n=25), recent humans (n=40). Comparative fossil sample composed of* Ar. ramidus *ARA-VP-7/2G,* Au. afarensis *A.L. 333-56,* Au. robustus*/early* Homo *SKX 2954,* H. naledi *U.W. 101-1318 and U.W. 102-028, Neandertals (n=4, Shanidar 4 and 5, Spy 22C, and Tabun 1-166), and early* H. sapiens *('early* Homo*') (n=5, Dolní Věstonice 16, Qafzeh 9, Ohalo II, Barma Grande 2 and Arene Candide 2). Regarding* Ar. ramidus *ARA-VP-7/2G, all data are taken published values in Lovejoy et al. (2009) apart from DP height of the base (10.1mm), which has been adjusted from the published value after re-measurement on the original fossil, and interarticular length (56mm), which was measured on the original fossil by TLK and G. Suwa.*

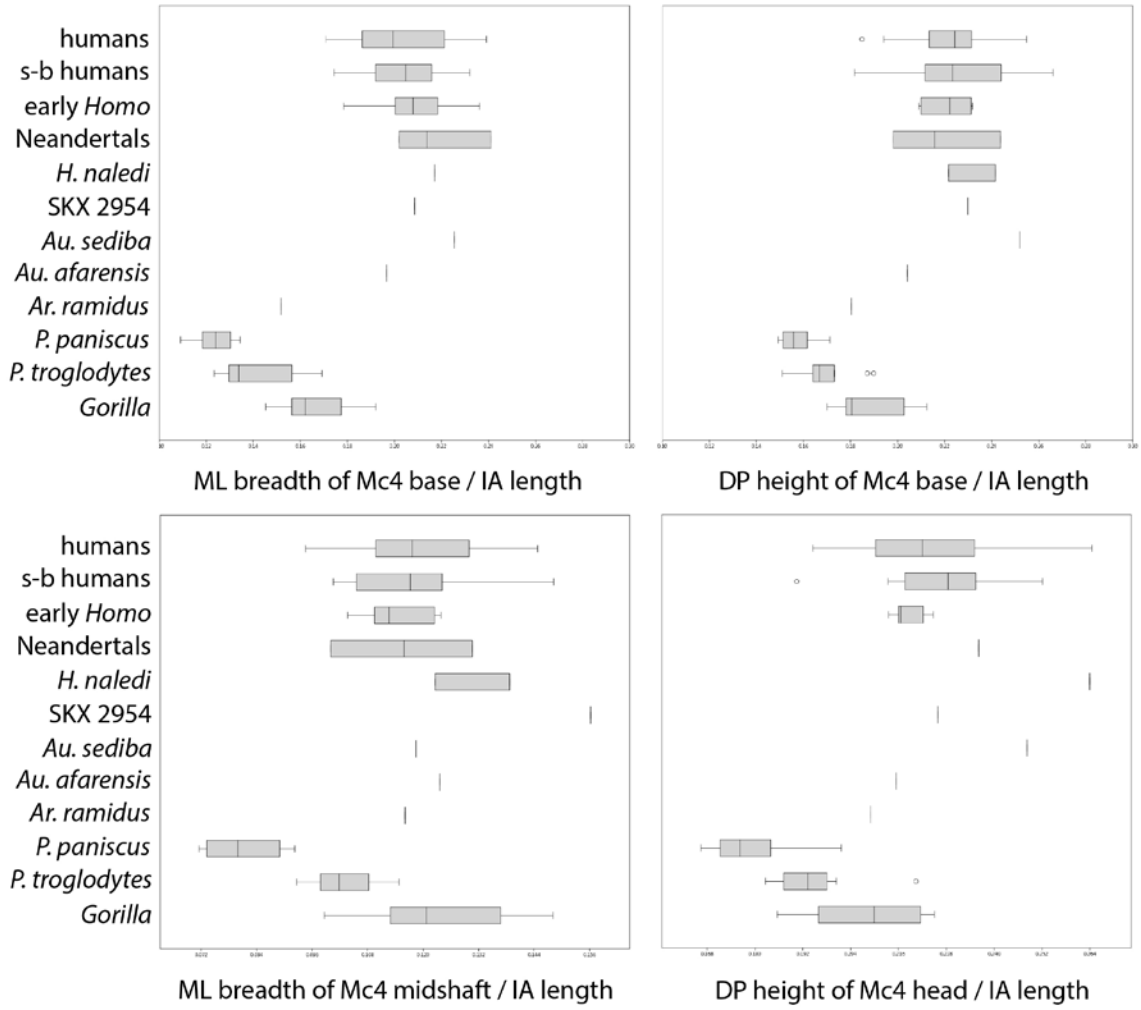

Figure 28. Comparative analysis of the MH2 U.W. 88-118 fifth metacarpal morphology. Box-and-whisker plots of fifth metacarpal (Mc5) shape, in which each variable is shown as a ratio of interarticular (IA) length: mediolateral (ML) breadth (top, left) and dorsopalmar (DP) height (top, right) of the Mc5 base, ML breadth at midshaft (bottom, left) and DP height of the head (bottom, right). Comparative extant sample includes Gorilla *sp. (n=9),* P. troglodytes *ssp. (n=11),* P. paniscus *(n=11), recent small-bodied (s-b) Khoisan humans (n=25), recent humans (n=37). Comparative fossil sample composed of* Ar. ramidus *ARA-VP-6/500-036,* Au. afarensis *(n=3, A.L. 333-14, -89 and -141),* Au. africanus *StW 63,* Au. robustus*/early* Homo *SK(W) 14147 (SKW 27),* H. naledi *U.W. 101-1309, Neandertals (n=3, Shandiar 4 and 5, and Tabun 1-164), and early* H. sapiens *('early* Homo*') (n=5, Dolní Věstonice 16, Qafzeh 9, Ohalo II, Barma Grande 2, and Arene Candide 2). Regarding* Ar. ramidus*, all data are derived from published values in Lovejoy et al. (2009).*

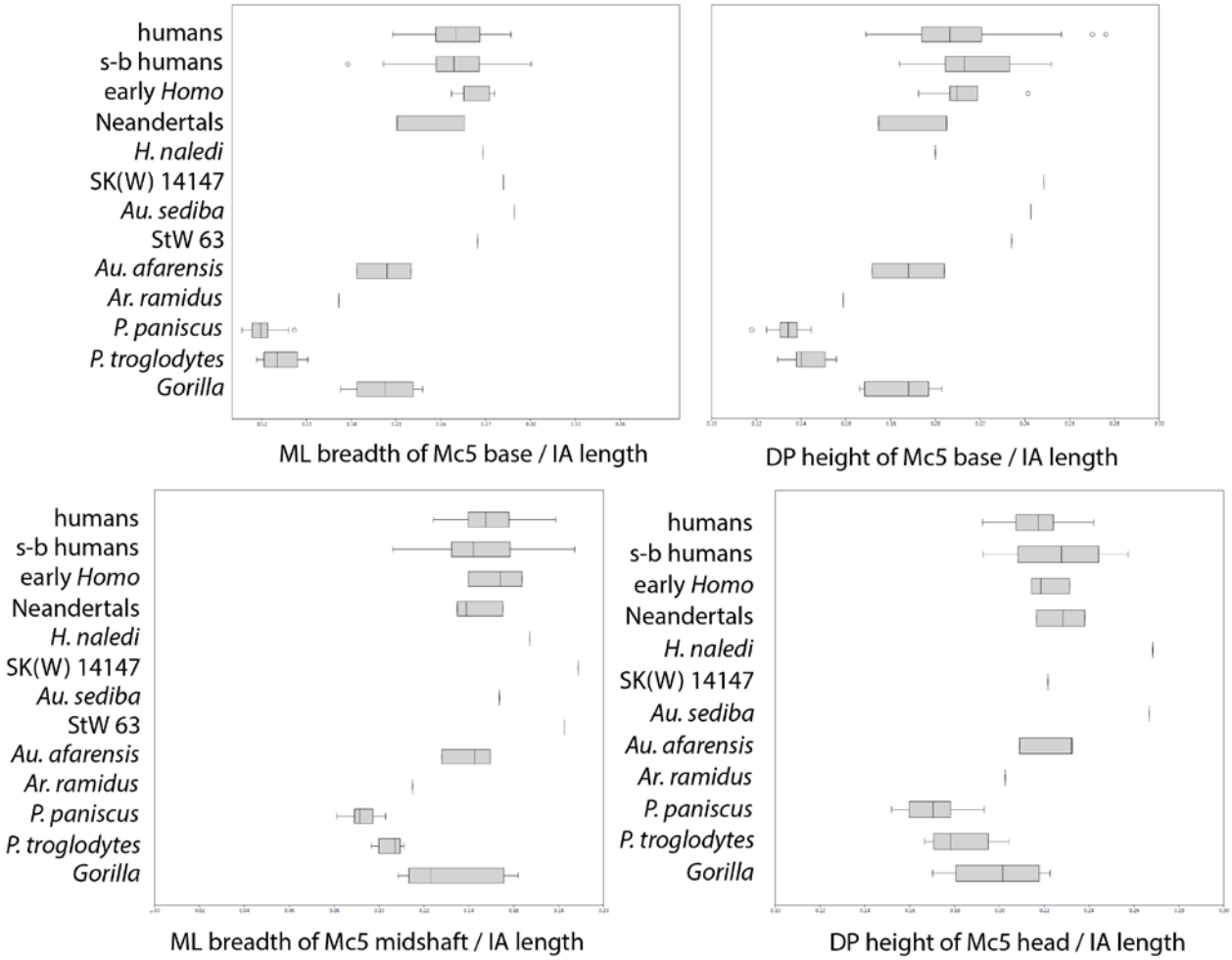

Figure 29. Comparative analysis of the MH2 pollical proximal phalanx (left, U.W. 88-91 and right, U.W. 88-160) morphology. Box-and-whisker plots of pollical proximal phalanx (PP1) shape, in which each variable is shown as a ratio of maximum or total length: mediolateral (ML) breadth of the PP1 base (top, left), midshaft (top, right) and distal trochlea (bottom, left) and dorsopalmar (DP) height of the trochlea (bottom, right). Comparative extant sample includes Gorilla *sp. (n=8),* P. troglodytes *ssp. (n=10),* P. paniscus *(n=10), recent small-bodied (s-b) Khoisan humans (n=24), recent humans (n=38). Comparative fossil sample composed of* Ar. ramidus *ARA-VP-7/2I,* Au. afarensis *(n=2, A.L. 333-69 and A.L. 438-4, total length is estimated in the latter),* Au. africanus *StW 575,* H. naledi *(n=3, U.W. 101-428, -1055 and -1721), Neandertals (n=7, Shandiar 4, 5 and 6, Kebara 2, Tabun 1, Moula-Guersy M-E1-123 and Spy 25H), and early* H. sapiens *('early* Homo*') (n=4, Dolní Věstonice 14 and 16, Qafzeh 9, Ohalo II).* Ar. ramidus *values derived from published values in Lovejoy et al. (2009) apart from midshaft ML breadth (5.4mm) measured on original fossils by TLK.*

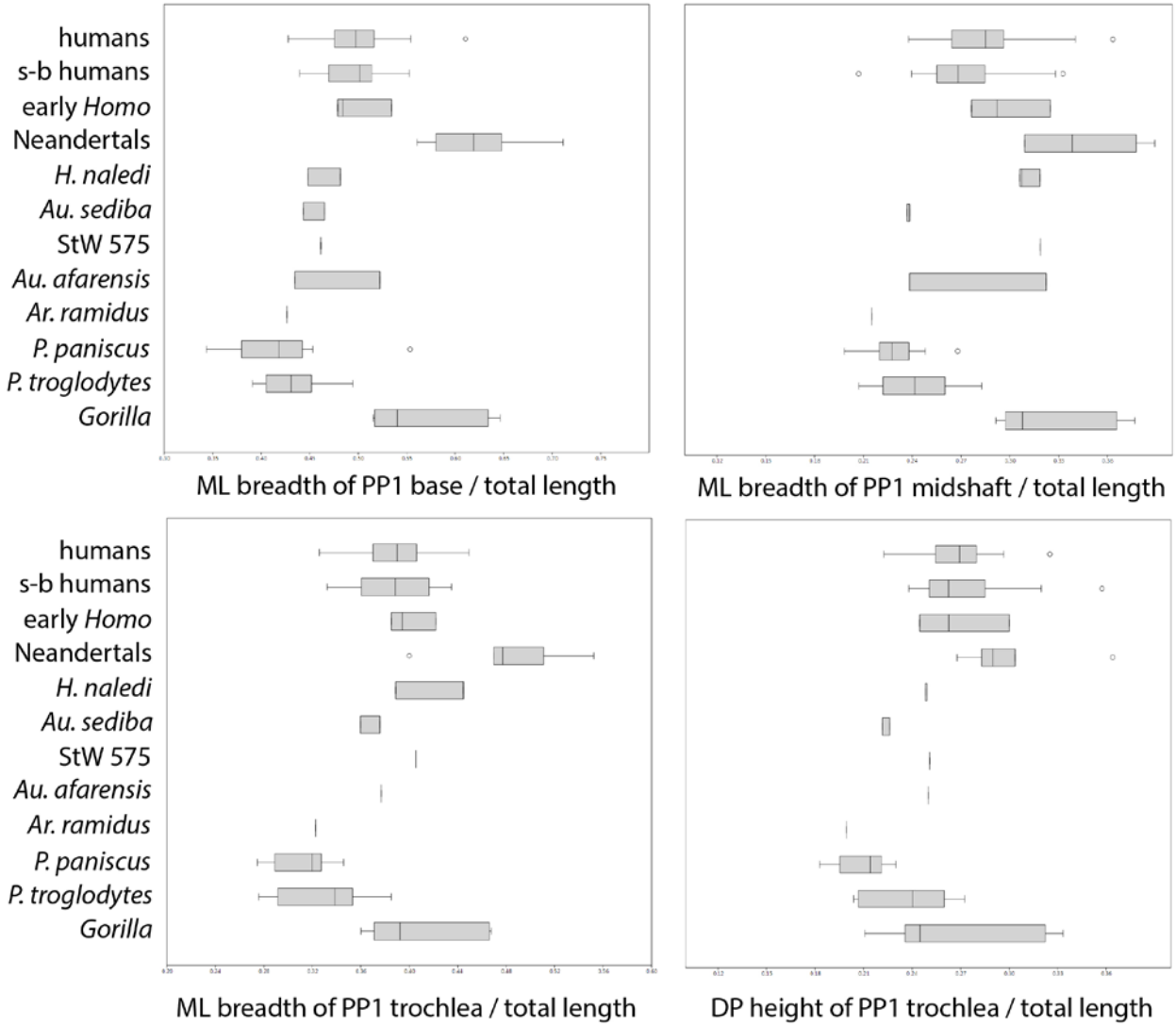

Figure 30. Phalangeal curvature of the MH2 non-pollical proximal phalanges in comparison to other fossil hominins and extant catarrhines. Variation in PD curvature of the dorsal surface of proximal phalanges of rays 2-4, quantified as the first polynominal coefficient using methods described in Deane and Begun (2008). Although there is substantial overlap in degree of curvature across taxa, Au. sediba *curvature is less than the median value of* Ar. ramidus*,* Au. afarensis*,* H. naledi *and OH 7, but greater than that of* Au. africanus *and hominins from Swartkrans. Image adapted from Kivell et al. (2015).*

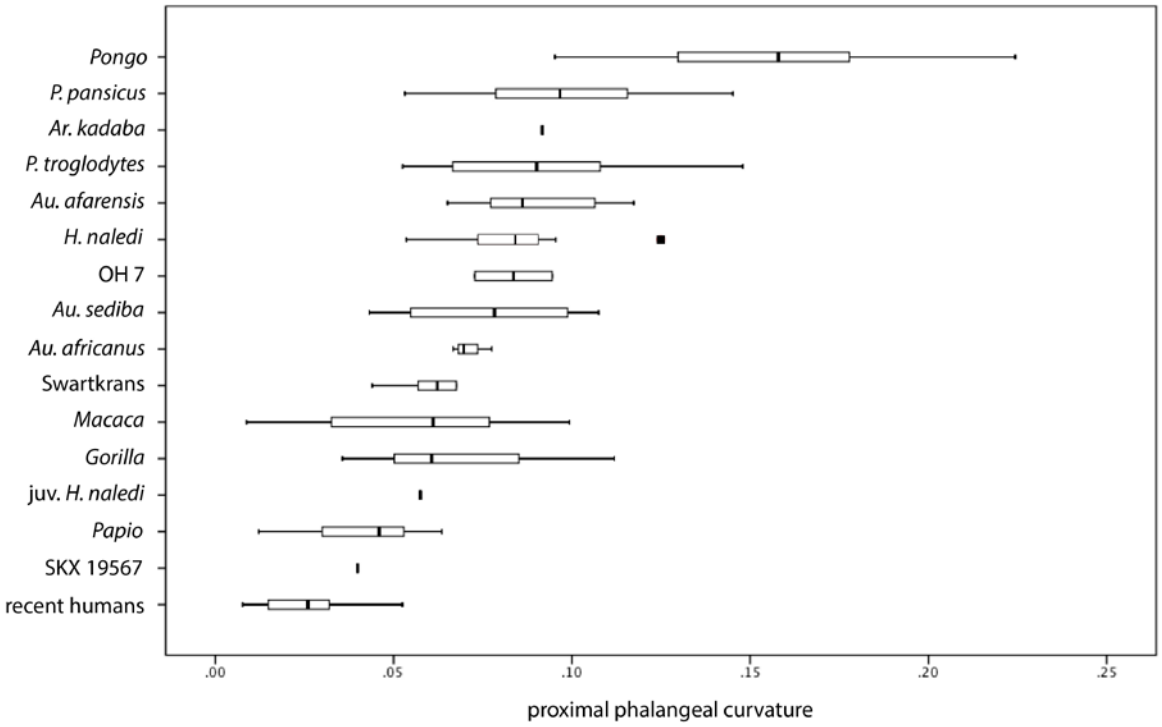

Figure 31. Comparative analysis of the MH2 non-pollical proximal phalanx morphology, including U.W. 88-164 (PP2), -120 (PP3), -108 (PP4) and -121 (PP5). Box-and-whisker plots of proximal phalanx (PP) shape, in which each variable is shown as a ratio of total length: mediolateral (ML) breadth of the base (top, left), at midshaft (top, right) and the distal trochlea (bottom, left), and dorsopalmar (DP) height of the trochlea (bottom, right). Comparative extant sample includes Gorilla *sp. (n=10 individuals),* P. troglodytes *ssp. (n=6),* P. paniscus *(n=5), recent small-bodied (s-b) Khoisan humans (n=6), recent humans (n=17). Comparative fossil sample composed of* Ar. ramidus *(n=5 specimens, ARA-VP-6/500-022, -030 and -069, ARA-VP-7/2H, and ARA-VP-6/507),* Au. afarensis *(n=9, A.L. 288-1x, A.L. 333-19, -57, -62, -63 and -93, A.L. 333w-4, A.L. 1044-1, A.L. 444-4),* Au. africanus *(n=2, StW 28 and -293),* Au. robustus*/early* Homo *(n=3, SKX 5018, -15468 and -2741), cf.* H. erectus *OH 86 PP5 (Domínguez-Rodrigo et al. 2015),* Homo *sp. ATE9-2 PP5 (Lorenzo et al. 2015),* H. naledi *(n=13, U.W. 101-558, -754, -923, -1025, -1326, -1327, -1328, -1454, -1460, -1643, -1644, -1645, -1725),* H. floresiensis *LB6/8 (Larson et al. 2009), Neandertals (n=5 individuals, Shandiar 4 , 5 and 6, Tabun 1, Kebara 2 in addition to Spy 24A, -24B, -24C, -426a, -748a, and -766a), and early* H. sapiens *('early* Homo*') (n=8 individuals, Dolní Věstonice 3, 13, 14, 15 and 16, Qafzeh 8 and 9, Ohalo II). Regarding* Ar. ramidus*, all data derive from published values in Lovejoy et al. (2009), except for ML breadth at midshaft, which was measured on the original fossils by TLK, and the following values that have been adjusted from Lovejoy et al. (2009) following re-measurement of original fossils by G. Suwa: ARA-VP-6/500-069 ML breadth of base (13.8mm) and ARA-VP-6/507 DP height of trochlea (8.5mm).*

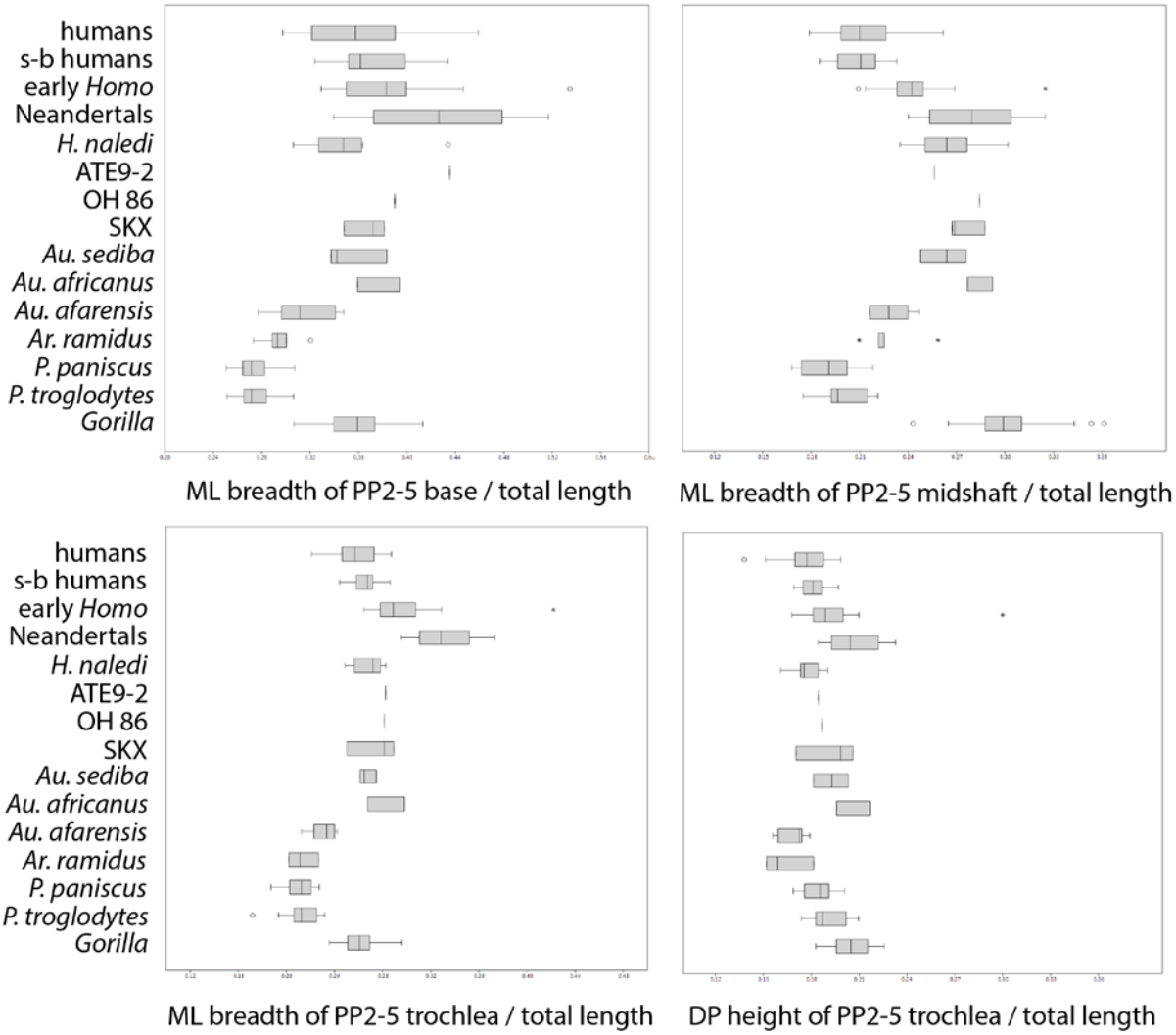
humans
s-b humans
early Homo
Neandertals
H. naledi
ATE9-2
OH 86
SKX
Au. sediba
Au. africanus
Au. afarensis
Ar. ramidus
P. paniscus
P. troglodytes
Gorilla
ML breadth of PP2-5 base / total length
ML breadth of PP2-5 midshaft / total length
ML breadth of PP2-5 trochlea / total length
DP height of PP2-5 trochlea / total length

1
2

Figure 32. Comparative analysis of the MH2 intermediate phalanx morphology, including U.W. 88-161 (IP3), -122 (IP4) and -162 (IP5). Box-and-whisker plots of intermediate phalanx (IP) shape, in which each variable is shown as a ratio of total length: mediolateral (ML) breadth of the base (top, left), at midshaft (top, right) and the distal trochlea (bottom, left), and dorsopalmar (DP) height of the trochlea (bottom, right). Comparative extant sample includes Gorilla *sp. (n=9 individuals),* P. troglodytes *ssp. (n=4),* P. paniscus *(n=4), recent small-bodied (s-b) Khoisan humans (n=6), recent humans (n=15). Comparative fossil sample composed of* Ar. ramidus *(n=4 specimens, ARA-VP-6/500-002, -059, -078 and -092),* Au. afarensis *(n=7, A.L. 333-32, -46, -64, -88, -149 and -150, and A.L. 333x-18),* Au. africanus *(n=1, StW 331),* Au. robustus*/early* Homo *(n=6, SKX 5019, -5020, -9449, -13476, -35439, and -36712),* H. naledi *(n=11, U.W. 101-381, -777, -924, -1027, -1308, -1310, -1311, -1325, -1646, -1647, and -1648),* H. floresiensis *(n=2, LB1/48 and LB6/9; Larson et al. 2009), Neandertals (n=7 individuals, Shandiar 4 , 5 and 6, Amud 1, Tabun 1, Kebara 2, Moula-Geursy M-G1-154 in addition to Spy 222b, -390a, 430a and -484a), and early* H. sapiens *('early* Homo*') (n=10 individuals, Dolní Věstonice 3, 13, 14, 15, 16, 34 and 53, Qafzeh 8 and 9, and Ohalo II). Regarding* Ar. ramidus*, all data derive from published values in Lovejoy et al. (2009), except for ML breadth at midshaft, which was measured on the original fossils by TLK, and the following values that have been adjusted from Lovejoy et al. (2009) following re-measurement of original fossils by G. Suwa: total length of the IP in ARA-VP-6/500-059 (35mm), ARA-VP-6/500-092 (37mm) and ARA-VP-6/500-002 (24.4mm) and ML breadth of base in ARA-VP-6/500-078 (12.9mm).*

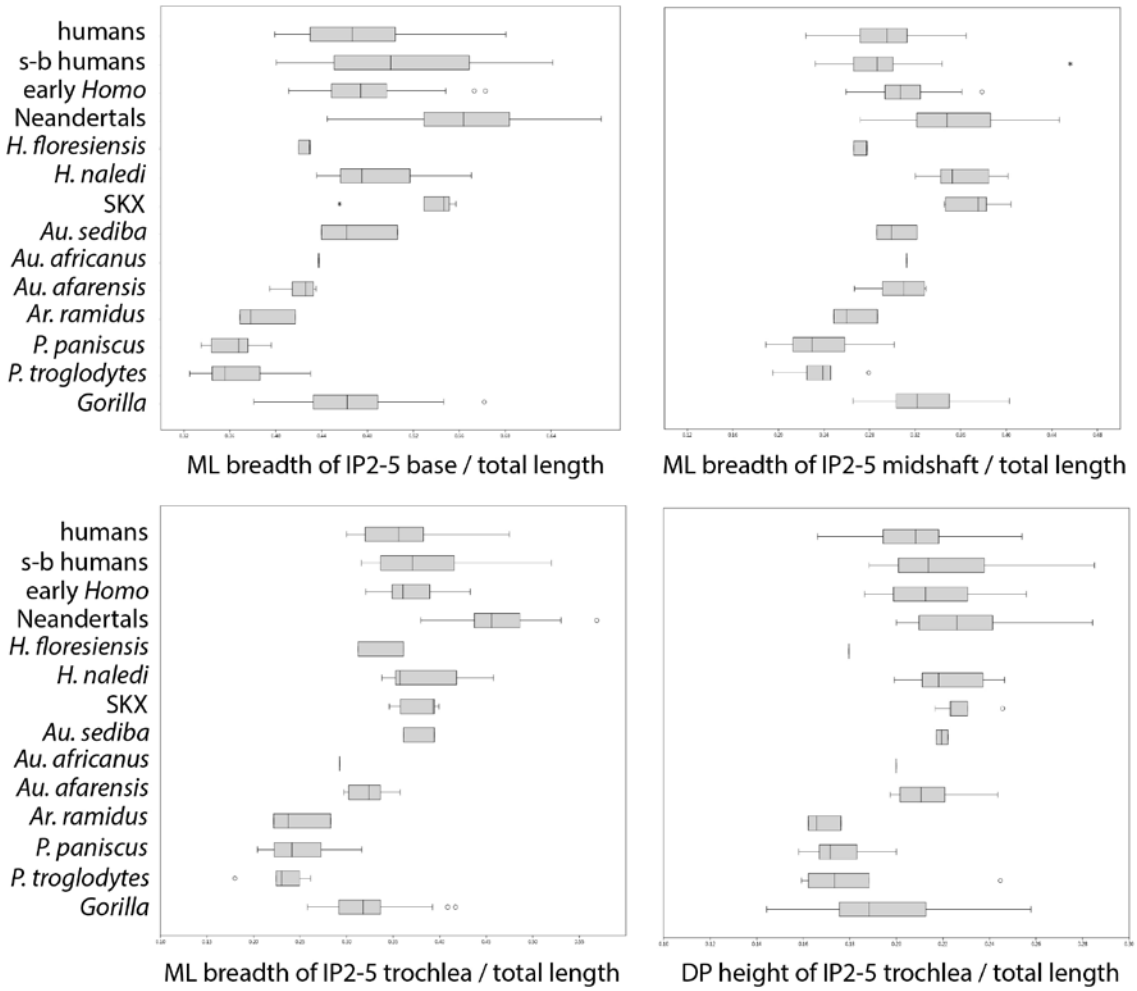
humans
s-b humans
early Homo
Neandertals
H. floresiensis
H. naledi
SKX
Au. sediba
Au. africanus
Au. afarensis
Ar. ramidus
P. paniscus
P. troglodytes
Gorilla
ML breadth of IP2-5 base / total length
ML breadth of IP2-5 midshaft / total length
ML breadth of IP2-5 trochlea / total length
DP height of IP2-5 trochlea / total length

1
2

Figure 33. Comparative analysis of the MH2 U.W. 88-124 distal pollical phalanx morphology. Box-and-whisker plot of the mediolateral (ML) breadth of the distal pollical phalanx (DP1) apical tuft relative to total DP1 length. Comparative extant sample includes Pan *sp. (n=7), recent small-bodied (s-b) Khoisan humans (n=22), and recent humans (n=34). Comparative fossil sample composed of* Ar. ramidus *ARA-VP-6/500-049,* Au. afarensis *A.L. 333-159,* Au. africanus *StW 294,* Au. robustus *TM 1517k,* Au. robustus*/early* Homo *SKX 5016,* H. habilis *OH 7 FLK-NN-A,* H. naledi *U.W. 101-1351 and -1453, Neandertals (n=5 individuals, Shandiar 3, 4, 5 and 6, and Kebara 2), and early* H. sapiens *('early'* Homo*) (n=2 individuals, Dolní Věstonice 16 and Ohalo II).* Ar. ramidus *total DP1 length from Lovejoy et al. (2009) and ML breadth of apical tuft (4.3mm) measured on original fossil by TLK. Due to preservation, both total length and apical tuft breadth are estimated in U.W. 101-124 and thus results should be interpreted with caution.*

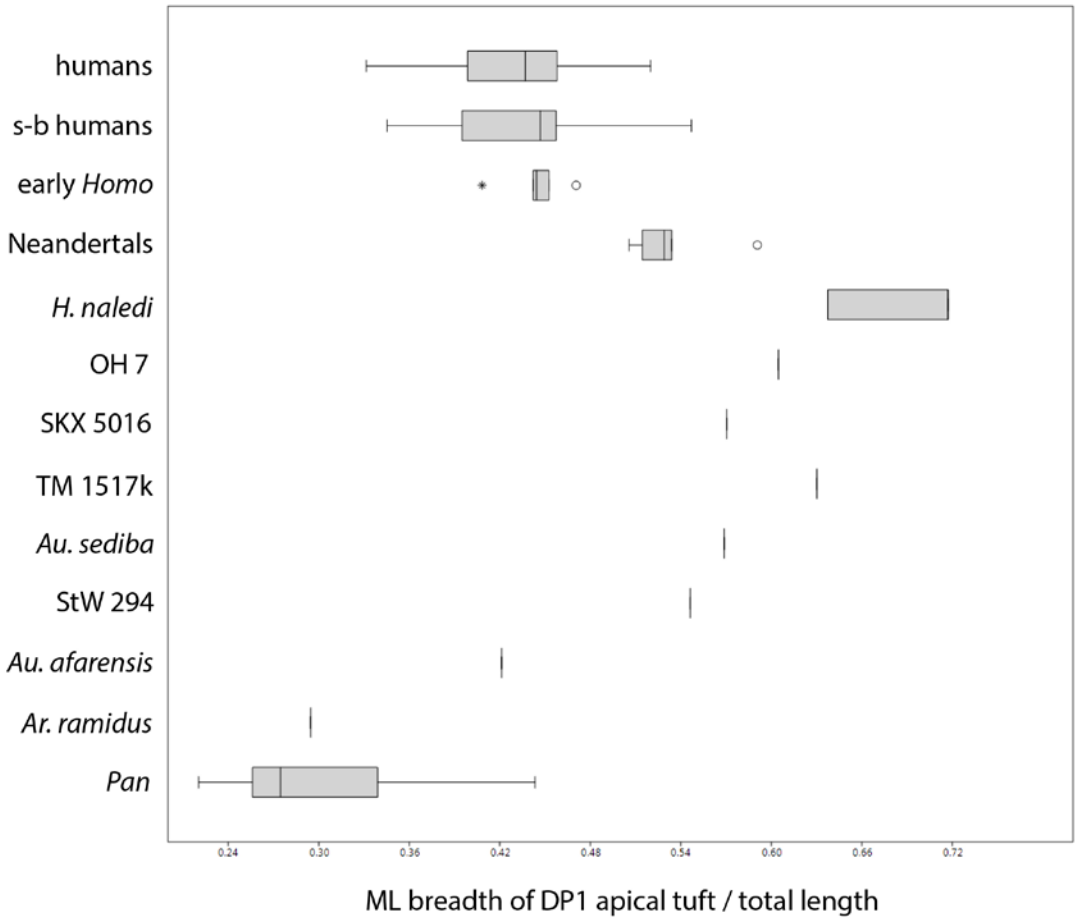

TABLES

Table 1. *Au. sediba* MH1 and MH2 hand bones.

Specimen #[1]	Element	Preservation
MH1 hand bone (juvenile)		
U.W. 88-112	L Mc3[2]	missing distal epiphysis and eroded proximal end
MH2 hand bones (adult)[3]		
U.W. 88-158	R scaphoid	complete, excluding small fragment at tip of tubercle
U.W. 88-159	R lunate	complete, excluding small palmar-medial fragment of distal end
U.W. 88-157[4]	R triquetrum	complete and undistorted
U.W. 88-156	R capitate	complete, excluding small fragments from dorsolateral corner and palmar beak of distal end
U.W. 88-105	L capitate	complete and undistorted
U.W. 88-95	R hamate	complete, excluding tip of hamulus
U.W. 88-106	L hamate	complete and undistorted
U.W. 88-119	R Mc1	complete and undistorted
U.W. 88-115	R Mc2	complete and undistorted
U.W. 88-116	R Mc3	complete and undistorted
U.W. 88-117	R Mc4	complete and undistorted
U.W. 88-118	R Mc5	complete and undistorted
U.W. 88-160	R PP1	complete, excluding fragments from palmar surface of base, some erosion on head
U.W. 88-91	L PP1	complete and undistorted
U.W. 88-164	R PP2	complete and undistorted
U.W. 88-109	L PP2	lateral half of bone, broken at sagittal midline
U.W. 88-120	R PP3	complete and undistorted
U.W. 88-182	L PP3	proximal half, broken just distal to the midline
U.W. 88-108	R PP4	complete, missing small fragment from palmar surface of base and palmar, lateral edge of head
U.W. 88-110	L PP4	fragment of proximal end
U.W. 88-121	R PP5	complete and undistorted
U.W. 88-123	R IP2	complete, but preserved in breccia and shaft distorted a distal end
U.W. 88-161	R IP3	complete and undistorted
U.W. 88-122	R IP4	complete, excluding small fragment from palmar surface of base
U.W. 88-162	R IP5	complete and undistorted
U.W. 88-124	R DP1	missing most of base and small fragments from medial and palmar surface side of apical tuft

[1] Abbreviations: ‘L’, left; ‘R’, right; ‘Mc’, metacarpal; ‘PP’, proximal phalanx; ‘IP’, intermediate phalanx; ‘DP’, distal phalanx.

[2] Kivell et al. (2011) reported U.W. 88-112 as a right Mc3, rather than left.

[3]Kivell et al. (2011) reported a U.W. 88-111 as a manual left DP4 or DP5 associated with the MH2 skeleton, but this bone is now considered to be a pedal distal phalanx (see DeSilva et al, this volume).

[4]This specimen was mistakenly listed as U.W. 88-163 in Kivell et al. (2011)

Table 2. Linear measurements of MH2 carpal bones.

Description	Measurement (mm)[1]	
	MH2 right	MH2 left
Scaphoid U.W. 88-158[2]		
PD[3] length of scaphoid body	12.2	-
DP height of scaphoid body	20.8	-
ML breadth of scaphoid body (excluding tubercle)	9.9	-
tubercle projection (following Trinkaus 1983)	11.7	-
PD length of radial facet	11.3	-
PD height of radial facet	13.7	-
DP height of lunate facet	8.9	-
PD length of lunate facet	7.9	-
DP height of capitate facet	11.1	-
PD length of capitate facet	9.2	-
DP height of trapezium-trapezoid facet	14.6	-
ML breadth of trapezium-trapezoid facet	7.6	-
Lunate U.W. 88-159		
PD length of lunate body	9.4	-
DP height of lunate body	12.8	-
ML breadth of lunate body	11.5	-
DP height scaphoid facet (at distal edge)	9.6	-
PD length of scaphoid facet	6.6	-
DP height of capitate facet	10	-
ML breadth of capitate facet	5.4	-
DP height radial facet	12.6	-
ML breadth of radial facet	11.2	-
DP height of triquetrum facet	6.7	-
PD length of triquetrum facet	7.6	-
Triquetrum U.W. 88-157		
ML breadth of triquetrum body	14.2	-
DP height of triquetrum body	11.5	-
PD length of triqetrum body	8.3	-

DP height of lunate facet	7.8	-
PD length of lunate facet	7.4	-
ML breadth of hamate facet	11.3	-
DP height of hamate facet	10.2	-
ML breadth of pisform facet	6.1	-
PD length of pisiform facet	5.7	-
Capitate U.W. 88-156 (R) and U.W. 88-105 (L)		
PD length of capitate body	17.7	17.8
DP height of capitate body	16.1	16.2
ML breadth of capitate body	[12.3]	12.8
minimum ML breadth of the capitate neck	9	9.5
ML breadth of proximal facet	10	10.1
DP height of proximal facet	10.1	10.8
DP height of hamate facet	9.3	9.4
PD length of hamate facet	15.4	15.7
PD length of Mc2 facet	4.2	4.6
DP height of Mc2 facet	8.2 pres.	11.2
ML breadth of Mc3 facet	[11]	12
DP height of Mc3 facet	11.4	12.7
Hamate U.W. 88-95 (R) and U.W. 88-106 (L)		
PD length of hamate	[16.6]	16.6
PD length of hamate body (excluding hamulus)	15.6	16.4
DP height of hamate	18.4	19.2
DP height of hamate body (excluding hamulus)	11.4	11.6
ML breadth of hamate body	14.1	13.6
DP height of capitate facet	8.8	9.2
PD length of capitate facet	13.9	14.2
DP height of triquetrum facet	9.2	9.6
PD length of triquetrum facet	14.3	13.7
ML breadth of Mc4 facet	8.3	8.4
DP height of Mc4 facet	10.7	11
ML breadth of Mc5 facet	7.9	7.7
DP height of Mc5 facet	8.2	8

[1] All measurements are the maximum of that dimension, unless otherwise noted. Additional metric data are also provided in the text for some carpal bones.
[2] Note that the PD and DP dimensions of the scaphoid follow the orientation in Figure 3.
[3] Abbreviations: ‘PD’, proximodistal; ‘DP’, dorsopalmar; ‘ML’, mediolateral; ‘R’, right; ‘L’, left; ‘pres.’, preserved; [x], value estimated with confidence based on preserved morphology; ‘-‘, bone not preserved, or morphology not preserved well enough to estimate the value.

Table 3. Linear measurements of MH1 and MH2 metacarpals (Mc).

Description	**Measurement (mm)**					
Specimen #: **U.W. 88**	**MH2 Mc1 -119**	**MH2 Mc2 -115**	**MH1 Mc3 -112**	**MH2 Mc3 -116**	**MH2 Mc4 -117**	**MH2 Mc5 -118**
Total length	39.5	53.3	44.7 pres. [53]	48.6	44.5	41.7
Interarticular length	37.7	50	-	48.4	43.9	41
DP[1] height of proximal base	12.7	13.9	13.9 pres. [11.5]	13.8	11.1	10
ML breadth of proximal base	10.7	13.1	10.3 pres. [16.5]	10.5	9.9	11.9
DP height of proximal facet	9.9	12.1	-	[9.3]	10.2	7.8
ML breadth of proximal facet	10.5	10.2	-	[12.2]	[7.4]	8.5
DP height at midshaft	6.3	7.4	9	7.3	6.6	5.3
ML breadth at midshaft	7.3	5.6	7.3	5.5	5.2	6.3
DP height of distal head	11.2	12.1	-	11.6	10.9	10.9
ML breadth of distal head	10.3	10.3	-	10.4	10	9.4

[1] Abbreviations the same as in Table 2.

Table 4. Linear measurements of MH2 proximal phalanges.

Description	**Measurement (mm)**								
Specimen #: U.W. 88-	**Ray 1 right -160**	**Ray 1 left -91**	**Ray 2 right -164**	**Ray 2 left -109**	**Ray 3 right -120**	**Ray 3 left -182**	**Ray 4 right -108**	**Ray 4 left -110**	**Ray 5 right -121**
Total length	[23.5]	24.5	31.5	31.5	34.7	26.0 pres.	[33.6]	14.3 pres.	[27.9]
ML[1] breadth of proximal base	[10.6]	11.4	11.3	-	11.7	11.3	11.5	[10.3]	10.7
DP height of proximal base	7.6 pres.	9	9.2	[9]	10.9	10.2	[9.6]	-	8.9
DP height of proximal facet	[7.8]	7.8	7.9	[7.7]	9.1	9	[8.4]	[8.3]	7.2
ML breadth of proximal facet	[9.6]	9.7	10	-	9.5	8.9	9.3	[8.7]	9.1
DP height at midshaft	5.3	5.6	5.5	[5.9]	6.9	5.9	6.5	-	[4.2]
ML breadth at midshaft	5.7	5.8	7.8	-	9.2	8.7	9.1	-	7.7
DP height of distal trochlea	[5.3]	5.5	6.4	[6.3]	6.7	-	[6.1]	-	-
ML breadth of distal trochea	[8.6]	[9.2]	8.7	-	9.1	-	[8.9]	-	-

[1] Abbreviations the same as in Table 2.

Table 5. Linear measurements of MH2 intermediate and distal phalanges.

Description	**Distal phalanx**[2]	**Intermediate phalanges**			
	Ray 1	**Ray 2**	**Ray 3**	**Ray 4**	**Ray 5**
Specimen #: U.W.88-	**-124**	**-123**	**-161**	**-122**	**-162**
Total length	15.1 pres.[16]	16.6 pres. [18.3]	22.2	21.6	17.5
ML[1] breadth of proximal base	-	[9.8]	9.7	10	8.9
DP height of proximal base	-	-	8.7	-	-
DP height of proximal facet	-	-	6.2	-	-
ML breadth of proximal facet	-	-	8	8.4	[7.6]
DP height at midshaft	5.1	-	5	4.1	3.9
ML breadth at midshaft	5	[6.7]	6.3	6.9	5.2
DP height of apical tuft[3]/trochlea	4..4	-	4.9	[4.8]	[3.8]
ML breadth of apical tuft/trochlea	7.7 pres. [9.1]	[7.1]	8	7.8	6.9

[1] Abbreviations the same as in Table 2
[2] All measurements are in mm.
[3] Reference to the apical tuft applies to the distal phalanx only, while trochlea applies to the intermediate phalanges.

Table 6. Hand proportions in extant and fossil taxa.

			Ratio (%)[1]					
Taxon	**Sex**	**n**	**PP1:Mc1 TL**	**PP3:Mc3 TL**	**PP3:Mc3 IA**	**IP3:Mc3 TL**	**PP4:Mc4 TL**	**Ray 1: Ray 3**
EXTANT[2]								
Gorilla	M & F	9	56	64.3	67.5	44.9	63.8	39.7
			3.5	2.3	2.7	1.8	5.3	1.4
P. troglodytes	M & F	9	67.6	67.5	69.1	49.2	68.5	36.3
			3.7	1.1	1.1	1.9	1.5	1
P. paniscus	M & F	10	64.6	61.9	63.5	44.1	63	36.3
			3	1.9	2	1.4	1.5	0.9
H. sapiens	M	18	68.8	67.2	71.3	44	73.7	54
			4.4	3.4	3.8	2.2	4.5	2
	F	23	68.3	67.3	71.8	44.1	74.6	53.1
			2.6	3	3.1	1.9	3.4	1.9
s-b *H. sapiens*	M	12	67.4	67.5	71.5	43.8	74.7	55.3
			3.4	3.8	4	2.4	3	2.3
	F	13	68.1	67.4	71.3	42.8	75.8	54.5
			2.4	2.3	2.3	2	9.4	1.8
FOSSILS								
Early *H. sapiens*								
Ohalo II H2			67	68.1	69.5	45.8	69	52.4
Arene Candide 2			73.7	68.5	72	45.7	74.9	56.6
Barma Grande 2			70.3	64.2	67.3	44.1	72.2	56.1
Qafzeh 9			73.8	74.7	76.6	49.9	82.3	56.6
Qafzeh 8			-	-	-	49.6	-	-
H. neanderthalensis								
Kebara 2			67.7	67.8	71.2	44.8	-	51.4
Shanidar 4			62.4	60.8	65.7	40.1	67[3]	52.4
Tabun 1			64.4	67.4	70	-	-	-
Other hominins								
H. naledi Hand 1			65.5	73.3	73.9	46.1	77.5	57.6

Au. sediba MH2	62	71.4	71.7	45.7	75.5	60.7
Au. afarensis composite[4]	66	67.3	69	42.9	70	51.7
Ar. ramidus ARA-VP-6/500	-	-	-	-	80.3	-

[1] All values are presented as percentages, with the mean value above and standard deviation below.
[2] Abbreviations: 's-b', small-bodied, Khoisan individuals. 'TL', total length; 'IA', interarticular length
[3] ratio calculated using IA length of Mc4
[4] hand bones not associated with the same individual

Table 7. Summary of key morphological features of the *Au. sediba* hand and how they compare with other hominins.[1]

Primitive or similar to (most) other australopiths and *Ardipithecus*
large trapezoid facet and "closed" distomedial border of scaphoid
"waisted" capitate body
absence of saddle-shaped hamate-Mc5 articulation
small and relatively curved trapezium-Mc1 articulation
gracile Mc1 shaft with poorly-developed entheses
distally-extended first *M. dorsal interosseous* insertion on Mc1 shaft
asymmetrical metacarpal heads
ML narrow Mc1 head
absence of Mc3 styloid process
moderate curvature of proximal phalanges
prominent flexor sheath ridges of proximal phalanges
DP1 with ML broad apical tuft
Derived or similar to (some) *Homo* species
scaphoid's trapezium facet extends onto tubercle
triquetrum morphology suggests possibly small, rather than rod-shaped, pisiform
hamate hamulus shape with limited distal projection
relative size of hamate's Mc4/Mc5 facets that do not extend onto the hamulus
intrinsic thumb proportions with relatively long Mc1 and relatively short PP1 (most similar to Neandertals)
DP1 with well-developed proximal and distal fossae and FPL tendon attachment
Distinct or of unknown polarity

triquetrum morphology with tubercle-like palmar-medial extension
ML narrow lunate (most similar to Miocene ape morphology)
extremely long length of thumb, and especially Mc1, relative to third digit
palmar beak on Mc1 head (also found only in SK 84)
poorly developed and proximally-positioned *M. opponens pollicis* insertion on Mc1 shaft
generally gracile metacarpal shafts with relatively large heads and bases (although MH1 Mc3 shaft is relatively broad)
overall shape and flexor attachment morphology of intermediate phalanges
dorsal and palmar trapezoid facets on capitate
laterally-oriented captiate-Mc2 articulation

[1] Features are organised into hypothesised categories based on general similarities to all or most species within a particular genus (i.e., *Australopithecus, Homo*). However, given the mosaic of morphologies that are found across the hominin fossil record, particularly traditionally "derived" features in early hominins [e.g. *Orrorin* (Almécija et al. 2010)] or traditionally "primitive" features in recent hominins [e.g. *H. floresiensis* (Tocheri et al. 2007) or *H. naledi* (Kivell et al. 2015)], the polarity of any given feature is not always clear.

1